Topological changes in sheared two-dimensional foams

by

Aled Wyn

University of Wales Aberystwyth (UWA)
2009

THESIS
submitted to The University of Wales
by
Aled Wyn, B.Sc, M.Sc (Wales)
In Candidature for the Degree of
PHILOSOPHIAE DOCTOR

Declaration

This work has not previously been accepted in substance for any degree and is not being concurrently submitted in candidature for any degree.

Signed . . . . . (candidate)

Date . . . . . .

Statement 1

This thesis is the result of my own investigations, except where otherwise stated. Where ***correction services** have been used, the extent and nature of the correction is clearly marked in a footnote(s).

Other sources are acknowledged by footnotes giving explicit references.
A bibliography is appended.

Signed . . . . . (candidate)

Date . . . . . .

[*this refers to the extent to which the text has been corrected by others]

Statement 2

I hereby give consent for my thesis, if accepted, to be made available for photocopying and for inter-library loan, and for the title and summary to be made available to outside organisations.

Signed . . . . . (candidate)

Date . . . . . .

Summary

This thesis concerns the response of two-dimensional foams to applied shear based on numerical simulations in the quasistatic limit. The effect of liquid fraction and area-disorder on the discrete topological changes (T1s) which occur as a foam flows are probed at several length scales and related to the response of the ordered hexagonal honeycomb.

At the macroscopic scale, many T1s combine and the yielding of the foam can be characterized through the harmonics of the stress. Stress harmonics obtained from simulations of dry two-dimensional foams are in good agreement with experimental data for foams and other yield stress materials.

At the mesoscopic scale, several T1s occur in a certain region of the foam causing the flow to localize in a region of width proportional to the square root of area-disorder. For dry two-dimensional foams I present a one-dimensional measure and a tensorial measure of foam structure which can identify the localized region from a single still image. The width of the localized region increases linearly with liquid fraction and for sufficiently high values of liquid fraction and area-disorder, the T1s fill the channel and no localization is observed.

At the microscopic scale, the links between neighbouring bubbles define a pair of orientations that characterize the local bubble configurations at the instant of a T1. Macroscopic flow behaviour originates at the microscopic scale and I show that the yield stress is directly related to the orientation of the T1 events.

Liquid fraction and area-disorder have, in general, the same effect at each length scale. The yield stress decreases with increasing liquid fraction and area-disorder; and the amount of flowing foam and the orientations of a T1 increase with increasing liquid fraction and area-disorder. The response of disordered foams is shown to be different to that of ordered foams in each case.

This work is dedicated to
Cerys

Acknowledgements

I'd like to express my gratitude to my supervisor, Simon, for patiently putting up with me for three years and to the rest of the foams research group, Tudur and Sian, for valuable input and discussion. I'd like to thank my second supervisor Dave for checking up on me, John for advice on statistics and the remainder of IMAPS, past and present, who have contributed to my education. In addition, I'd like to thank Ken Brakke for developing the Surface Evolver and financial support from the EPSRC (EP/D048397/1) is gratefully acknowledged. Finally, I'd like to thank my wife, Cerys, for her support and patience throughout, and my daughter, Ava, for keeping things interesting.

Figure 1: An experimental collaborator.

Contents

Chapter 1

Introduction

Foams are complex fluids which have wide ranging application, both industrial and commercial. They consist of gas bubbles dispersed in liquid. The films, which separate the bubbles, meet at channels called Plateau borders [1] which themselves meet at vertices called Plateau border junctions (figure 1.1). This simple local structure can lead to complex dynamic phenomena, which can be split into four broad categories:

- **Foam drainage**, which is the study of how the liquid flows through the Plateau border network and films under gravity. If flow is assumed to be through the Plateau borders only and of Poiseuille type then the following drainage equation can be derived [3]:

$$\frac{\partial \phi}{\partial \bar{t}} + \frac{\partial}{\partial z}\left(\phi^2 - \frac{\sqrt{\phi}}{2}\frac{\partial \phi}{\partial z}\right) = 0, \tag{1.1}$$

  where ϕ, $\bar{t}$ and z are dimensionless parameters representing liquid fraction, time (the time-scale is set by the liquid viscosity) and vertical position respectively. This equation may be used, for example, to find the equilibrium distribution of liquid in a foam.

- **Coarsening**, in which gas diffuses from one bubble to another through the liquid films, driven by the pressure difference between bubbles. The rate of change

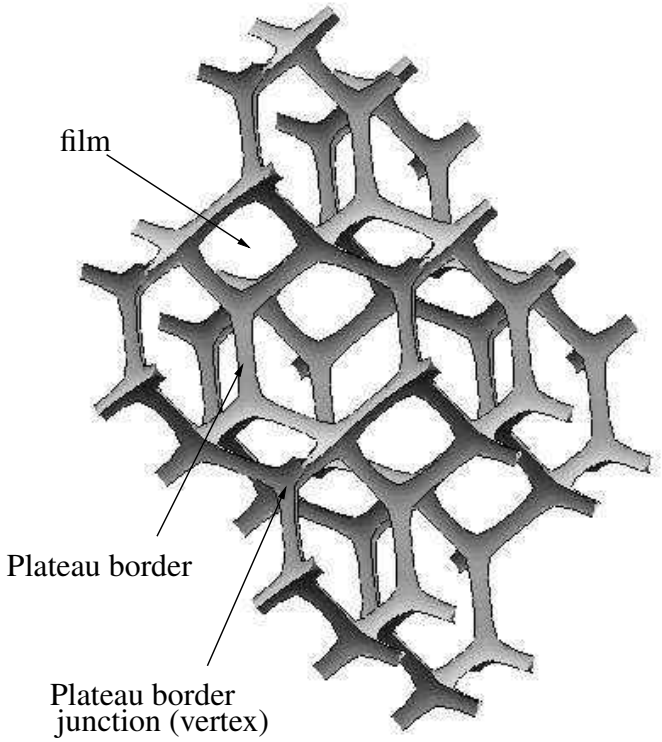

Figure 1.1: Three-dimensional foam structure (adapted from [2]): Films (transparent) meet at Plateau borders which themselves meet at Plateau border junctions.

of bubble volume with time can be expressed exactly in terms of a measure of the bubble's linear size (an average of chord lengths) and the total length of the surrounding Plateau border network [4]. In two dimensions, the rate of change of bubble area, A, with time, t, is given by the von Neumann law [5, referenced in 2]:

$$\frac{\mathrm{d}A}{\mathrm{d}t} = k(n-6) \tag{1.2}$$

where n is the number of sides of the bubble and k a constant.

- **Film rupture / foam collapse**, the study of what causes films to rupture, bubbles to coalesce and ultimately a foam to fracture and collapse. Rupture is typically attributed to films becoming too thin, perhaps because of being stretched [6] or as liquid drains from them [7] or evaporates, or as a result of the presence of

antifoam particles [8].

- **Rheology**, which concerns the flow of the foam and the movement of individual bubbles. Foams exhibit both solid-like and liquid-like behaviour due to their peculiar local structure, possessing elastic, plastic and viscous properties which make them useful prototypical systems for studying complex fluids such as pastes, gels and emulsions.

Each aspect plays an important role in different situations. This thesis concerns the flow (rheology) of foams. Numerical bubble-scale simulations are performed in order to predict their properties and mechanical response. In particular, I shall examine the effect of the liquid content and the level of disorder of a foam on the structural changes which occur as it flows. The structural changes at small length scale in turn affect the phenomena of yielding and shear banding at larger length scales.

1.1 Motivation

Foams are familiar to us all. We encounter them daily, whether it be while grooming in the bathroom, washing the dirty dishes or sitting on our padded office chair. Whilst foams are used in many everyday situations, their applications in industry are also extensive. Examples of foam use include:

- **Fire fighting**

  The lower density of foams compared to liquid is one aspect that makes them useful for fighting fires, particularly those involving liquids [9]. In circumstances where addition of liquid to cool the fire would aid the spreading of the fire, foams are able to form a layer on top of the burning liquid, both cooling the fire and denying it oxygen.

- **Enhanced Oil Recovery**

  Foams are injected into oil reservoirs to improve the efficiency of oil recovery in one of two ways [10]. Foam can be used to *plug* regions of the reservoir which are unproductive or from which oil has already been extracted. A second, more ambitious approach, involves creating large foam-filled regions within the oil reservoir in order to redirect the flow of the injected liquid by exploiting the foam's yield stress.

- **Separation of precious minerals from ores**

  Minerals can be separated from extracted ores through the process of foam flotation [11]. Air is pumped into a solution containing the minerals to be separated. With the right mixture of chemicals, the desired mineral is attracted to the air bubbles which form a foam at the top of the liquid and the undesired compounds are left in the solution. The process may be repeated if required.

- **Personal care and drug products**

  A foaming property in personal care products often shows no evidence of increasing the product's efficiency but is nevertheless demanded by the consumer and is therefore an important consideration for the manufacturer [12]. Shaving foam is a good example of a product where a foaming property is expected from the consumer, but there is good evidence that a non-foaming gel will perform all the tasks required from a shaving foam with equal efficiency. A foaming property is useful however for drug products which require injection into a body cavity since the foam increases the probability that the drug will come into contact with all surfaces needing treatment.

- **Wet processing in the textile industry**

  Foams are used in place of liquids in processes such as dyeing, printing and fin-

ishing of textiles to cover a greater area of the fabric, using less liquid, leading to greater savings and shorter drying times [13].

There are also many examples of solid foams that are fabricated from liquid precursors, including metals and foods, which were liquid foams at one stage of manufacture.

Such a vast and growing number of applications pose questions regarding the dynamics of foams. During enhanced oil recovery, foams flow through porous rock, and there are many instances where a foam must flow through a pipe e.g. in firefighting, food manufacture and after the foam is collected from flotation. Predicting foam response in these situations is useful and requires an understanding of how a foam responds to applied stresses. To probe the effect of an applied stress on the flow of a foam, I perform simulations in a simplified geometry, where a foam sample is placed between parallel walls and sheared by moving one of these walls.

1.2 Foam fundamentals

1.2.1 Structure and liquid fraction

Aqueous or, more generally, liquid foams consist of gas bubbles dispersed in liquid. They bear many similarities to emulsions, which comprise one liquid dispersed within another continuous liquid. The gas is sometimes referred to as the dispersed phase, and the liquid as the continuous phase. The volume fraction of the liquid phase, ϕ_l, characterizes the amount of liquid present in the foam. The gas fraction, $\phi_g = 1 - \phi_l$ may also be used but I use the liquid fraction throughout.

Whilst the macroscopic behaviour of foams is complex, the bubble scale structure is remarkably simple. Each film minimizes its surface energy which is equal to the product of surface area and surface tension, γ, and is made up of two air-liquid interfaces which

have mean curvature

$$\kappa = \frac{1}{2}\left(\frac{1}{r_1} + \frac{1}{r_2}\right) \tag{1.3}$$

where r_1 and r_2 are the principal radii of curvature. The pressure difference across each film, ΔP, is given by the Laplace-Young law [2], taking into account that a film consists of two air-liquid interfaces:

$$\Delta P = 2\gamma\kappa. \tag{1.4}$$

Plateau [1] established the following rules for a dry foam (the limit $\phi_l \to 0$) at equilibrium from empirical observation:

- Three films meet at angles of 120° creating liquid channels called Plateau borders.
- Plateau borders meet fourfold at Plateau border junctions at tetrahedral angles, $\cos^{-1}(-1/3) \approx 109.47°$.

These rules were proved by Taylor [14] to arise as a consequence of minimization of surface energy.

The Plateau borders form a continuous network of liquid and at low liquid fraction, the liquid is contained mainly in the Plateau borders. As the liquid fraction increases, the Plateau borders become shorter and thicker, Plateau border junctions swell and then merge. Strictly speaking, Plateau's laws only apply in the dry limit, but they are a good approximation at low liquid fraction, where only threefold Plateau borders and fourfold Plateau border junctions are present [15], At a critical high liquid fraction, at what is known as the rigidity-loss transition ($\phi_l \approx 0.36$ [16–18]), there is a transition from a foam to a bubbly liquid. As a consequence, foam simulation has proved increasingly difficult either as the liquid fraction is increased from the dry limit [19–21] or decreased from the rigidity-loss transition [16; 22–24], and many studies are restricted either to the dry limit or to the wet limit, leaving the intermediate range of liquid fraction relatively unexplored.

A foam structure can also be described statistically. Early work by Matzke [25] found that pentagonal films were most common in a monodisperse foam (those where the volume of each bubble is equal) and the average number of films per bubble was 13.70. Simulations by Kraynik *et al.* [26; 27] were in good agreement and extended the study to polydisperse foams (those with bubbles of different volume). They found that the number of films per bubble decreased with increasing polydispersity and that the average number of sides to a film also decreases with increasing polydispersity.

1.2.2 Two-dimensional foams

Three-dimensional foams are challenging to study both computationally [26–28] and experimentally [29]. Accurately *seeing* inside the foam is a significant obstacle for experimentalists, whilst the complexity of the algorithms involved (e.g. in implementing changes in topology), coupled with the high demand on computer power and memory, limits the extent of numerical simulation. Working in two dimensions provides many simplifications, whilst still providing useful information about foam response [16; 19–24; 30–43]. Although promoted as a recent technique, and certainly used to good effect in the last ten to fifteen years, the idea is approaching its centenary. There are currently three main methods of realizing a two-dimensional foam experimentally (figure 1.2), sometimes referred to as *quasi-two-dimensional* foams:

- A single layer of bubbles floating freely on a liquid pool, known as a Bragg bubble raft ($\mathcal{LA}$) [44], promoted recently by Dennin and co-workers [45–56].

- A single layer of bubbles is confined between two glass plates, known as a Hele-Shaw cell ($\mathcal{GG}$) [57], used in recent years by Debrégeas and co-workers [40; 58; 59] and Raufaste *et al.* [60].

- A hybrid method in which a single layer of bubbles is confined between a liquid

pool and a glass plate ($\mathcal{LG}$) [61–63], recently utilized by Katgert *et al.* [64; 65], Dennin and co-workers [45; 49] and Graner and co-workers [66–69]

Advantages of two-dimensional experiments include the ability to see each bubble and track its position and shape using image analysis. The disadvantage is that additional effects arise as a consequence of the confinement. It has been demonstrated that the external friction introduced between the glass plates and the bubbles has a significant effect on the flow of the bubbles which must be taken into account [24; 43; 49; 64; 65; 70; 71].

Surfactants (e.g. washing up liquid) are introduced to lower the surface tension of the liquid and stabilize the foam. Surfactant molecules have a hydrophobic head and a hydrophilic tail, causing them to line the air-liquid interfaces and help prevent film rupture. As in three dimensions, the chemistry of the surfactant solution can have a large effect on foam response, since it changes the local boundary conditions for flow [72].

In two dimensions, the mathematical idealization of a dry foam at equilibrium is that films are circular arcs which meet threefold at 120° angles at point vertices representing Plateau borders which are perpendicular to the plane of the foam. Figure 1.3 (a) and (b) show the similarity in appearance between a quasi-two-dimensional foam, in this case a Hele-Shaw cell ($\mathcal{GG}$), and the mathematical idealization of a two-dimensional foam. The actual structure of an ordered quasi-two-dimensional foam in a Hele-Shaw cell can be seen in figure 1.2 (b) (ii). With only one finite radius of curvature, r, the curvature is given by $\kappa = 1/r$ and the Laplace-Young law reduces to

$$\Delta P = \frac{2\gamma}{r}. \tag{1.5}$$

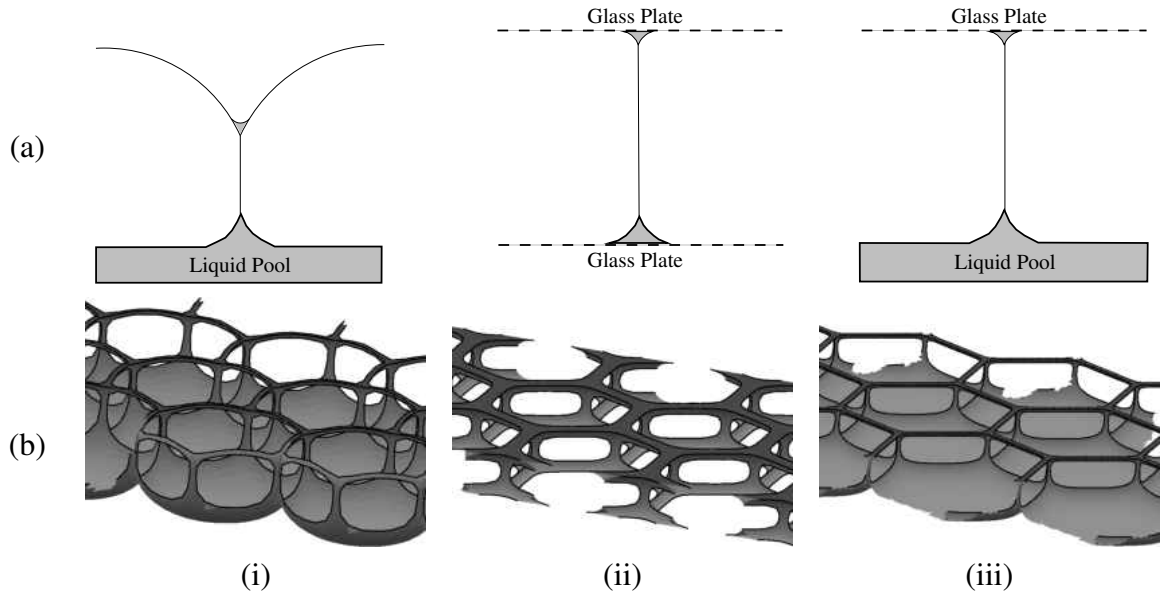

Figure 1.2: Quasi-two-dimensional foams: realizations of two-dimensional foams for experiment from different perspectives courtesy of (a) Vaz & Cox [73] and (b) Cox & Janiaud [74]. (i) A single layer of bubbles floating on a liquid pool ($\mathcal{LA}$). (ii) A single layer of bubbles confined between glass plates ($\mathcal{GG}$). (iii) A single layer of bubbles confined between a liquid pool and a glass plate ($\mathcal{LG}$).

This implies that each film has constant mean curvature, so that it must be an arc of a circle. The surface energy is given by the line tension of the films multiplied by their length and, as in the three-dimensional case, the threefold vertices with 120° angles arise as a consequence of minimization of this energy.

At finite liquid fraction, Plateau borders are no longer points but have finite size (figure 1.3 (c) and (d)). There is a 0° contact angle (i.e. a smooth transition) between the air-liquid interfaces forming a Plateau border and the air-liquid-air interfaces separating bubbles. The *decoration theorem* [2] states that if an equilibrium dry foam is 'decorated' with threefold Plateau borders such that the Plateau borders do not touch, then the result is an equilibrium ("wet") foam with finite liquid fraction. As a result, the dry foam limit can be used as an approximation of a low but finite liquid fraction.

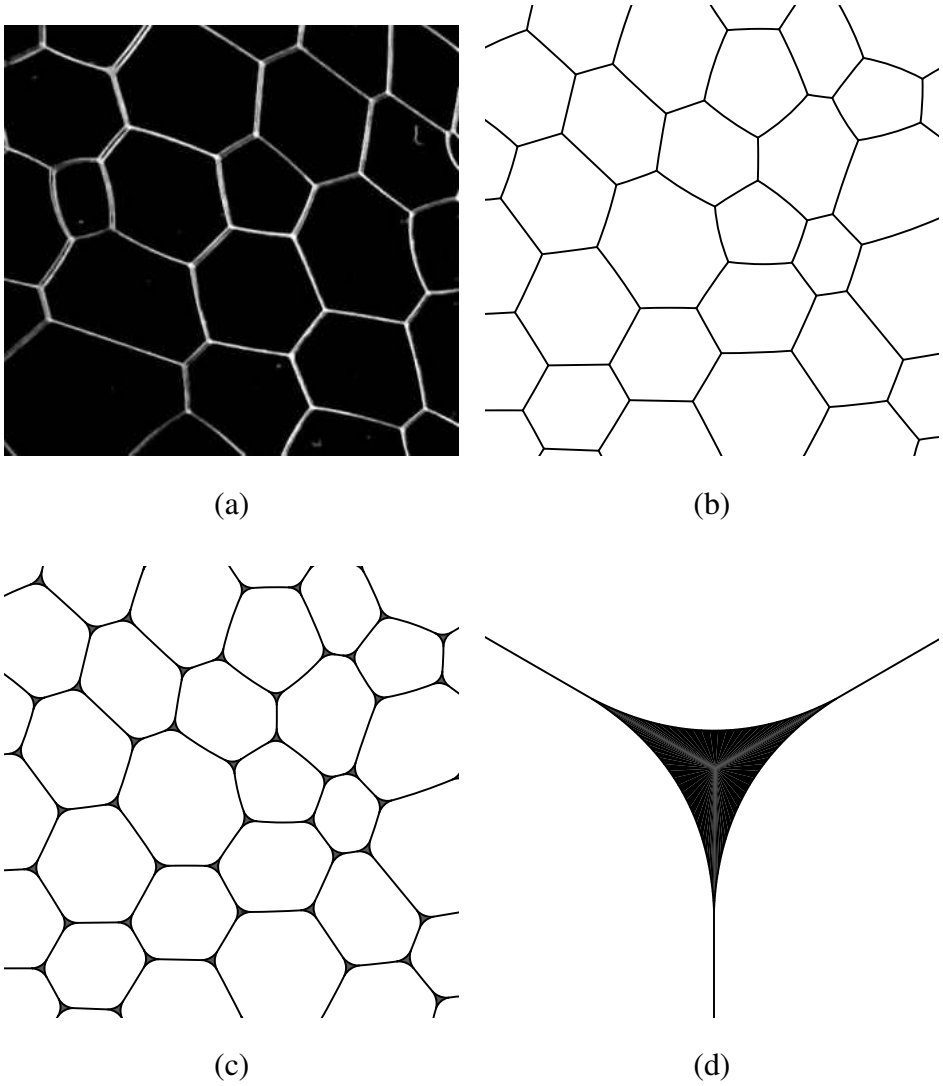

Figure 1.3: (a) A quasi-two-dimensional foam ($\mathcal{GG}$) used in experiment (picture courtesy of S. A. Jones). (b) The mathematical idealization of a dry two-dimensional foam: three films meet at 120° angles at point vertices representing Plateau borders. (c) At finite liquid fraction, Plateau borders have finite cross-section and must be included explicitly in the mathematical model. (d) Close-up of a single Plateau border. The contact angle where air-liquid interfaces meet air-liquid-air interfaces is 0°.

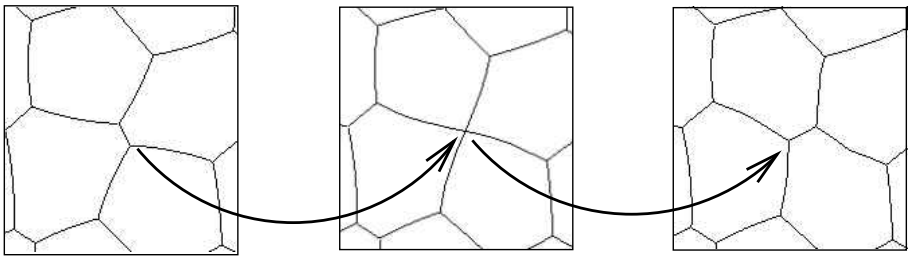

Figure 1.4: A T1 topological rearrangement (picture courtesy of Cox *et al.* [41]), a fundamental process in the flow of foams. Bubbles change neighbours as a film shrinks to zero length, to be replaced by a new film with different orientation and connectivity.

1.2.3 Topological changes

Foams dissipate energy through discrete changes in topology, which are a manifestation of plasticity. There are several types of topological change in three dimensions but the crucial topological change allowing the flow of a two-dimensional foam is the T1 topological change (figure 1.4) [75]. As a film shrinks to zero length, an unstable fourfold vertex is formed, which dissociates into two new threefold vertices. The topology (number of neighbours, loosely speaking) of the bubbles involved has changed. Bubbles that were nearest neighbours before the T1 become next nearest neighbours and *vice-versa*.

1.2.4 Disorder

The disorder of a foam can be characterized in terms of volumetric (area in two dimensions) or topological dispersity. A hexagonal (honeycomb) structure is perfectly ordered: it has all bubbles areas equal (zero area-disorder) and all bubbles have six sides (zero topological disorder). If the plane is partitioned into regions of equal area, the partition that has least perimeter is the hexagonal structure [76], i.e. the hexagonal foam is the monodisperse foam of minimum energy. Hexagonal foams therefore provide a good starting point for the study of foams [30; 32; 34; 35], but are not always representative of real, disordered foams.

The second moment of the distribution of the areas of the bubbles is often used to quantify the level of disorder in a two-dimensional foam [69; 77], here normalized by the square of average bubble area:

$$\mu_2^A = \left\langle \left(\frac{A}{\langle A \rangle} - 1 \right)^2 \right\rangle, \tag{1.6}$$

where A is the bubble area and $\langle . \rangle$ denotes an average over an entire foam sample. It is representative of how far a foam sample is from being monodisperse foam.

The topological disorder, i.e. the deviation from a fully hexagonal sample, can be characterized by the second moment of the distribution of the number of neighbours per bubble, n:

$$\mu_2^n = \langle (n-6)^2 \rangle. \tag{1.7}$$

Quilliet et al. [69] show that both measures are correlated if a foam is annealed through several oscillatory shear cycles to a deep energy minimum. T1 topological rearrangements cause μ_2^n to fluctuate, whilst μ_2^A is often constant over the timescale of an experiment, or fixed in theoretical calculations. Since this will be the case in what follows (i.e. there will be no coarsening or film rupture), I will use μ_2^A to describe the level of foam disorder.

1.2.5 Confining geometries

Experimental and theoretical studies of foams in two dimensions are performed under a wide variety of geometries with different boundary conditions and it will be beneficial to take a moment to define them (figure 1.5):

- **Linear Couette** shear describes the confinement of bubbles between parallel walls. Where the walls end there can be an open pool of bubbles (experiment) or a periodic boundary condition (theory and simulation). If the foam sample is

large enough, this has the effect of having a foam of infinite length and eliminates many artifacts arising from having a foam of finite length. The foam is sheared by moving either wall, or both walls in opposite directions [16; 22; 39–41; 71].

- **Cylindrical Couette** shear refers to the confinement of bubbles between concentric cylinders. Again, the foam is sheared by moving either wall, or both walls in opposite directions [40; 50–56; 58; 59; 64; 70].

- **Fully periodic** shear is possible in simulation or continuum theory only. It refers to a foam sample (a representative element) with periodic boundary conditions in both the x and y directions (figure 1.6), and is essentially an infinite sample and is therefore useful while trying to eliminate boundary effects. It can therefore be thought of as a section of foam in the middle of a very large foam, far from any boundaries. Films crossing periodic boundaries (dashed lines) reappear at the opposite boundary. Care must be taken however to avoid introducing artifacts through having too small a sample. Shear is introduced by changing the shape of the periodic box [30; 37; 38; 43; 77; 78].

- **Pure shear** describes a foam which is wholly confined between two sets of parallel walls [66; 69; 79; 80].

1.3 Rheology of foams

Foams are elasto-visco-plastic complex fluids which exhibit rich flow behaviour that remains to be fully understood [81]. The strain, a measure of the relative deformation of the foam, and the stress, the force per unit area within the foam, have an intricate relationship. Foams respond like elastic solids to small applied strains, with shear stress proportional to applied strain via a shear modulus, G. As the applied strain is increased

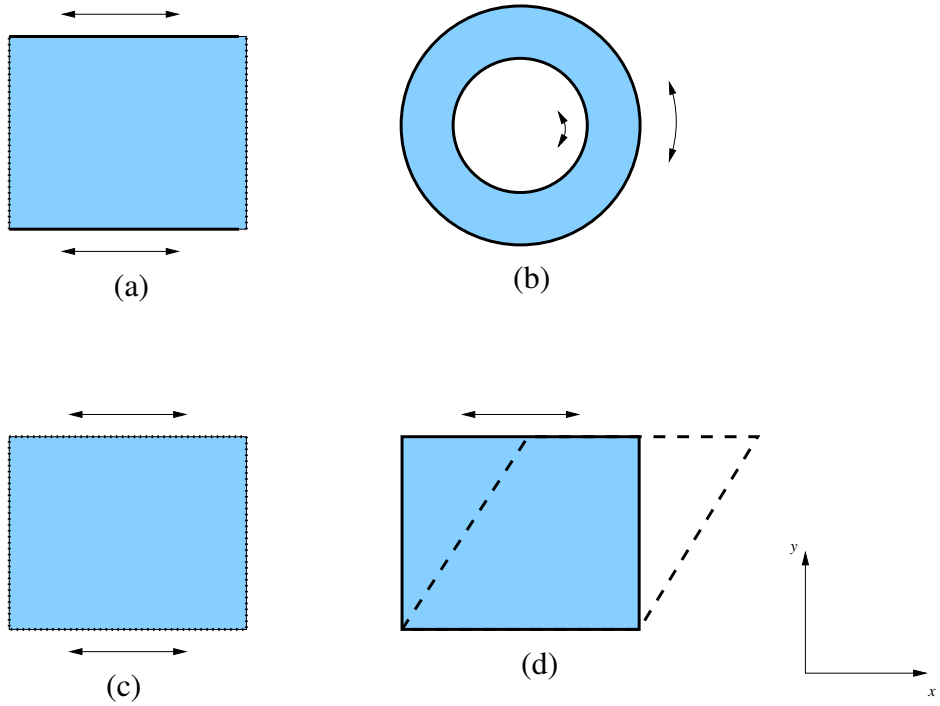

Figure 1.5: Two-dimensional foam studies use the following main geometries, solid lines represent solid boundaries and lightly dashed lines represent boundaries which may be periodic. (a) Linear Couette: The foam sample is placed between parallel walls and sheared by moving either or both walls. In theoretical or numerical work, periodic boundary conditions may be employed at the ends of the channel. (b) Cylindrical Couette: The foam sample is confined between concentric cylinders and sheared by moving either or both walls. (c) Fully periodic boundary conditions: The foam is fully periodic in both the x and y directions. The foam is sheared by changing the shape of the periodic box (figure 1.6). This method is possible with numerical or theoretical work only. (d) Pure shear: The foam is confined by two sets of parallel walls and sheared by moving three of the walls e.g. to a position shown by the bold dashed line.

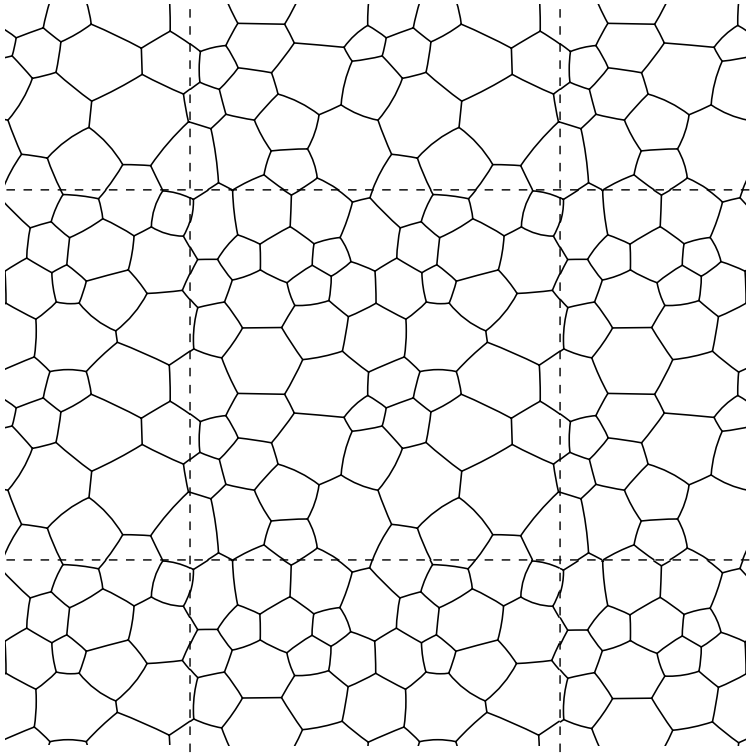

Figure 1.6: A representative element with periodic boundary conditions: Vertices or films crossing a periodic boundary (dashed) reappear at the opposite boundary. The same portion of foam is repeated endlessly, with the effect of creating a very large foam with relatively few bubbles, eliminating the need for a solid boundary which may affect the behaviour of the bubbles. The foam can be sheared by changing the periodic boundary conditions, creating a parallelogram, forcing the foam to respond to restore equilibrium.

they undergo plastic structural changes and at high rates of shear they flow like viscous liquids.

The elasticity arises from the increase in surface area in response to an applied strain [82]. The shear modulus scales with interfacial area per unit volume (perimeter per unit area in two dimensions) [83; 84] and in two dimensions has been shown to decrease with increasing area-disorder [77]. The shear modulus of both foams and emulsions decreases with increasing liquid fraction [17; 18; 21] and vanishes at the rigidity-loss transition ($\phi_l \approx 0.36$) [16].

As the applied strain is increased, foams dissipate energy through discrete plastic changes in topology (T1s), during which bubbles change neighbours. T1 transitions in three-dimensions are complex [84; 85] but there is only one kind in two dimensions, described in section 1.2.3. With further applied strain, T1s occur with greater frequency, in proportion to the applied strain [37; 86], the shear stress exceeds a critical *yield stress* and the foam flows like a non-Newtonian viscous liquid. Other mechanisms of energy dissipation include viscous dissipation as the films stretch [33; 35; 87] or relax after a topological change [88]. Energy is also dissipated as the liquid in the Plateau borders is sheared as the bubbles slide past each other [16; 89] or along a bounding glass plate in a quasi-two-dimensional experiment [24; 42; 71].

The yield stress, τ_y, of foams has been studied by many authors. It has been shown to decrease with increasing liquid fraction in experiment [17], in numerical work with two-dimensional ordered foams [30] and in simulations of disordered foams under extensional shear [21]. Like the shear modulus, the yield stress vanishes at the rigidity-loss transition where the foam loses any solid-like characteristics and is better described as a bubbly liquid.

After the foam yields, it flows as a fluid with effective viscosity orders of magnitude greater than that of the liquid phase [90; 91]. Experimental data of the velocity

profiles of two-dimensional foams has been fitted to the Herschel-Bulkley [92] constitutive relation (or a slight variation) for the stress, τ, by some authors [55; 64]. The Herschel-Bulkley model is given by

$$\begin{aligned} \dot{\gamma} &= 0 \qquad \text{for } \tau < \tau_y \\ \tau &= \tau_y + \xi_H \dot{\gamma}^{n_H} \quad \text{for } \tau > \tau_y \end{aligned} \tag{1.8}$$

where ξ_H and n_H are material parameters. Others observe a flow profile consistent with shear-thinning power law behaviour [56] and no yield stress:

$$\tau = \xi_P \dot{\gamma}^{n_P} \tag{1.9}$$

where ξ_P and n_P are material parameters. The absence of a yield stress in this case is surprising given that foams are yield stress fluids. Several authors have observed co-existing regions of flowing and static foam, where the flowing region is consistent with flow profiles of either a power law fluid [54] or flow profiles which decay exponentially with increasing distance from the moving wall [59].

Observations in three-dimensions in the parallel plate geometry have shown fluctuating velocity profiles [29] whilst others have found discontinuous flow profiles [93; 94] in the cylindrical Couette geometry. Each study is different and a comprehensive picture of the flowing nature of foams remains elusive, though recent advances in continuum theory and numerical simulations [24; 70; 71] can explain many experimental observations in terms of the external friction present in two-dimensional experiments.

Models of continuum foam rheology aim to incorporate all components of foam response [71; 95; 96] by averaging macroscopic quantities over regions of the foam sample. They have proved successful in capturing many aspects of foam response, including shear localization in the presence of external dissipation or a non-homogeneous

stress profile, but none have predicted coexisting flowing and static regions in the absence of either of these factors; nonetheless, localization *has* been observed in quasi-static bubble-scale simulations of foam rheology in linear Couette shear [40]. Recent developments with a continuum model [97] suggest that a non-monatonic relationship between stress and applied strain could account for the localization in these cases but the discrete nature of the bubbles play a role in the foam rheology and it is not always clear when the foam may be treated as a continuum fluid and when it must be regarded as a discrete system. For example, recent work by Goyon *et al.* [98] with concentrated emulsions demonstrated that below the jamming point (i.e. concentrations of the continuous phase above the rigidity-loss transition) flow curves relating local shear rate to local shear stress for emulsions in a wide gap Couette viscometer superimpose onto the same master curve for different applied torques. The same was observed in a narrow microchannel with different pressure drops. Furthermore, the flow curves are well described by the Herschel-Bulkley model (equation (1.8)). However, above the jamming point, whilst the Herschel-Bulkley model was able to reproduce the flow curves for the cylindrical Couette geometry, the flow curves from the narrow microchannel no longer fell onto a master curve and the Herschel-Bulkley model fails.

1.4 Summary

Foams are widely used commercially and industrially. Their simple local structure leads to complex flow behaviour which is not yet fully understood. Investigation of foam behaviour can be simplified by restricting the number of dimensions to two, whilst still obtaining meaningful information about foam behaviour.

At low stresses foams deform elastically. At stresses above the yield stress, foams flow through irreversible topological changes and in some instances regions of flowing

and static foam coexist. The focus of this thesis is to investigate, through numerical simulation, the effect of liquid fraction and area-disorder on the T1 topological changes and the resulting effect on the yielding and flow of a two-dimensional foam. Bubble-scale simulations are used since this will allow precise control over the liquid fraction and area-disorder and allow the location of the T1s to be recorded, which is not possible using continuum models.

The thesis will proceed as follows. Methods of foam simulation are reviewed in Chapter 2. The merits of each method are presented and my chosen method described in detail. The *yield stress* of a foam has been shown in different situations to depend on liquid fraction, I consider the effects of liquid fraction and area-disorder on the yield stress in linear Couette shear and probe the solid-liquid transition through oscillatory shear simulations in Chapter 3.

The yielding occurs as a macroscopic manifestation of many T1s. Initially T1s occur without any apparent spatial pattern, but it has been shown in experiments using a wide gap Couette viscometer [54; 59] and also in linear Couette shear in the presence of external friction [49; 64; 65], that after this initial transient, the T1s become localized in a band. The result is coexisting regions of flowing and static foam, often referred to as shear banding or shear localization. The occurrence of, and explanations for, shear banding form a controversial topic. Some argue that the shear banding arises as a result of introducing external friction through bounding glass plates [49; 71] whilst others have observed shear banding in the absence of external friction in simulation [40] or in the bulk of a three-dimensional foam [29]. I show in Chapter 4 that results that seem conflicting need not be contradictory, since there are other factors, namely area-disorder and liquid fraction, which influence shear localization in foams. I will also consider the flow of the bubbles in localized flows and identify structural features which characterize regions of flowing and static foam.

Finally in Chapter 5 I consider the local configuration of bubbles undergoing topological changes. A pair of orientations can be associated to each T1, relative to the direction of shear, which describes the local configuration of bubbles undergoing plastic rearrangement. It has been demonstrated that T1s have preferred orientations [46], suggesting specific local geometric configurations when bubbles undergo a T1. I consider the effect of liquid fraction and area-disorder on the orientation of T1 events and relate it to foam yielding and shear localization.

Parts of this thesis have been published [99; 100] and others are being prepared for publication [101; 102].

Chapter 2

Methods of foam simulation

2.1 Introduction

Simulations of foam rheology take many forms, with different methods appropriate in different situations. The significant choices to be made are based on an estimate of appropriate liquid fraction, rate of applied shear, accuracy in representing the foam structure, boundary conditions and computational time. A study of coarsening might require tens of thousands of bubbles to obtain adequate statistics, but the accuracy of the foam structure is less important and therefore it would be beneficial to choose a method which sacrifices structural accuracy for shorter computation time. On the other hand, in a rheological simulation, accurate control of liquid fraction and disorder may be required to study their role and therefore a smaller foam sample will be used and longer computation times tolerated. My chosen methods are based on a quasistatic assumption, in which the timescale at which the foam returns to equilibrium is shorter than all other timescales, and is implemented in the Surface Evolver software [103]. I begin by discussing the features of the most commonly used models for two-dimensional foam rheology, many of which have their three-dimensional counterparts, before highlighting the advantages of my chosen methods and describing them in detail.

2.2 Two-dimensional foam rheology simulation

A description of common simulation methods follows. The methods vary in terms of the approximations made and the amount of computational time required to run simulations. All methods described are poor approximations in comparison to the hydrodynamic simulations of Higdon [104] and Li *et al.* [105]. These methods involve solving the Stokes equation for the flow within each phase. In the work of Li *et al.* [105] the case of a fully periodic hexagonal foam is considered and the equations governing the flow are solved exactly subject to the assumption of a low Reynolds number. These calculations are time consuming and Higdon and co workers have developed algorithms with improved efficiency but even so using these methods would require too much computational time for the system sizes generally required for studies of foam rheology.

Simulations of foam rheology fall into two categories; those performed in the quasistatic limit and those which are not. As mentioned in the introduction, the underlying assumption of quasistatic foam simulation is that the timescale for the relaxation of the foam system is shorter than any others and therefore at any instant the foam can be considered to be in an equilibrium configuration. Foam simulation now becomes an optimization problem, where the minimum energy configuration of the system is sought. With the foam at equilibrium, it can be described precisely as circular arcs meeting threefold at point vertices at 120° angles. This aids simulation methods since it is a quick way of satisfying the Laplace-Young law introduced in Chapter 1, although not all quasistatic methods, e.g. the Q-Potts model, utilize this property. Rheological simulations are performed by imposing small perturbations on the foam system and then relaxing it to find a new equilibrium state; therefore the foam passes through a sequence of equilibrium configurations. The interpretation of the quasistatic assumption then is that the rate of relaxation of the foam system is much faster than any other mechanisms like shear or coarsening. It may also be useful to think of the foam as moving

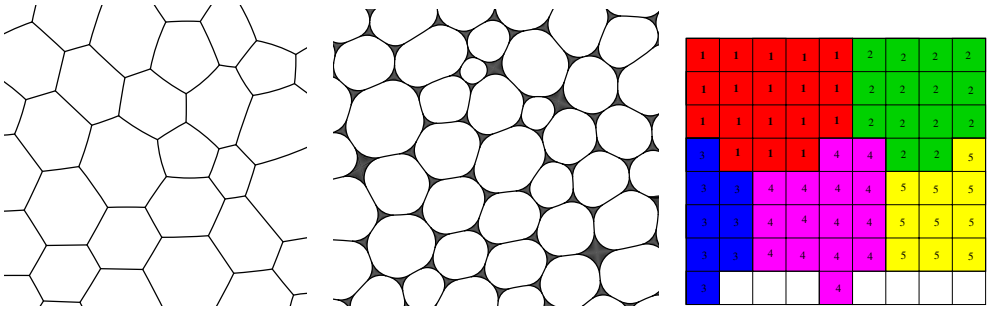

(a) (b) (c)

Figure 2.1: Quasistatic methods: (a) Typical output from the 2D-Froth method or Surface Evolver methods where the foam structure is accurately represented as circular arcs meeting threefold at vertices. (b) Typical output from PLAT or from Surface Evolver methods extended to include the Plateau borders. (c) The large Q-Potts model uses rectangular lattice sites to approximate the foam structure. Each group of sites with the same number represents a bubble.

infinitesimally slowly.

Non-quasistatic methods make sacrifices, usually in terms of structural resolution or computational time, to allow the inclusion of viscous dissipation. Such sacrifices are necessary since the structure of the foam no longer has a simple description when not at equilibrium. With dissipation included in the models, strain-rate dependent effects can be considered.

2.2.1 Quasistatic methods

2.2.1.1 2D-Froth

The 2D-Froth method of Kermode and Weaire [106] represents a foam system as circular arcs meeting threefold at vertices (figure 2.1 (a)). An equilibrium configuration of the foam satisfying Plateau's laws and the Laplace-Young law (see Chapter 1) is found by relaxing the foam in the *local* vicinity of each vertex in turn, until convergence is achieved. The method has been used with fully periodic boundary conditions to study coarsening [31], extensional shear [107] and simple shear [108]. A variation of the model was implemented by Herdtle and Aref [109] in the context of coarsening.

2.2.1.2 PLAT

PLAT is the extension of the 2D-Froth model by Weaire and co-workers to explicitly include the Plateau borders [20; 21; 36] and simulate wet two-dimensional foams (figure 2.1 (b)). There are two types of interfaces, which are represented as circular arcs, one separating adjacent bubbles and another separating bubbles and Plateau borders. A vertex now defines the point at which different types of interface meet. An equilibrium configuration is found in a similar way to that of the 2D-Froth method, with the pressure assumed to be the same throughout the liquid phase. The method has been used to study the rigidity-loss transition and properties of random wet foams through extensional shear of a fully periodic two-dimensional foam.

2.2.1.3 Large Q-Potts model

The large Q-Potts model uses a rectangular lattice divided into domains to describe a foam (figure 2.1 (c)). Each lattice site is assigned an integer value according to which bubble that site belongs to, and each group of lattice sites with the same number constitutes a bubble. The interfaces between lattice sites of differing values serve as the films between bubbles. The total energy of the foam is given by a Hamiltonian, which can be extended to enable shear of the foam [39]. The Monte Carlo simulation procedure using a modified Metropolis algorithm [110] proceeds by reassigning lattice sites if the change would result in a decrease in the energy of the system. Only lattice sites at an interface are tested and lattice sites are only reassigned to a neighbouring lattice site. The model has also been used by Raufaste *et al* [67] to simulate a Stokes experiment, in which foam flows around an obstacle, to study coarsening by Thomas *et al.* [80] and Glazier *et al* [111], and to study drainage by Jiang and Glazier [112]. Attempts have been made to extend the model beyond the quasistatic limit but results remain unconvincing [39].

2.2.1.4 Surface Evolver methods

The Surface Evolver [103] is free software for minimizing the energy of surfaces and is described in detail in section 2.4. It provides the necessary framework within which to perform quasistatic simulation of both dry and wet foams (figure 2.1 (a) and (b)), namely the capacity to accurately represent and subsequently view foam structures and a means to evolve toward an equilibrium configuration through the global minimization of surface energy. This differs from the approach of 2D-Froth and PLAT where foam structures are computed by local equilibration of the structure. Potential differences between the methods of equilibration may come to light by comparing the distribution of the number of sides of Plateau borders as a function of liquid fraction. The relative ease of use of the Surface Evolver has made it popular with many authors for studying foam and structure [26; 27; 74], rheology [40; 41; 43; 58; 77; 80; 83; 84; 99; 113; 114] and coarsening [78; 115] in both two and three dimensions.

2.2.2 Non-quasistatic methods

2.2.2.1 Vertex model

The Vertex model, first implemented by Fullman [116, referenced in 42] to study grain growth in metals, was adapted by Okuzono *et al.* [37; 38] to study foam rheology using periodic boundary conditions. Applicable in the dry limit ($\phi_l \to 0$), the foam is approximated by modelling films as straight lines meeting threefold at vertices (figure 2.2 (a)). The foam evolves by considering the motion of the vertices. The equations of motion for a vertex are derived from a force balance between the frictional force (e.g. from viscous dissipation) and the potential force arising from the surface free energy of the system. The Vertex model has also been used by Cantat & Delanney [117] to study the migration of a large bubble in plug flow.

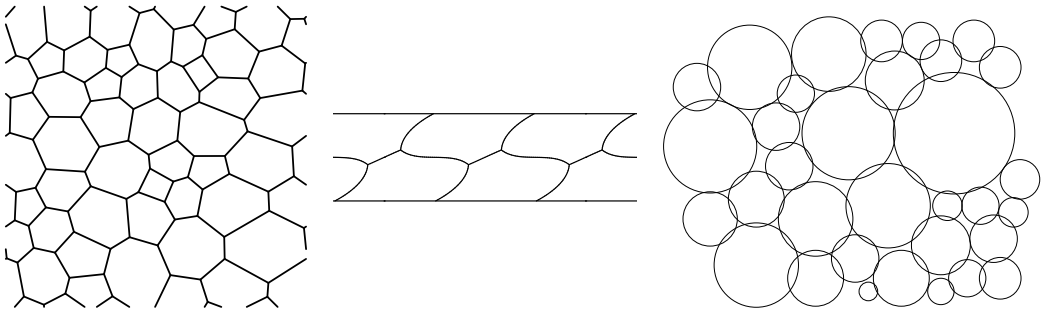

(a) (b) (c)

Figure 2.2: Non-quasistatic methods. (a) Vertex model. Films are approximated by straight lines meeting threefold at vertices. (b) A staircase structure sheared with the Viscous Froth model. Films are not circular arcs since the foam is not at equilibrium, but the model maintains an accurate description of the foam structure by discretizing films into short edges. (c) The Bubble model: Bubbles are approximated as circular discs which are allowed to overlap.

2.2.2.2 Viscous Froth model

The Viscous Froth model [42] incorporates viscous drag from bounding plates in two-dimensional simulations by augmenting the Laplace-Young relationship between curvature and bubble pressures with a drag coefficient, λ_d:

$$\Delta P - 2\gamma\kappa = \lambda_d v \tag{2.1}$$

where v is the normal velocity of the film. The model maintains an accurate description of the foam structure by discretizing each film into a number of straight edges. The model has been implemented in the Surface Evolver with fully periodic boundary conditions [43], for staircase foam structures [43; 118] (figure 2.2 (b)) and in the cylindrical Couette geometry [43].

2.2.2.3 Bubble model

Durian's approach with the bubble model [16; 22] differs from the others described, noting that in the wet limit bubbles do not deform and are circular. The foam struc-

ture is approximated by representing each bubble as a circular disc (figure 2.2 (c)). As the liquid fraction is decreased, discs are allowed to overlap, and repel via a one-sided spring-like force. As a result, the approximation of the foam structure becomes increasingly less realistic as the dry limit is approached. Nevertheless the bubble model still predicts the shear modulus to a high degree of accuracy. Viscous dissipation is included via a drag force on each disc from each neighbouring disc proportional to the velocity difference between them. Durian used the model to study linear Couette shear of two-dimensional foams [16; 22]. The model has been extended to three dimensions by Gardiner *et al.* [28; 119] to study shear and coarsening and recently Langlois *et al.* [24] have extended the two-dimensional model to include external viscous dissipation from bounding plates above and below the foam.

2.2.2.4 Lattice gas method

The lattice gas method has been implemented for foams by Sun & Hutzler [120; 121]. A fluid or gas *particle* is used to represent a collection of fluid or gas molecules and each particle moves between lattice sites on a hexagonal lattice. Predefined collision rules are applied when particles collide and each particle's velocity is updated. The entire range of liquid fraction is accessible up to the rigidity-loss transition. The method was used to investigate the coordination number of a foam [120], the average number of neighbours of a bubble, against liquid fraction and to study T1 rearrangements through simulation of a Stokes experiment [121].

2.3 Advantages and disadvantages of methods

I employ two methods of foam simulation implemented in the Surface Evolver [103] described in the next section. The first is for dry foams i.e. foams with liquid frac-

tion tending to zero, and the second for wet foams, where the liquid fraction can be varied in the range $0 < \phi_l < 0.16$. Each method is appropriate in different situations. The dry method is less demanding of computer power and memory and therefore many more bubbles can be simulated than with the wet method. The dry method is however limited to effective liquid fractions up to around 0.01 (this is discussed in Chapter 3) and is therefore not appropriate for considering the effects of varying liquid fraction. The main advantage of the quasistatic Surface Evolver methods used here over other methods described in the previous section is the precision with which the foam is represented. Other methods such as the Bubble model, Q-Potts model and Vertex model make approximations to the foam structure, whilst the method used here represents the foam structure exactly, and measured quantities such as shear stress and surface energy are therefore precise. The most obvious disadvantage is the inability to consider strain-rate dependent effects. In addition, these methods are relatively slow compared to those with poorer structural resolution. Whilst the dry foam model can realistically simulate several thousands of bubbles, the wet method is restricted to one or two hundred bubbles. Even the thousands possible for the dry method is small compared to the tens of thousands possible with the Q-Potts model. It is worth noting that the software PLAT is quicker than Surface Evolver methods, possibly because of the difference in the way an equilibrium foam configuration is found; or because it is purpose written software. The functionality and adaptability of the Surface Evolver makes it a more appropriate choice in this circumstance.

There is a certain level of ambiguity associated with quasistatic simulation. Only the final equilibrium configuration of the foam after a perturbation is of concern and not how it was attained. It is therefore possible to have more than one valid equilibrium configuration after a perturbation, depending on the minimization algorithm used. Whilst this is not ideal, it is unavoidable and I perform many simulations in order to

obtain an overall picture of foam response as opposed to relying heavily on the outcome of individual simulations. I note that similar obstacles arise in foam experiments where foam properties can be history dependant. Thus, performing a large number of simulations or experiments might lead to important averaging.

2.4 The Surface Evolver

The Surface Evolver [103] is freely available software[1] which is designed to minimize the energy of surfaces subject to user defined constraints. The program consists of a command window and a display window where the surface is displayed (figure 2.3). Surfaces are constructed using vertices, edges, facets and bodies. Vertices are points in space. Edges are lines or curves connecting vertices. Facets consist of a directed loop of edges and bodies are collections of facets. In three dimensions, curved surfaces are discretized by triangulation of the surface into three sided facets, which are allocated a surface tension of one unless otherwise specified.

In two dimensions, the Surface Evolver has a mode called *the STRING model* in which the surface tension resides in the edges and not the facets and it is this mode I use for my simulations. Films can be represented precisely as circular arcs (figure 2.1 (a)) and each body is defined to have one facet which represents each bubble.

The Surface Evolver changes the surface by moving the vertices in an attempt to minimize the energy function E. The energy function can take many forms but for the case of a two-dimensional soap froth we have

$$E = \sum_i \gamma_i l_i + \sum_j \left(A_{j0} - A_j \right) P_j \tag{2.2}$$

where the first sum is a sum over the edges, each of length l_i and surface tension γ_i, and

[1] The Surface Evolver can be downloaded at http://www.susqu.edu/brakke/evolver/evolver.html

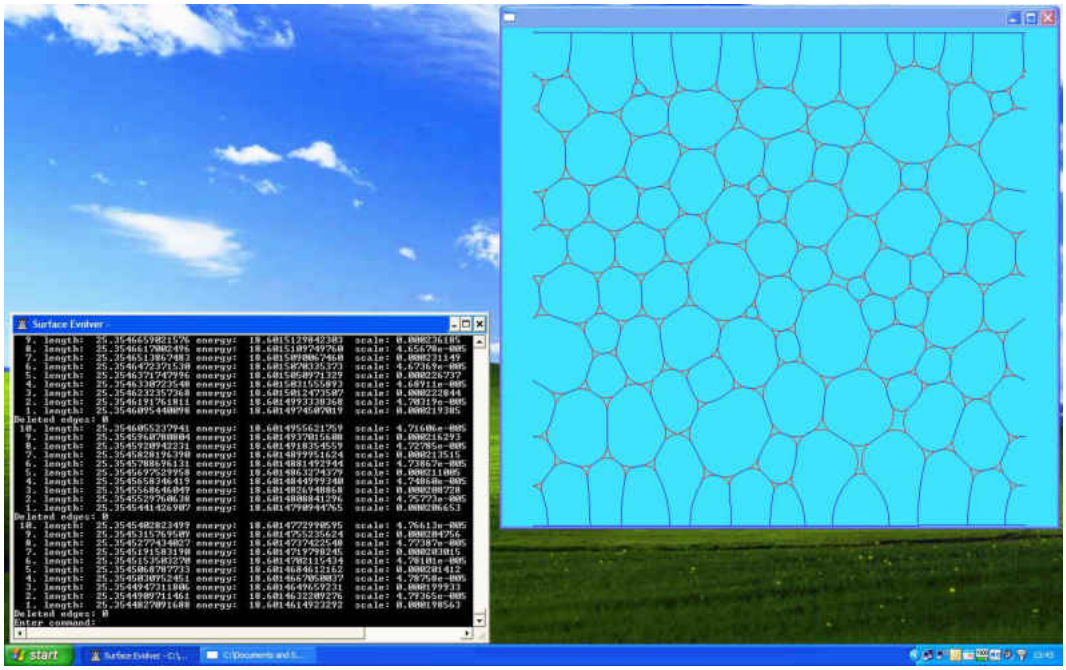

Figure 2.3: The Surface Evolver consists of a command window where instructions are given and a display window which shows the current state of the surface.

the second sum is a sum over all bodies (representing the bubbles), with A_j the current area of body j, A_{j0} the target area of body j and P_j is the pressure inside body j. The second sum is to ensure that the area of each body remains close to the specified target area. By minimizing the energy function, E, the pressure of each bubble is determined as a Lagrange multiplier, P_j [122].

The main iterative step of energy minimization in the Surface Evolver is a *gradient descent* method. The negative gradient of the energy is calculated from the forces on each vertex and the vertices are moved in the appropriate direction by a scale factor multiplied by the force at each vertex. The Surface Evolver has other methods for minimizing the energy. In addition to the gradient descent method I use the conjugate gradient method and Hessian minimization. The conjugate gradient method adds an orthogonal vector to the direction of steepest gradient before moving in a direction roughly perpendicular to that vector. This is far more efficient than the gradient descent method. A more direct way to find the minimum energy is to calculate the Hessian

matrix of the energy and solve for the motion that gives zero gradient [103]. However, care must be taken when using the Hessian, since it can be unpredictable if used too far from a local minimum.

After each gradient descent or Hessian iteration, the total surface area and energy of the surface is printed. If the surface tension is set to one throughout then these two quantities are numerically equal. After a gradient descent iteration, the scale factor is also printed. This can be set by the user or left in optimization mode.

A further important feature in the Surface Evolver is the ability to perform T1s, described in section 1.2.3, which are fundamental to the flow of foams. Short edges can be deleted to create fourfold vertices which can subsequently be *popped*: here the Surface Evolver replaces the fourfold vertex with two threefold vertices joined by an edge. Depending on the local configuration of edges, the new edge will either have the same adjoining facets as the old edge (a "failed" T1), or the edge will now be between two new facets and a T1 will have occurred.

Taking all of the above into account, the Surface Evolver provides the necessary framework within which to conduct simulations of two-dimensional foam rheology whilst retaining accurate structural information about the foam under consideration.

2.5 Dry foam preparation

Here I present the method used for simulating dry two-dimensional foams with liquid fractions in the limit of $\phi_l \to 0$, although a non-zero liquid fraction is achievable and it is possible to simulate foams with liquid fraction up to $\phi_l \approx 0.01$ (see below).

To create a dry foam in a channel of length L between parallel plates a distance W apart in the Surface Evolver I begin with a Voronoi tessellation of two-dimensional space which is periodic in the x and y directions (figure 2.4). The structure is imported

into the Surface Evolver and peripheral edges at the top and bottom are deleted to leave a structure which is periodic in the x direction only. Edges at the top and bottom are fixed to constraints to create walls at $y = 0$ and $y = W$ and then the structure is relaxed toward an equilibrium configuration by minimizing the free energy of the system, E, using the methods described in section 2.4, where each edge is given tension $\gamma_1 = 2$, representing two air-liquid interfaces each with tension 1. When an edge falls below a minimum *cut-off* length, l_c, it is deleted and the resulting fourfold vertex is *popped* resulting in a T1 topological change. The process of energy minimization and T1 initiation is repeated until the energy of the system has converged to 16 significant figures.

To obtain a specific distribution of bubble areas, a target area can be set for each bubble which acts as a constraint during the minimization procedure to ensure that each bubble area will evolve toward its desired area. When using disordered foams, I allocate the bubble areas according to a Weibull distribution with probability density function (PDF):

$$f(A;\beta,\lambda) = \frac{\beta}{\lambda}\left(\frac{A}{\lambda}\right)^{\beta-1} e^{-(A/\lambda)^{\beta}}. \tag{2.3}$$

$\lambda > 0$ is the scale parameter which depends on the average bubble size, $\lambda\Gamma(1 + 1/\lambda) = \langle A\rangle$ where Γ is the Gamma function, and $\beta > 0$ is the shape parameter which determines the area-disorder. The second moment of this distribution is [99]

$$\mu_2^A = \frac{\Gamma\left(1+\frac{2}{\beta}\right)}{\Gamma\left(1+\frac{1}{\beta}\right)^2} - 1. \tag{2.4}$$

The limit $\beta \to \infty$ corresponds to a monodisperse foam ($\mu_2^A = 0$) and decreasing β leads to foams with increasing area-disorder. In practice, monodisperse foams are created by setting each bubble area equal to the average bubble area, $\langle A\rangle$. For $\beta \leq 1$, bubbles with zero area are possible therefore I keep $\beta > 1$. Since the bubble samples to be studied are finite, the value of μ_2^A calculated from the sample may differ slightly to

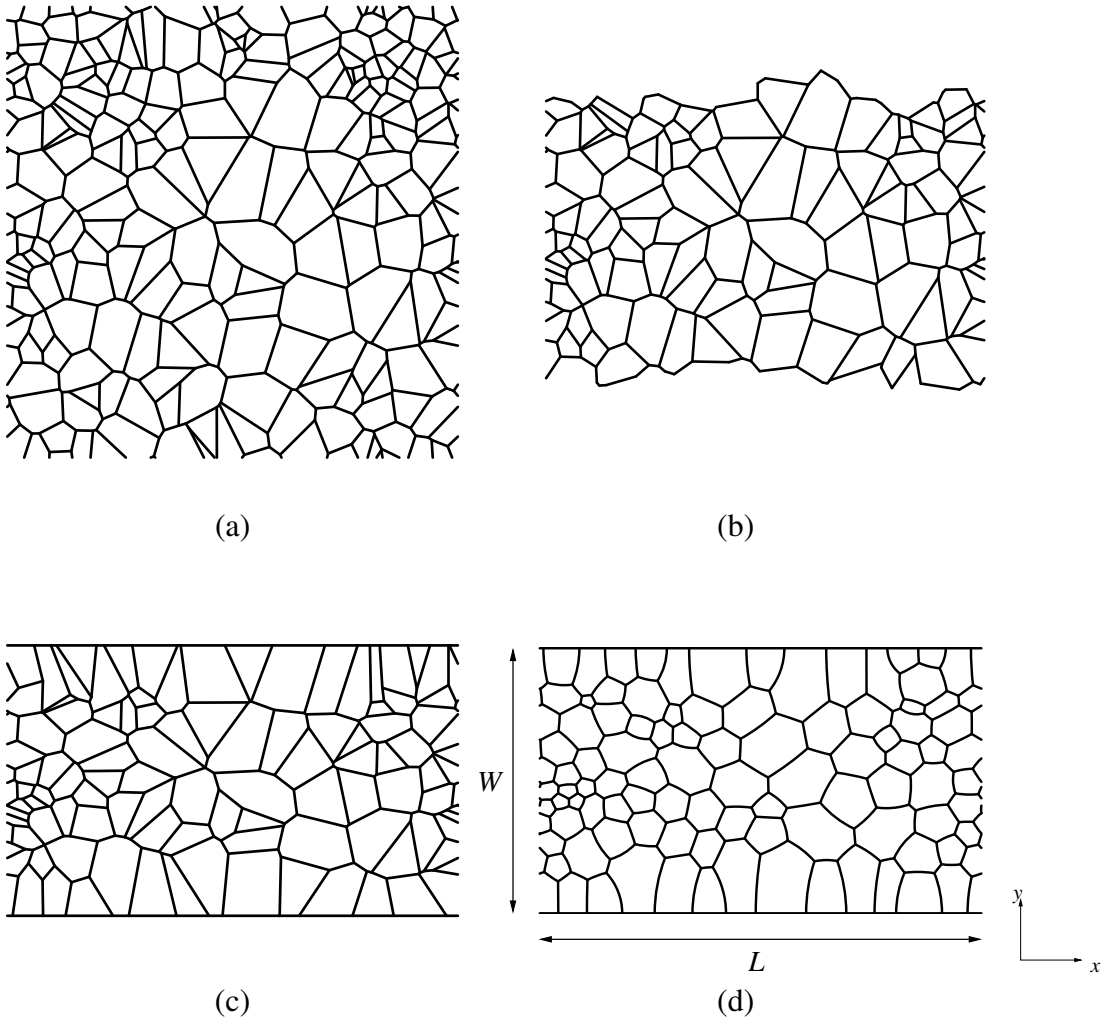

Figure 2.4: The procedure for creating dry foams between parallel plates in the Surface Evolver [99]: (a) A fully periodic tessellation of two-dimensional space created by Voronoi construction [123]. (b) Edges at the top and bottom are deleted to create a structure which is periodic in the x direction only. (c) The peripheral edges are set to constraints to form walls. (d) The straight line edges are converted to circular arcs and the structure is relaxed to give an equilibrium foam configuration from which a rheological simulation can begin.

the value expected from the assigned distribution. The effect of varying β can be seen in figures 2.5 and 2.6. As $\beta \to \infty$ the distribution becomes narrower and the peak moves toward the average bubble area. As β is decreased, the distribution becomes broader with a preference toward smaller bubbles.

Although this is a method for simulating dry foams, the cut-off length, l_c, is a measure of the effective liquid fraction. A T1 is initiated when two Plateau borders touch, i.e. the length of the film joining the Plateau borders, l_2, is zero (figure 2.7). l_c is therefore the value of l_1 when $l_2 = 0$. For dry foams, the Plateau borders are very small, and are therefore represented as point vertices, situated at their geometric centre. When $l_1 = l_c$, this is equivalent to Plateau borders touching and a T1 is initiated. Wetter foams have larger Plateau borders and therefore there is a smaller distance between the Plateau borders when a T1 is initiated. With Plateau borders omitted, this is represented by having a larger cut-off length. Cox *et al.* [124] derived the following relationship between cut-off length and liquid fraction based on a hexagonal foam:

$$\phi_l \approx 0.242 l_c^2 / \langle A \rangle . \tag{2.5}$$

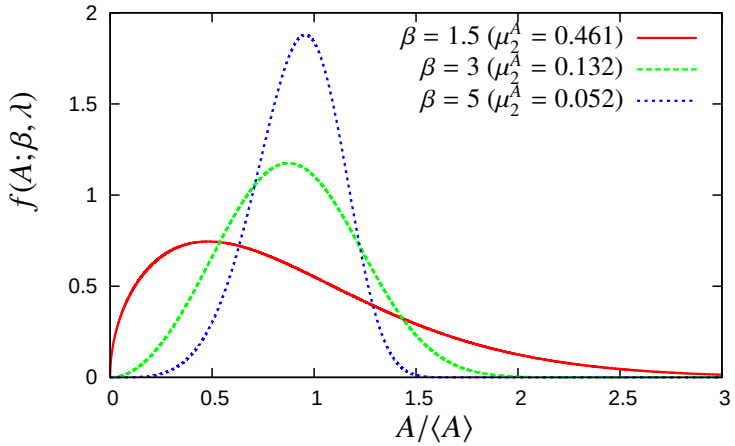

Figure 2.5: The Weibull PDF for different values of β. As β is decreased the distributions become broader and the area-disorder is increased.

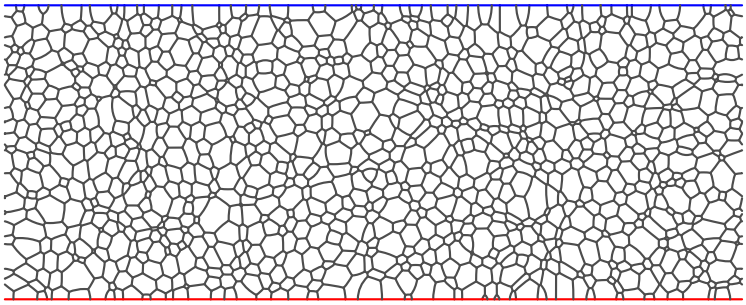

(a) $\beta = 1.5$

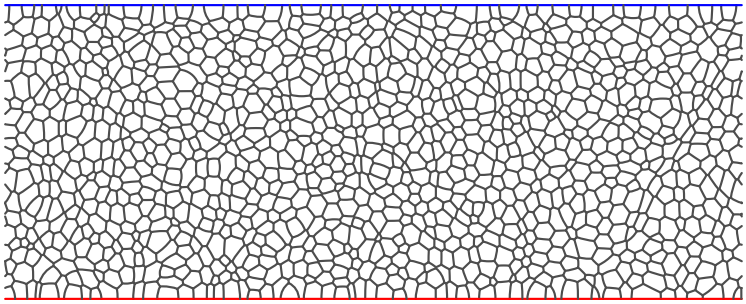

(b) $\beta = 3$

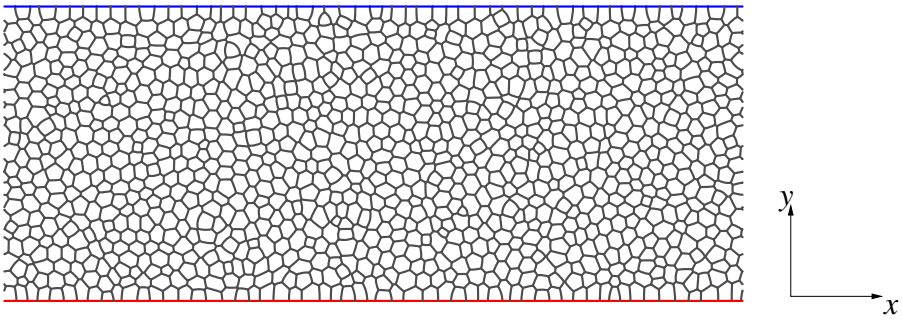

(c) $\beta = 5$

Figure 2.6: Dry foams of different area-disorder prepared in the Surface Evolver. The bubble areas are allocated via a Weibull distribution with parameter β which controls the area disorder.

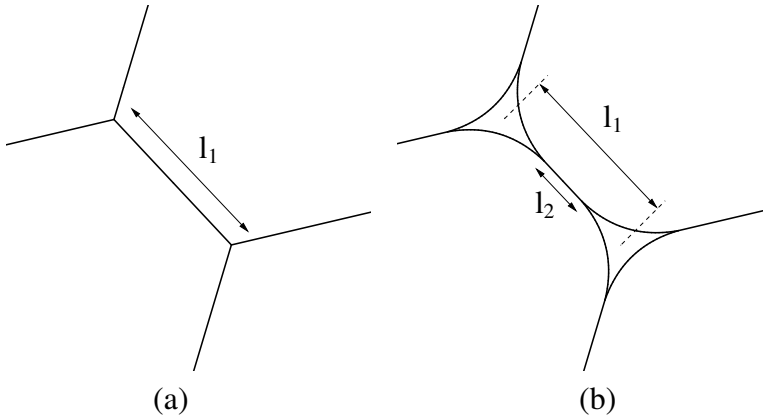

Figure 2.7: (a) For dry foams T1s are initiated when an edge falls below a cut-off length l_c. The cut-off length determines the effective liquid fraction. In real foams, T1s begin when two Plateau borders touch (i.e. the distance between the Plateau borders, l_2, is zero), illustrated in (b).

My simulations of wet foams, described below, place an upper limit on the validity of this method (see Chapter 3) but at low liquid fraction quantitative measurements can be obtained.

2.6 Wet foam preparation

To simulate foams with higher liquid fraction, the liquid in the Plateau borders must be included explicitly. With the following method it is theoretically possible to study foams with liquid fraction in the range $0 < \phi_l < 0.16$, but my simulations will be restricted to the range $0 < \phi_l < 0.1$ since the computation time gets very long even with relatively few bubbles. To create a wet foam, I begin with an equilibrium dry foam structure, created as in section 2.5, and "decorate" it with Plateau borders (using code adapted from that supplied with the Surface Evolver source code). That is, each threefold vertex is replaced by a three sided Plateau border. The exception is the vertices at the walls: I changed the Surface Evolver code so that these are not decorated, in order to simplify the numerical algorithm. The wall vertices will be fixed in the same manner as for the dry foam simulations so that they are not in a position to undergo T1s; decorating them

with Plateau borders would introduce unnecessary complexity. I presume that omission of the Plateau borders at the wall will not affect the outcome of the simulation.

There are now two different types of interfaces: Air-liquid-air interfaces between neighbouring bubbles and air-liquid interfaces between bubbles and Plateau borders (figure 2.8). Air-liquid-air interfaces have tension γ_1 as for dry foams whilst air-liquid interfaces are given tension γ_2, and the contact angle between the two different types of interface is given by

$$\alpha = \cos^{-1}\left(\frac{\gamma_1}{2\gamma_2}\right). \tag{2.6}$$

For foams, I expect $\gamma_1 = 2\gamma_2$ leading to a contact angle α of 0°, i.e. a smooth transition, between the two types of interface, but non-zero contact angles can arise in emulsions [125; 126]. Setting $\alpha = 0$ in my simulations is difficult in practice since the contact angle may become negative and the Plateau border films may overlap. This configuration, whilst unphysical, is energetically favourable and simulations cannot recover. Therefore I keep the contact angle small, $1.15 < \alpha < 11.36$, and consider the effect of changing the contact angle (see sections 3.3.2.1 and 5.2).

Initially the foam is decorated with small three-sided Plateau borders. Each Plateau border is represented as a facet in the Surface Evolver and the facets are defined collectively as one body with a target area which can be specified to set the liquid fraction. The target areas of the bubbles are also reduced slightly to ensure that the total area of liquid and air remains fixed. The distribution of bubble areas is therefore inherited from the parent dry foam, and the level of disorder remains similar. If the required bubble areas are to be different from those resulting from the Voronoi procedure, it is more efficient to do so before introducing the Plateau borders.

The equilibrium configuration is found by minimizing the energy function in the same manner as for dry foams. Examples of equilibrium wet foams of different liquid fraction are shown in figure 2.9. The process for performing T1s is more difficult than

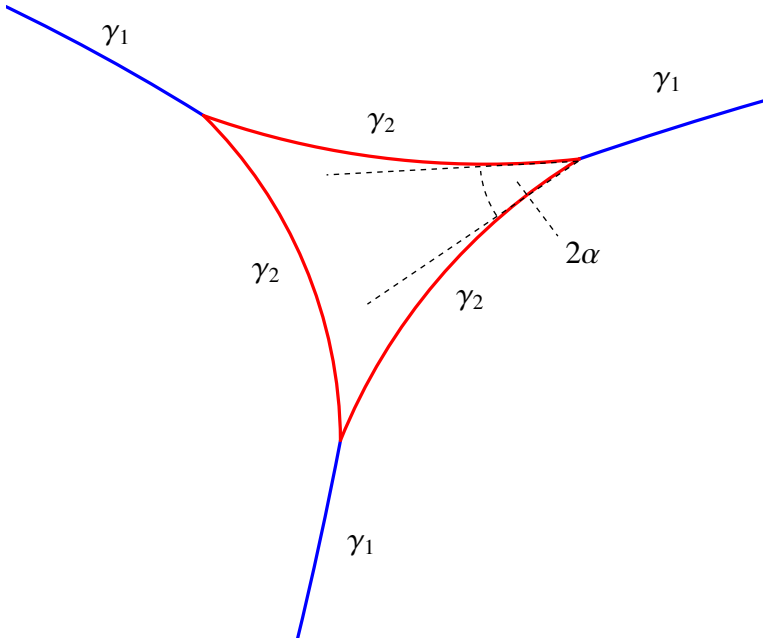

Figure 2.8: To create wet foams, point vertices in dry foams are replaced by three sided Plateau borders. There is a contact angle, α, between air-liquid-air interfaces separating two bubbles and air-liquid interfaces between the bubbles and the Plateau borders, determined by their interfacial tensions, γ_1, γ_2.

for dry foams. When two Plateau borders touch, they merge to form a fourfold Plateau border. This is done by removing the edge between the two threefold Plateau borders (creating a fourfold vertex) and using the Surface Evolver's POP_DISJOIN feature to replace the fourfold vertex with two twofold vertices which are *not* connected by an edge. For each of the new twofold vertices, one of the adjoining edges is deleted to leave a fourfold Plateau border with four edges.

Depending on the liquid fraction, this fourfold Plateau border is not necessarily unstable (figure 2.10). It will persist until two of the Plateau border interfaces meet, forming a new air-liquid-air interface between two threefold Plateau borders. This is done by periodically testing each fourfold Plateau border for overlapping edges. Each edge is a circular arc. If the distance between the centres of the two longest arcs is less

than the sum of their radii then the arcs are split in two to form two twofold vertices. The twofold vertices are merged to form two threefold Plateau borders sharing the new merged vertex. This vertex is popped in the usual manner to insert a new edge between the threefold Plateau borders.

Fourfold Plateau borders have been observed in two-dimensional simulations at $\phi_l \approx 0.02$ [21], but are rare in unstrained foams with liquid fraction less than 0.04. Plateau borders with five or more sides are also possible at liquid fractions greater than approximately 0.06. I adapted this existing code [103] to deal with Plateau borders with any number of sides by modifying it to compare each pair of Plateau border edges for any overlap. Previously the code would have failed since Plateau borders with more than four sides would not always be able to dissociate into two smaller Plateau borders.

2.7 Simulating shear

To simulate the linear Couette shear of either a dry or a wet foam between parallel walls described above, I begin by fixing the vertices at the walls, in their equilibrium positions, to create a no-slip boundary condition at the walls. This means that the vertices will not be moved during the energy minimization process. This is a realistic boundary condition since in many experiments sandpaper or small teeth are placed at the walls to ensure that the first layer of bubbles does not slip.

I then apply a strain increment by moving all vertices affinely according to their y-position (see figure 2.11 (a)) i.e. a distance

$$\delta x = \frac{y}{W}\delta x_{\text{wall}} \tag{2.7}$$

where δx_{wall} represents the distance the top plate has moved and W is the channel width. Note that the vertices at the bottom plate ($y = 0$) do not move. The resulting increment

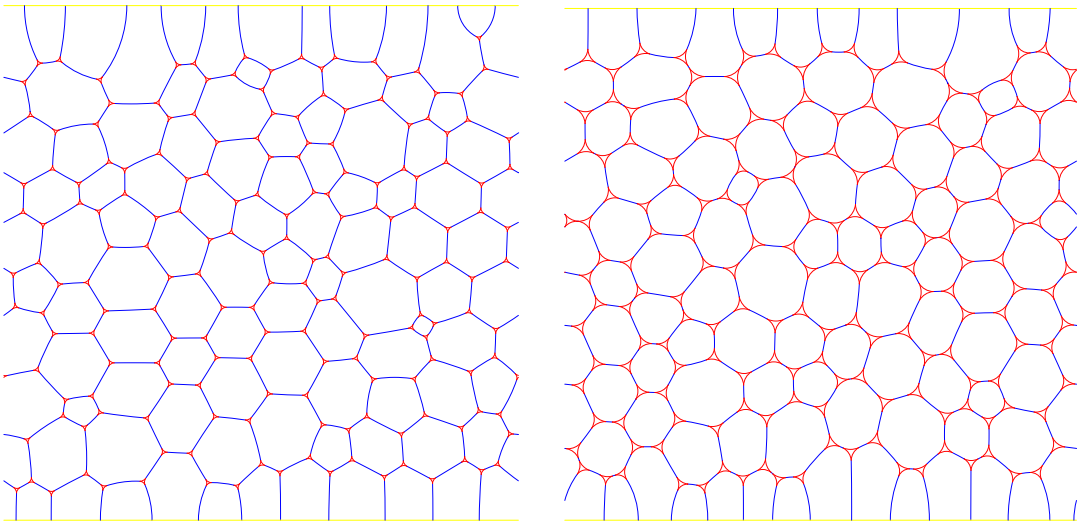

$\phi_l = 0.005$ $\phi_l = 0.03$

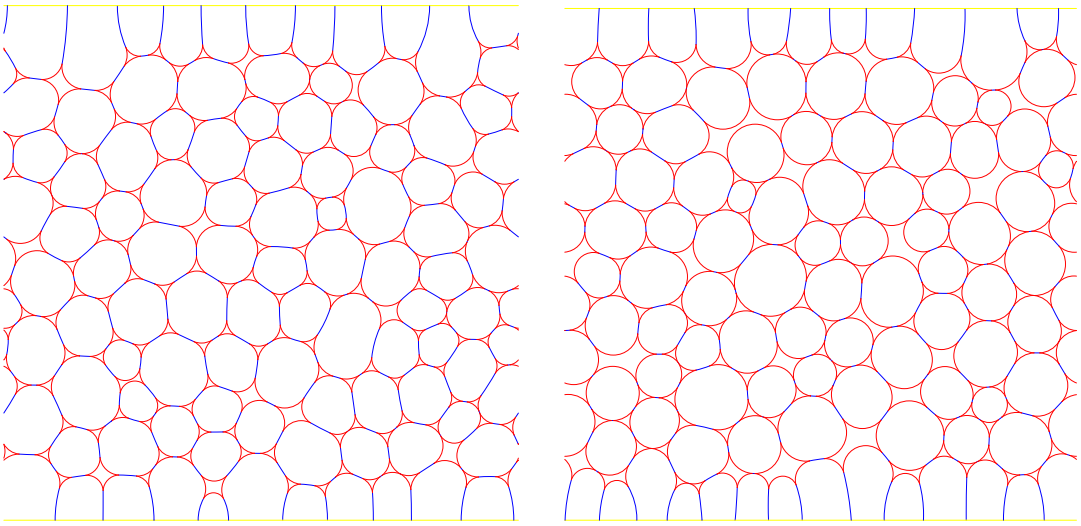

$\phi_l = 0.05$ $\phi_l = 0.09$

Figure 2.9: Examples of equilibrium wet foams between parallel walls for different values of liquid fraction, ϕ_l.

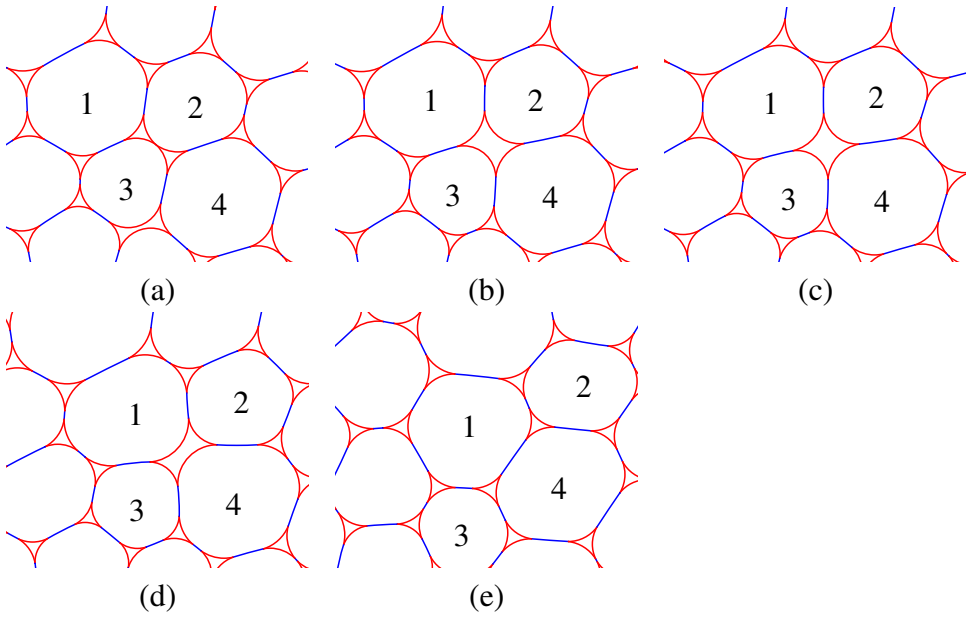

Figure 2.10: The T1 process for a wet foam. (a) The T1 begins when two threefold Plateau borders touch. (b) The Plateau borders merge to form a fourfold Plateau border. (c) The fourfold Plateau border is not necessarily unstable and can persist. (d)-(e) Two Plateau border films become closer together; when they touch the fourfold Plateau border dissociates back into two threefold Plateau borders.

in total strain is

$$\delta\epsilon = \delta x_{\text{wall}}/W \tag{2.8}$$

I then iterate to an equilibrium configuration of the foam, initiating any T1s when an edge length falls below the minimum cut-off length, as described in sections 2.5 and 2.6.

The alternative to shearing the foam affinely is to move only the vertices at the top plate an amount δx_{wall} (see figure 2.11 (b)). The displacement of each vertex is given by the following equations for boundary shear:

$$\delta x = \begin{cases} \delta x_{\text{wall}} & (y = W) \\ 0 & (y \neq W) \end{cases} \tag{2.9}$$

which results in the same increment in total strain as for applying affine shear. In the quasistatic limit ($\delta x_{\text{wall}} \to 0$), both functions are equivalent and therefore as long as I

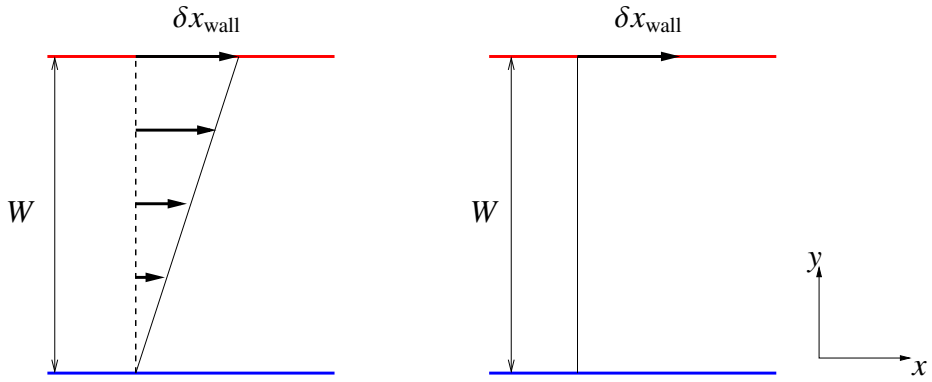

(a) Affine shear (b) Boundary shear

Figure 2.11: Two methods for shearing the foam. (a) All vertices are moved an amount proportional to their y-position. (b) Only the vertices at the boundary are moved. In the quasistatic limit, both methods are more-or-less equivalent, but the energy of the structure will converge in less time after shearing the foam affinely.

ensure that δx_{wall} is small enough that I make a good approximation to the quasistatic limit, either method may be used. The advantage of shearing the foam affinely is that the energy converges more quickly (figure 2.14(b)).

Throughout, I perform a selection of simulations using the boundary shear method to verify that the same range of behaviours is observed as for shearing the foam affinely. Note that the result will never be identical to that of shearing the foam affinely due to inherent ambiguity associated with quasistatic simulation discussed in section 2.2.1, i.e. the sequence in which T1s occur will different in each case, but I expect the overall range of behaviours to be the same and measured quantities like the yield stress to be the same to within reasonable error. Figure 2.12 (a) and (b) show two foam structures at a strain of $\epsilon = 3$ which have been sheared with affine and boundary shear, starting from the same initial configuration. The final configurations are different and the shear stress *versus* applied strain is shown in figure 2.12 (c) for each method. In this case, the average shear stress after the transient using the two methods differ by only 1.5% and the maximum shear stresses differ by less than 1%.

The choice of δx_{wall} is therefore very important since I must ensure that the sim-

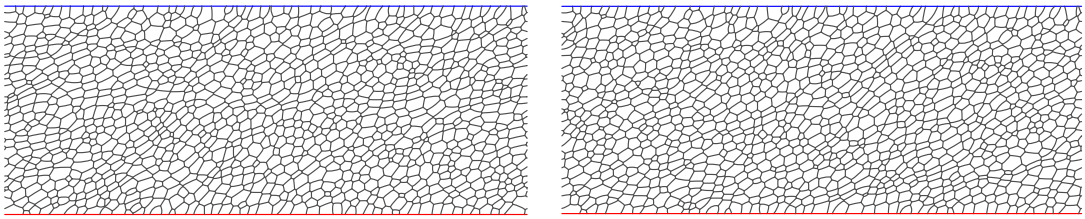

(a) Affine (b) Boundary

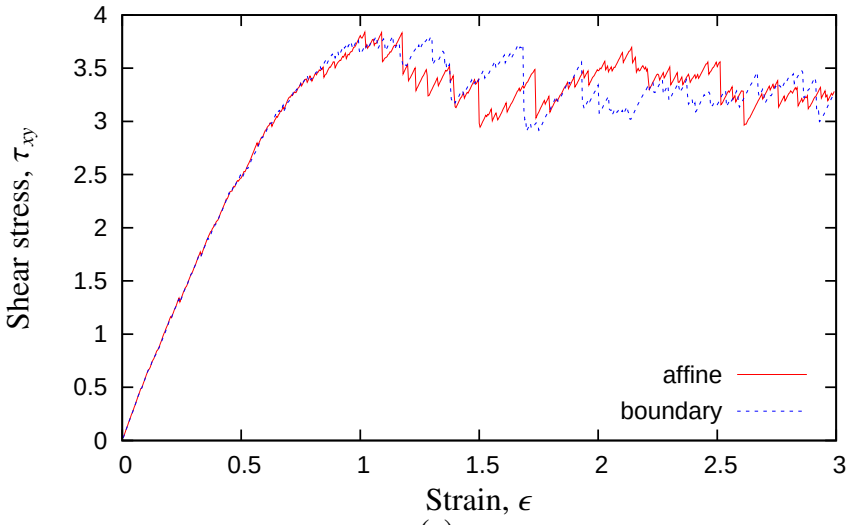

(c)

Figure 2.12: (a) and (b) show foam structures at a strain of $\epsilon = 3$ sheared with affine shear and boundary shear respectively. Both foams started from the same initial configuration, but the final configurations are different. (c) The stress strain relationship during the shear of the foam in (a) and (b). Whilst the relationship is different since the order of T1s is different, the maximum stress and average stress after the transient differ by only a small amount.

ulations are performed in the quasistatic limit. The result of a simulation must not be significantly different if δx_{wall} is made smaller. In figure 2.13 (a) the shear stress, τ_{xy}, is plotted against strain for different values of δx_{wall} for a simulation of a dry two-dimensional foam, sheared between parallel walls. The shear stress will be defined later on, but I use it here to illustrate the effect of varying δx_{wall}. For decreasing values of δx_{wall}, the average shear stress at strains above 2 does not vary by more than approximately 5% (figure 2.13 (b)).

The average area of the bubbles in the simulations whose stress strain relationships are given in figure 2.13 (a) is $\langle A \rangle = 0.0229$, and bubbles have typical size $\sqrt{\langle A \rangle} = 0.151$. The largest value of δx_{wall} is of the same order of magnitude as a typical bubble width and is not therefore suitable. For the smaller values of δx_{wall}, the choice would depend on other considerations affecting simulation time, such as the number of bubbles and type of shear.

The dependence of simulation time on the number of bubbles, N_B, is slightly greater than $O(N_B)$ (figure 2.14). Strain increments which induce plastic rearrangements take longer to converge than those which do not (figure 2.14 (a)). Affine shear is more efficient than boundary shear (figure 2.14 (b)). Strain increments which do not induce plastic rearrangements take approximately the same amount of time to converge regardless of the magnitude of the strain increment, therefore smaller strain increments would take longer to reach a given strain (figure 2.14 (c)).

In each study, a balance must be found between the magnitude of δx_{wall}, the number of bubbles and the simulation time. Throughout this work, δx_{wall} is chosen carefully. I keep $\delta\epsilon < 0.01$ and $\delta x_{\text{wall}} / \sqrt{\langle A \rangle} < 0.17$ throughout.

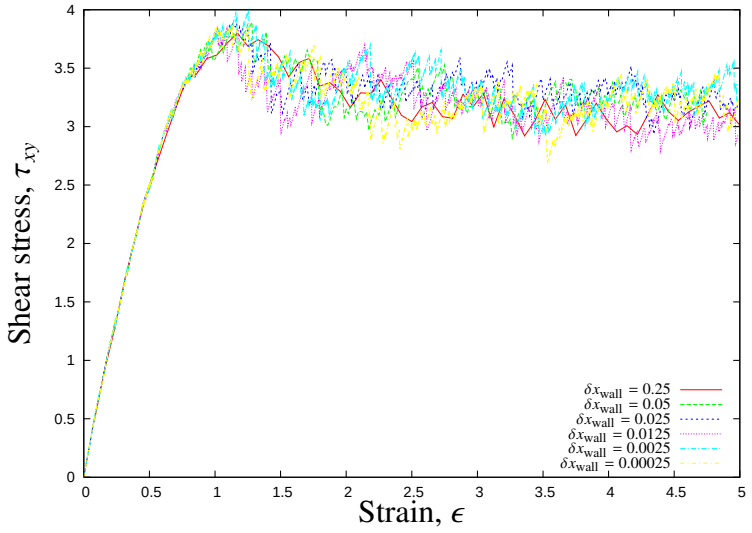

(a)

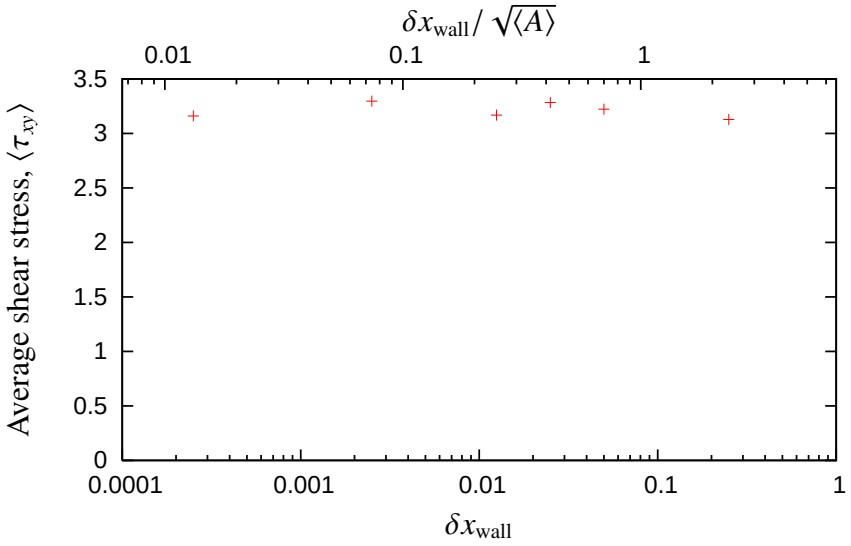

(b)

Figure 2.13: (a) Shear stress versus strain for the same initial foam configuration sheared with different values of strain increment $\delta\epsilon = \delta x_{\text{wall}}/W$. (b) The average shear stress, $\langle \tau_{xy} \rangle$, for strains greater than two *versus* δx_{wall}. The variation in the average shear stress after the transient between simulations of different δx_{wall} is about 5%.

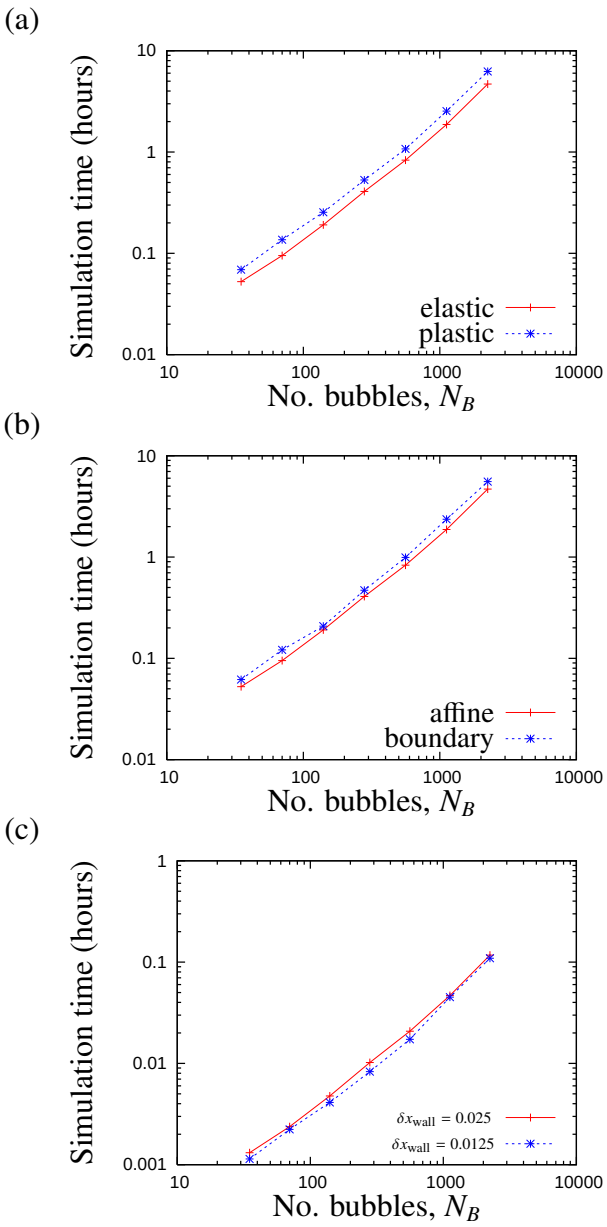

Figure 2.14: Factors affecting simulation time (processor speed 3.2Ghz). (a) The time taken to impose a strain of one during the elastic and plastic regimes. Simulation times are shorter in the elastic regime than the plastic regime since there is less structural relaxation after T1s. (b) The time taken to impose a strain of one for affine shear and boundary shear for the same value of δx_{wall}. Shearing the foam affinely is quicker than applying boundary shear. (c) The average simulation time per strain increment for different values of δx_{wall} during a total imposed strain of one. Halving the strain increment roughly doubles the simulation time because two steps are required to reach the same strain.

2.8 Summary

There are many different approaches to foam simulation in the literature and the choice of method should be appropriate to the goal of each study. Investigation of the effect of liquid fraction and area-disorder on the flow of a foam requires precise control over these parameters therefore I choose quasistatic methods, implemented in the Surface Evolver, in which the foam structure can be represented to a high degree of accuracy.

In the next chapter I consider the transition of a two-dimensional foam between solid-like and liquid-like behaviour, looking in particular at the dependence of the yield stress on liquid fraction and area-disorder.

Chapter 3

Yielding

3.1 Introduction

Foams, like gels, pastes and emulsions, are yield stress fluids. At stresses below the *yield stress*, foams behave as elastic solids, and above it they flow like visco-elastic liquids. The transition from solid-like to liquid-like behaviour is called *yielding*, and is often probed through oscillatory shear experiments [17; 18; 127–129]. In this chapter I study the transition from solid-like to liquid-like behaviour through oscillatory shear simulations and consider factors affecting the yield stress through linear Couette shear simulations.

The stress in a two-dimensional foam is a tensor given by integrating the tension forces along each edge [77]:

$$\boldsymbol{\tau} = \begin{pmatrix} \tau_{xx} & \tau_{xy} \\ \tau_{yx} & \tau_{yy} \end{pmatrix} = \frac{2}{A_{\mathrm{TOT}}} \gamma \int_{\mathrm{edges}} \mathbf{t} \otimes \mathbf{t} \, \mathrm{d}l \tag{3.1}$$

where A_{TOT} denotes the total area of the foam, $\mathbf{t}$ the tangent to the edge and γ the tension of an air-water interface. Air-liquid-air films which comprise two interfaces are counted

twice. The component of stress acting parallel to the plane of shear is the off-diagonal component of the stress, known as the shear stress, τ_{xy} or τ_{yx}. Whilst the concept of a yield stress is simple, defining it is not. There are several different definitions in the literature:

1. The shear stress, τ_y^p, at which the first plastic deformations (T1s) occur and therefore the deformation is no longer completely reversible (i.e. the elastic limit).

2. The maximum shear stress the foam achieves under applied strain during the transient, sometimes referred to as the static yield stress, τ_y^s. This reflects the initial stress needed to be overcome for the foam to start flowing.

3. The average shear stress the foam achieves under applied strain after the transient regime, sometimes referred to as the dynamic yield stress, τ_y^d. This can be lower than the static yield stress and reflects the applied stress below which the foam does not flow.

4. The average shear stress the foam achieves under applied strain after the transient regime, in the limit that the ratio of viscous to surface tension forces (capillary number) tends to zero. This definition reduces to τ_y^d in the quasistatic limit.

5. In oscillatory shear experiments, when the stress amplitude is plotted against the strain amplitude the intersection of power law fits to the data at low and high strain amplitude defines a yield stress and strain.

The first three definitions are illustrated in figure 3.1 which shows a typical stress *versus* strain relationship for a dry foam undergoing linear Couette shear. During the transient, of order one, the stress increases with increasing applied strain and goes through a maximum. Thereafter the stress fluctuates about an average value. The first of the yield stress definitions is not appropriate for dry foams since trapped stresses can lead to

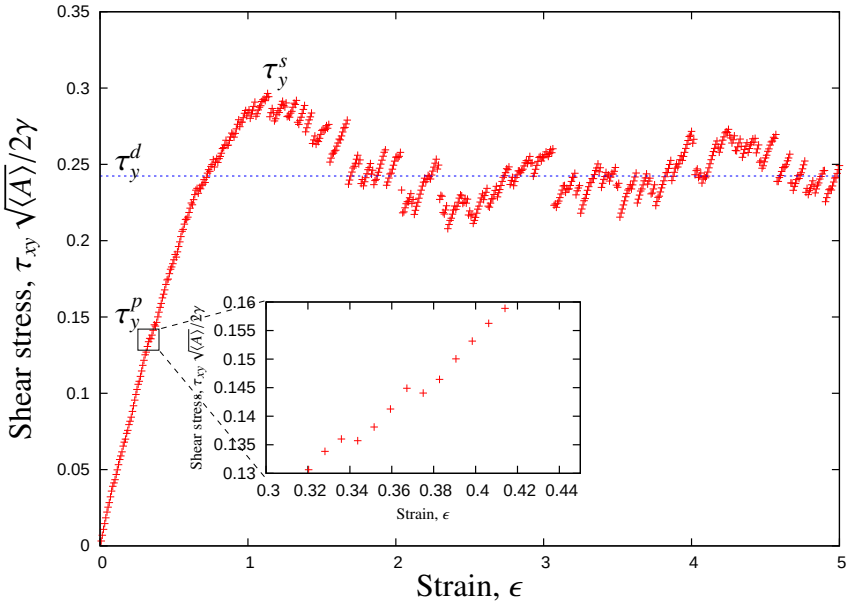

Figure 3.1: A typical stress-strain curve for a dry foam. The shear stress has been normalized by $2\gamma/\sqrt{\langle A\rangle}$. Possible definitions of the *yield stress* are indicated. τ_y^s: static yield stress. The maximum stress under applied strain. τ_y^d : dynamic yield stress. The average stress for strains greater than the transient. τ_y^p: the stress at which irreversible plastic events first occur, magnified in the insert.

short edges in a foam which could trigger a T1 at very small strains [29]. The fourth reduces to the first in the quasistatic limit and the fifth is useful only in oscillatory shear experiments, described in section 3.2. Whilst I shall perform some oscillatory shear simulations, the number of shear cycles required to extract a yield stress drastically increases computation time. Therefore it is not appropriate for determining the yield stress over a range of liquid fraction and/or area-disorder given the size of the foam and the number of simulations that would be required. There are even more ways of defining the yield stress in an engineering fashion, e.g. the point at which the linear relationship between stress and strain fails (ignoring small deviations due to T1s) but I do not consider them further. I will consider mainly the static and dynamic yield stress (i.e. the second and third definitions listed above) of foams in this chapter.

It is also possible to define a yield strain, ϵ_y, which is the strain at which the foam yields, but this also has a list of possible definitions. In the elastic regime, the shear

stress is proportional to the strain via a shear modulus G:

$$\tau_{xy} = G\epsilon. \tag{3.2}$$

Assuming that this relationship holds at the onset of yielding, one possible definition of the yield strain is in terms of the yield stress,

$$\epsilon_y = \tau_y/G, \tag{3.3}$$

but will differ according to which definition of yield stress is used. The opposite approach may also be taken, where the yield strain is measured and the yield stress calculated accordingly. To avoid over-complication, I will consider mainly the yield stress.

To facilitate comparison with other results in the literature I will use a non-dimensional stress $\tilde{\boldsymbol{\tau}}$ throughout:

$$\tilde{\boldsymbol{\tau}} = \frac{\sqrt{\langle A \rangle}}{2\gamma}\boldsymbol{\tau}, \tag{3.4}$$

and use the notation $\tilde{\tau}_y^s$ and $\tilde{\tau}_y^d$ for the non-dimensional static and dynamic yield stresses respectively.

The solid-liquid transition in foams and emulsions has been studied by many authors [17; 18; 127–129]. Oscillatory shear experiments are often performed, from which a storage modulus, G', and loss modulus, G'', can be found, which are measures of a material's elastic and dissipative properties respectively. The normalized storage and loss moduli of yield stress materials including foams, emulsions, pastes and gels have been found to fall on the same master curve when plotted as a function of strain amplitude, prompting suggestion of similar underlying mechanisms [81], e.g. elastic loading followed by an unloading through discrete rearrangements of the constituents. Elasto-visco-plastic models [95; 130; 131] accurately predict the storage and loss moduli but

an elasto-plastic model [128], neglecting viscous effects is a good approximation to the data for materials that are weakly dissipative. Higher harmonics of the stress were found experimentally by Rouyer *et al.* [128], and the ability to accurately predict these higher harmonics will be a good test of any constitutive relation for the stress, as well as for bubble scale numerical simulations.

The yield stress (or yield strain) plays an important role in the transition from predominantly solid-like to liquid-like behaviour. There have been several experimental studies of foam yielding in three dimensions. The static yield stress was found to decrease with increasing liquid fraction for foams and emulsions [17; 91; 127; 132–134], but the variance in the reported relationship between the yield stress and the liquid fraction suggests that further factors (e.g. wall slip) are involved in each study.

Princen [30] found that the static yield stress of a two-dimensional ordered hexagonal foam decreases with liquid fraction, whilst Hutzler *et al.* [21], through numerical simulations of disordered two-dimensional foams under extensional shear, showed that the dynamic yield stress of disordered two-dimensional foams also decreases with increasing liquid fraction.

Numerical simulations by Gardiner *et al.* [28] using the bubble model suggest that the static yield stress is reduced with increasing volumetric disorder whilst the dynamic yield stress remains the same, but only two bubble volume distributions were studied. Experimental observations by Khan *et al.* [91] found greater discrepancy between the static and dynamic yield stresses at low liquid fraction than at high liquid fraction but, even so, the difference between the static and dynamic yield stress was small. In oscillatory experiments with emulsions, Mason *et al.* [127] observe strong disagreement between the static and dynamic yield stress. In this case shear localization was observed, where different regions of the foam flows at different rates of shear; this will be studied further in Chapter 4.

The yield strain of a three-dimensional foam was found to increase with increasing shear rate [29] in experiment. Kraynik and Hansen [35] found that the dynamic yield stress of an ordered hexagonal two-dimensional foam increases with increasing shear rate, prompting them to define the yield stress as the average stress in the limit as capillary number, the ratio of surface tension to viscous forces, tends to zero (yield stress definition 4).

3.2 Solid-liquid transition

The solid-liquid transition in foams can be investigated by applying an oscillating strain to the foam sample and measuring the stress response. A sinusoidal strain signal of amplitude ϵ_0 is applied to the foam:

$$\epsilon(t) = \epsilon_0 \cos(2\pi t/T), \tag{3.5}$$

where T is the period of oscillation and t is the time. The shear stress response, $\tau_{xy}(t)$, is measured, and decomposed into a Fourier series:

$$\begin{aligned} \tau_{xy}(t) &= \sum_{n=1}^{\infty} [a_n \cos(2\pi nt/T) + b_n \sin(2\pi nt/T)] && (3.6) \\ &= a_1 \cos(2\pi t/T) + b_1 \sin(2\pi t/T) + \mathcal{H}\left(\tau_{xy}(t)\right) && (3.7) \end{aligned}$$

where

$$a_n = \frac{2}{T} \int_0^T \tau_{xy}(t) \cos(2\pi nt/T) dt \tag{3.8}$$

$$\text{and } b_n = \frac{2}{T} \int_0^T \tau_{xy}(t) \sin(2\pi nt/T) dt \tag{3.9}$$

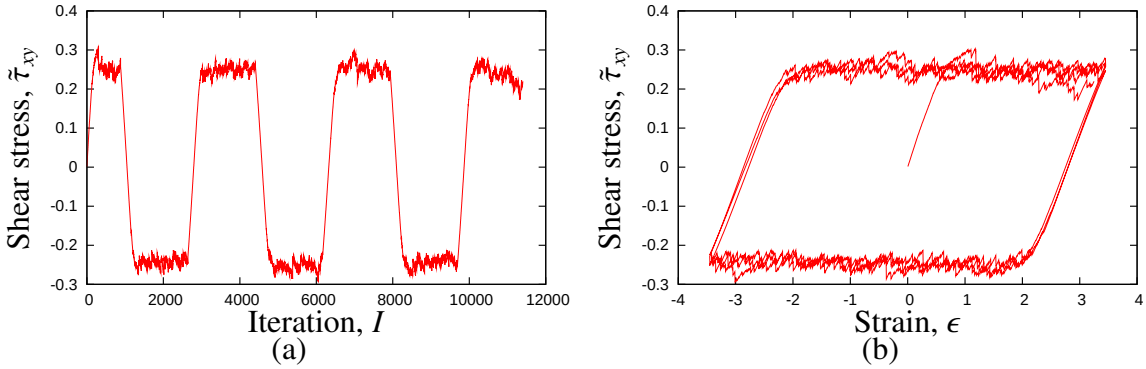

Figure 3.2: An example of the stress response of a dry two-dimensional foam to an oscillatory strain from one of my simulations for which the strain amplitude exceeds the yield strain. The shear stress is plotted against (a) iteration number, I, and (b) strain, ϵ.

are the coefficients of the harmonic components of the stress response. The first two terms in equation (3.7) are the primary harmonic components of the stress response. The final term $\mathcal{H}\left(\tau_{xy}(t)\right)$ contains all the contributions of the higher harmonic components.

The coefficients of the primary harmonic components, a_1 and b_1, when divided by the strain amplitude, give the storage and loss moduli, G' and G'', traditionally used to characterize a material's elastic and dissipative characteristics. Solid-like materials have $G' > G''$ and *vice-versa* for liquid-like materials.

In the linear viscoelastic regime, G', G'' completely characterize the stress response but as the response becomes non-linear, extra information is found in the higher harmonic components, $\mathcal{H}\left(\tau_{xy}(t)\right)$.

To examine the solid-liquid transition in dry two-dimensional foams I performed oscillatory shear simulations and calculate the harmonics from the stress response. Figure 3.2 shows the typical stress response of a dry two-dimensional foam to oscillatory shear in the quasistatic limit, for which the strain amplitude exceeds the yield strain. Figure 3.2 (a) shows the stress response *versus* iteration number whilst figure 3.2 (b) shows the stress response *versus* strain. The stress increases initially with iteration number and fluctuates about an average stress above the yield strain. When the direction of shear is

reversed, the stress strain relationship returns to linear until the foam yields once more and the stress fluctuates around an average value. The cycle is then repeated. Since the simulations were performed in the quasistatic regime, i.e. at very low frequency, the only option available is to vary the strain amplitude as a control parameter. However, this is the most appropriate option for studying the solid-liquid transition.

3.2.1 Method of oscillatory shear

Details of foam creation and shear in the linear Couette geometry are given in section 2.5. Since the simulations performed here are in the limit of low frequency and therefore there is no time-scale, the iteration number, I, plays the role of time. Oscillatory shear simulations require several shear cycles, which increases simulation times. Applying a strain signal which is sinusoidal with respect to iteration number further increases the simulation time: since the strain steps are now unequal, for the largest strain increment to remain below an acceptable level for quasistatic simulation, strain increments must become very small as $|\epsilon| \to \epsilon_0$.

To counteract this effect, I apply a saw-tooth strain signal with respect to iteration number. I then map the iteration number to the equivalent time, t, for a sinusoidal strain signal (figure 3.3). A saw-tooth strain signal is implemented by imposing constant strain increments up to the strain amplitude and then reversing the direction of shear. The period of oscillation is $T = 4\epsilon_0/\delta\epsilon$.

The function $t(I)$ which gives the "time" values for a sinusoidal strain signal from a saw-tooth signal of period T is

$$t(I) = \frac{T}{2\pi}\left\{\sin^{-1}\left(\frac{4I}{T} - k\right) + \frac{k\pi}{2}\right\} \tag{3.10}$$

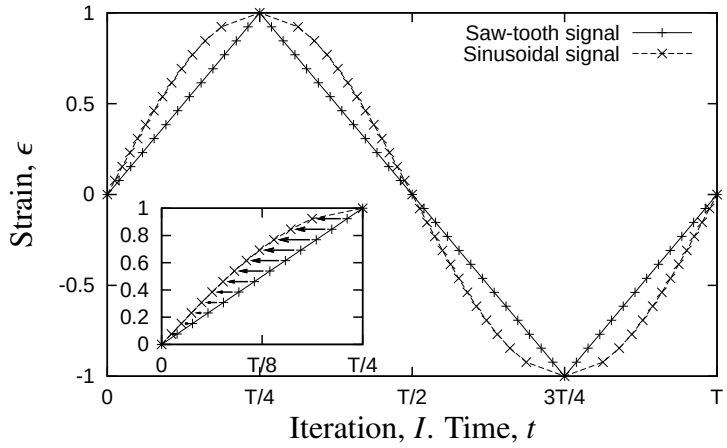

Figure 3.3: The applied saw-tooth strain signal *versus* iteration number and the corresponding sinusoidal strain signal *versus* "time" after the iteration number has been mapped according to equation 3.10.

where

$$k = 2\left\lfloor \frac{2I}{T} - \frac{1}{2} \right\rfloor + 2 \tag{3.11}$$

and $\lfloor\rfloor$ denotes the integer part.

This is an acceptable approach in the quasistatic limit, since it is the value of stress at a given strain which is important and not how that strain was reached. The ambiguity in which equilibrium state of foam is reached is the same as is encountered when using different but constant strain increments (see section 2.7).

The strain amplitude, ϵ_0, is varied in the range 10^{-2} to 20. The value of $\delta\epsilon$ is fixed for each simulation (i.e. for each strain amplitude) and is chosen to be sufficiently small such as to be a good approximation to the quasistatic limit (see section 2.7). Since the stress signal is to be integrated numerically with the trapezoidal method which is accurate to $O(\delta\epsilon^2)$, an extra condition is placed on the magnitude of $\delta\epsilon$ in that it must be sufficiently small to keep the error to an acceptable level during the integration, whilst still remaining large enough for the simulations to be completed in a reasonable time (up to 1 month for the largest strain amplitudes).

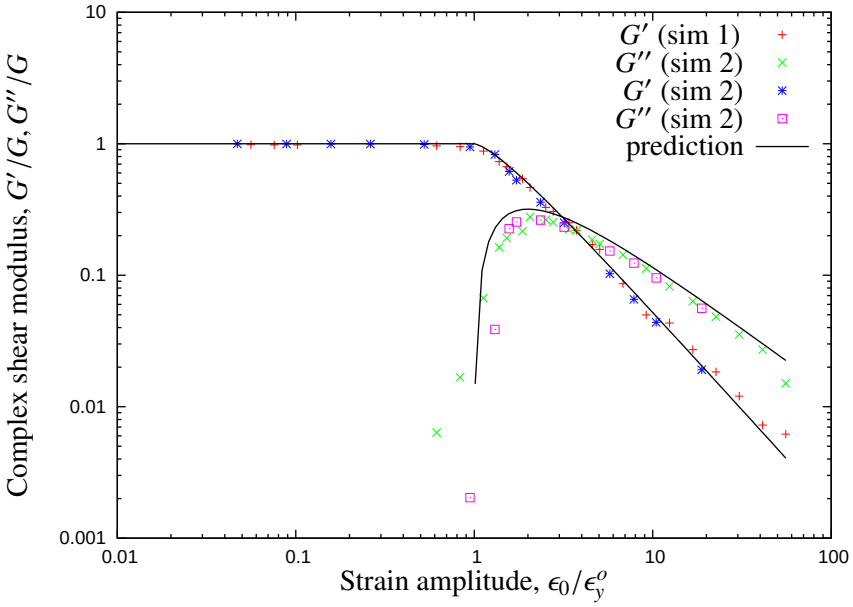

Figure 3.4: The storage and loss moduli as a function of strain amplitude for two foam samples, with the prediction of Rouyer *et al.* [128]

3.2.2 Storage and loss moduli

The complex shear modulus is given by

$$G^*(\epsilon_0) = \frac{2}{T\epsilon_0}\int_0^T \tau_{xy}(t)\exp(i2\pi t/T) = G' + iG'' \tag{3.12}$$

where the storage modulus, G', is a measure of the elastic response of a material and the loss modulus, G'', a measure of the dissipative response.

Figure 3.4 shows the storage and loss moduli for two simulated foams as a function of strain amplitude. Simulation 1 has $N_B = 560$ bubbles, $W = 1.6$ with approximately 10 bubbles between the plates and area-disorder, $\mu_2^A = 0.038$. Simulation 2 has $N_B = 1120$ bubbles, $W = 3.2$ with approximately 21 bubbles between the plates and area-disorder, $\mu_2^A = 0.052$. The data is normalized by the shear modulus, G, and oscillatory yield strain ϵ_y^o, which are calculated as follows [17; 127].

At low strain amplitude the response is purely elastic and G' is constant and at

high strain amplitude G' exhibits power-law behaviour. At intermediate values of strain amplitude there is transitional behaviour as the foam yields. To determine the shear modulus, G, I fit a horizontal line $G' = G$ to the data at low strain amplitude. To calculate the oscillatory yield strain, ϵ_y^o, I plot the stress amplitude against strain amplitude (data not shown) and fit a power law with exponent 1 to the data at low strain amplitude and a constant function to the data at high strain amplitude. The intersection of the two fits defines a yield stress and strain.

When normalized, the storage and loss moduli from both simulations fall on the same master curve. G' is almost constant at low strain amplitude, i.e. in the linear viscoelastic regime, whilst G'' is zero. This is to be expected since there is no viscous dissipation in the quasistatic limit and no plasticity (T1s) at low strain amplitude and therefore the response is purely elastic. As the yield strain is approached, G' starts to decrease and G'' becomes non-zero as some energy is dissipated through plastic rearrangements and the foam transits from solid-like behaviour to liquid-like behaviour. G'' passes through a maximum at approximately $2\epsilon_y^o$ and thereafter decreases with power-law behaviour.

The prediction of the elasto-plastic model of Rouyer *et al.* [128] is also plotted in figure 3.4. The model describes the stress strain relationship like that plotted in figure 3.2 as a simple combination of a spring and a slider. Elastic deformation below the yield strain is modeled as a spring with stress proportional to the applied strain. Plastic deformation above the yield strain is modeled as a slider where the stress remains constant, equal to the yield stress.

The result of the simulations is in excellent agreement with this simple model, which has only two free parameters: the shear modulus, G, and oscillatory yield strain, ϵ_y^o. The model assumes an abrupt transition from elastic to plastic behaviour, which is not the case in my simulations, leading to slight discrepancies near the yield strain. An elasto-

visco-plastic model, due to Marmottant *et al.* [95], uses a smooth transition between elastic and plastic behaviour and can also incorporate viscous dissipation, although this is not relevant here. Both models are in good agreement with experimental data for three-dimensional foams, pastes and emulsions and I find that the similarity also extends to two-dimensional dry foams.

3.2.3 Higher harmonics

The nonlinear stress response can be quantified by looking at the amplitude of the higher harmonics, h_n, where $n \geq 2$ and

$$h_n = \frac{2}{T}\left|\int_0^T \tau_{xy}(t)\exp(-i2\pi nt/T)dt\right|. \tag{3.13}$$

Following Rouyer *et al.* [128], I define the stress residual, q, to be the dimensionless root mean square variation of $\mathcal{H}\left(\tau_{xy}(t)\right)$,

$$q = \sqrt{\frac{\int \mathcal{H}\left(\tau_{xy}(t)\right)dt}{\int \tau_{xy}^2(t)dt}} = \sqrt{\frac{\sum_{i=1}^{4} h_{2i+1}^2}{h_1^2 + \sum_{i=1}^{4} h_{2i+1}^2}}. \tag{3.14}$$

The experimental data is obtained from three-dimensional foams in a cylindrical Couette geometry with liquid fraction $\phi_l \approx 0.075$, whilst the simulations were performed in the linear Couette geometry with dry two-dimensional foams of liquid fraction $\phi_l = 2.6 \times 10^{-4}$.

In agreement with the experimental data (figure 3.5), most of the nonlinear response is contributed by the third harmonic. The deviation from linear response increases with increasing strain amplitude and the jump in nonlinear behaviour at the yield strain is in agreement with experimental observations. The simulation data reaches higher values of strain amplitude than the experimental data and suggests a possible plateau in

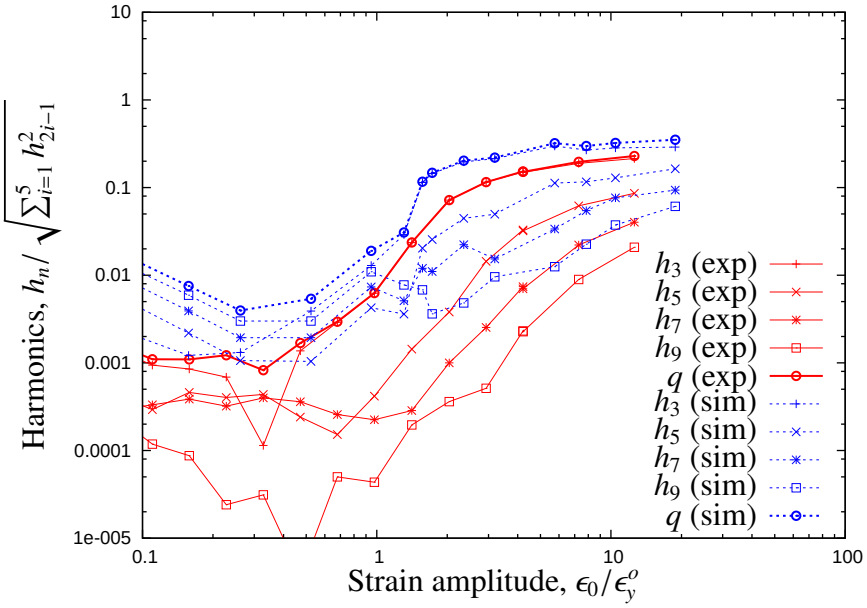

Figure 3.5: The stress residual, q, and the amplitude of the odd stress harmonics, h_n, for $n \geq 3$ as a function of strain amplitude, ϵ_0, normalized by the oscillatory yield strain, ϵ_y^o, for simulation and experiment. In both cases q and h_3 are almost indistinguishable.

nonlinear response as the strain amplitude is increased.

The simulations overpredict the harmonics, h_n, by a small amount but the agreement is still very good considering the differences between both studies in terms of dimension, liquid fraction, dissipation and, to a lesser extent, container geometry. These differences are likely to account for the discrepancy.

3.3 Yield Stress

3.3.1 Effect of area-disorder

First I consider the perfectly dry ordered case, studied analytically by Princen [30], as a reference with which to compare data for disordered foams. It will also provide a test for the simulation methods and later (section 3.3.2.1) will allow me to suitably fix the contact angle for wet foam simulations. An ordered dry foam can be created

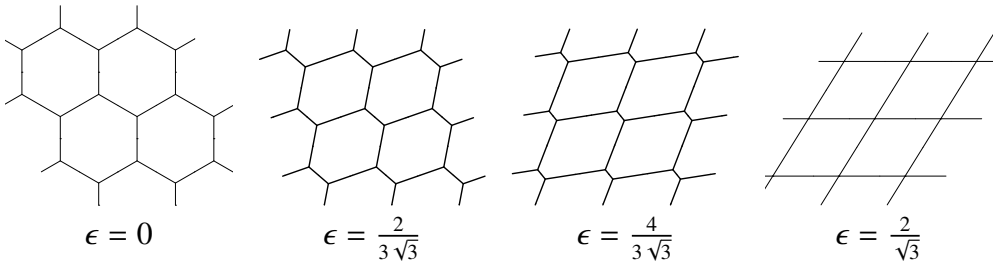

Figure 3.6: A perfectly ordered dry foam at different strains, created in the Surface Evolver using three films and periodic boundary conditions.

in the Surface Evolver with three films by using periodic boundary conditions and the foam structure at different strains is shown in figure 3.6. The stress-strain relationship is shown in figure 3.7, and is described by the following relationship in the dry limit [32]:

$$\tilde{\tau}_{xy} = \sqrt{\frac{\langle A \rangle}{3}} \frac{\epsilon}{\sqrt{\epsilon^2 + 4}}. \tag{3.15}$$

Simulation of the shear of the ordered dry foam in the Surface Evolver is in excellent agreement with the analytic result. Princen considered the static yield stress. The stress-strain curves for the hexagonal foam are periodic and do not therefore exhibit transient behaviour as is the case for disordered foams (figure 3.8). The definition of dynamic yield stress cannot therefore strictly be applied. However, in order to make comparison with the disordered case, I will use the average stress over an entire period as the dynamic yield stress in this case. Princen extended the analytical calculations to finite liquid fractions, and the values of static and dynamic yield stress at $\phi_l = 2.6 \times 10^{-4}$ will be used as a reference.

Bubble model simulations in three dimensions by Gardiner *et al.* [28] suggest that the static yield stress strongly decreases with volumetric disorder, but the nature of the decrease was not explored. I simulate shearing of dry two-dimensional foams of different area-disorder as described in section 2.5, to obtain the static and dynamic yield stress as a function of area-disorder. Dry foam simulations are used in this case (the effect of liquid fraction is considered later) for which simulations of over a thousand

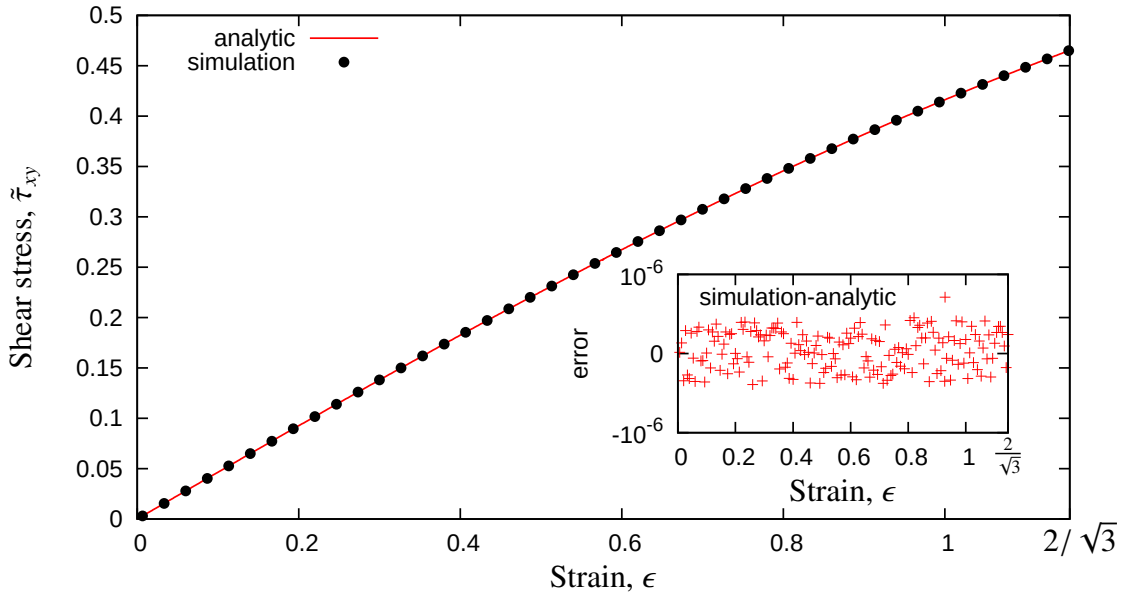

Figure 3.7: Shear stress *versus* strain for a perfectly ordered dry foam. Simulation using the dry method is in agreement with the analytic prediction, with error less than 10^{-6} (see inset).

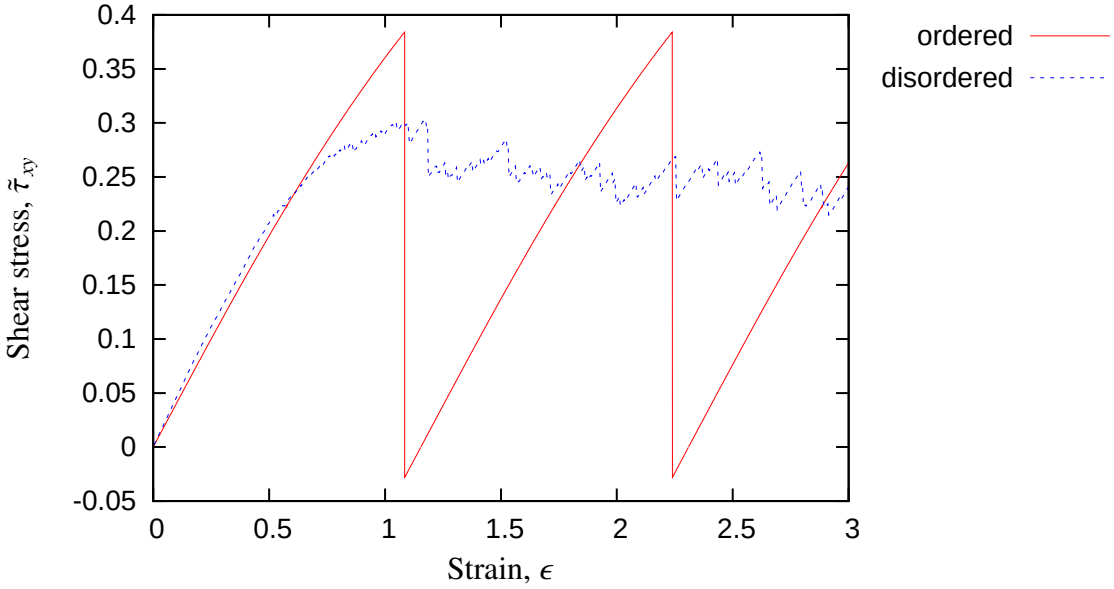

Figure 3.8: Stress-strain curves for an ordered foam and a disordered foam both with liquid fraction $\phi_l = 2.65 \times 10^{-4}$.

bubbles is possible in reasonable time. Each simulated foam consists of $N_B = 1120$ bubbles with $W = 3.2$ and approximately 21 bubbles between the parallel plates. The effective liquid fraction is $\phi_l = 2.6 \times 10^{-4}$.

Figure 3.9 shows the static and dynamic yield stress as a function of area-disorder. The values for a perfectly ordered foam are shown as large squares in figure 3.9 (a). The static yield stress appears constant at low area-disorder and decreases by approximately 20% at higher area-disorder. The dynamic yield stress appears to increase initially with increasing area-disorder before decreasing again as the area-disorder is increased further. The static yield stress does not converge to the value for a perfectly ordered foam as the area-disorder tends to zero but there is weak evidence that the dynamic yield stress may tend to the value for ordered foams as the area-disorder tends to zero. Nevertheless, the dynamic yield stress is, in general, greater than the value for the ordered case, even at low area-disorder, and it is important therefore that disordered foams are considered when trying to predict the response of a real foam. Stress *versus* strain relationships obtained from experiments also suggest that the static yield stress of disordered foams is over predicted by the ordered case and that the dynamic yield stress of disordered foams is under predicted by the ordered case (see section 3.4).

Figure 3.10 shows the difference between the static and dynamic yield stress as a function of area-disorder. $\tilde{\tau}_y^s - \tilde{\tau}_y^d$ decreases as the area-disorder is increased, which indicates that the stress overshoot observed in shear startup experiments decreases with increasing area-disorder. The decrease appears linear in $\ln\mu_2^A$ for the range of area-disorder considered and the difference between the static and dynamic yield stress will not go to zero for realistic values of area-disorder. The fit in figure 3.10 is given by

$$\tilde{\tau}_y^s - \tilde{\tau}_y^d = -12.8\ln\mu_2^A + 0.13. \tag{3.16}$$

(a)

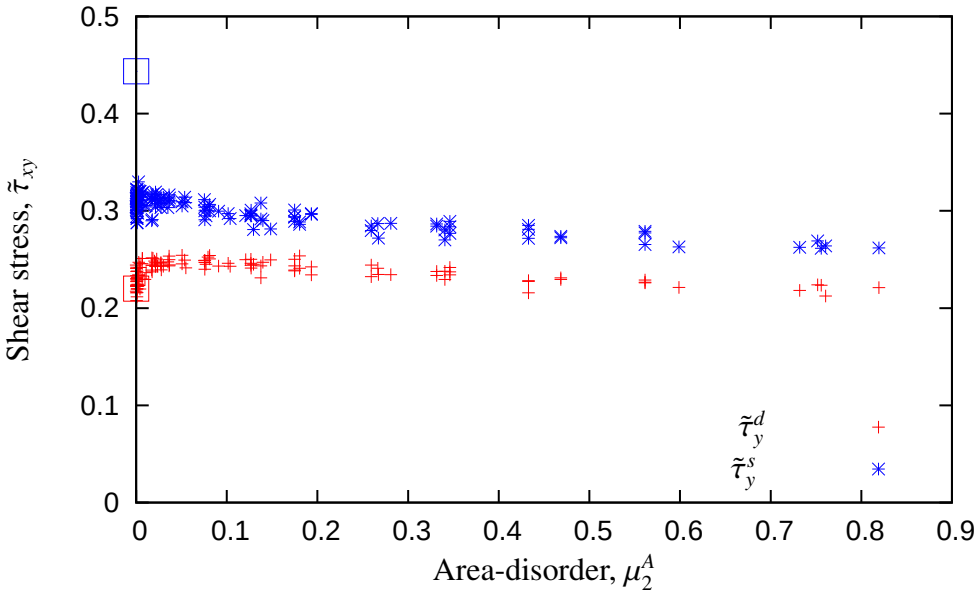

(b)

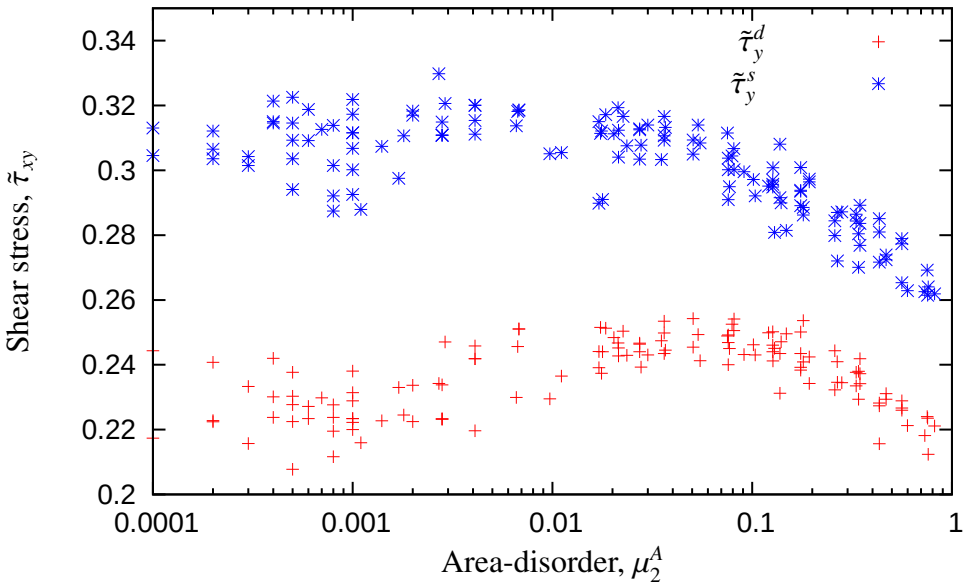

Figure 3.9: The static and dynamic yield stress *versus* area-disorder, using linear axes in the top figure and log-linear axes in the bottom figure. The values for an ordered foam are given as squares in the top figure. The variation at low area-disorder is clearer in the bottom figure. The static yield stress appears constant at low area-disorder but does not converge to the value of the perfectly ordered case as the area-disorder tends to zero. The dynamic yield stress appears to increase initially with increasing area-disorder from the value for a perfectly ordered foam. At higher area-disorder both the static and dynamic yield stress decrease with increasing area-disorder.

(a)

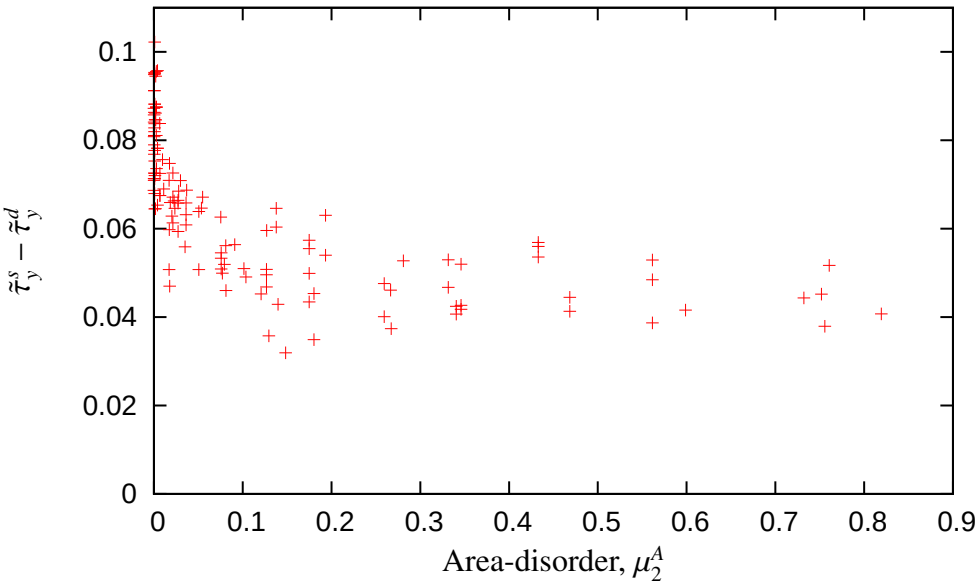

(b)

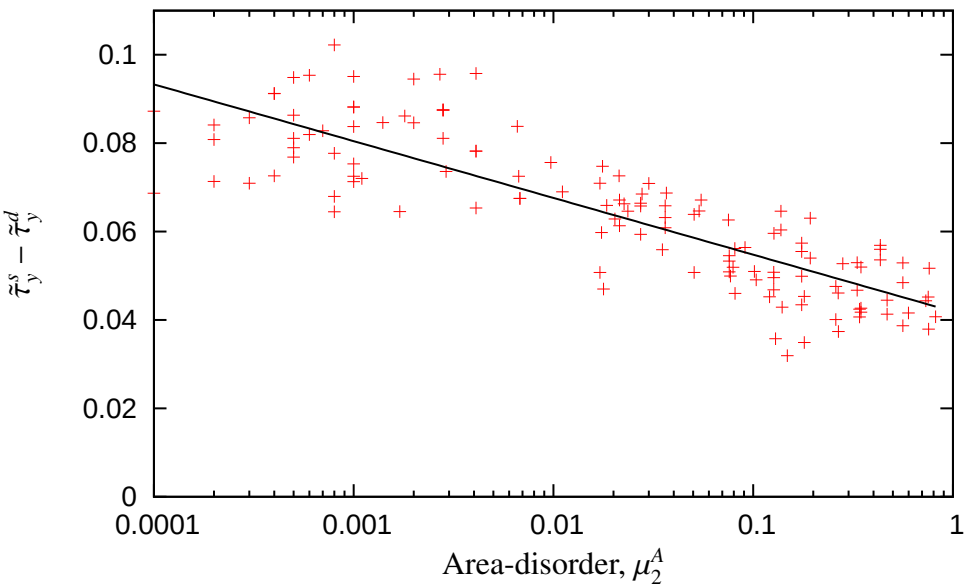

Figure 3.10: The difference between the static and dynamic yield stress decreases with increasing area-disorder, indicating that the stress overshoot on shear startup also decreases with increasing area-disorder. The fit is given by equation (3.16).

3.3.2 Effect of liquid fraction

To study the effect of liquid fraction on the yield stress of disordered foams in linear Couette shear, I shall use both the dry method with cut-off length and the wet method, described in sections 2.5 and 2.6, comparing with results for ordered hexagonal foams, extracted by reproducing the stress-strain curves from the work of Princen [30].

3.3.2.1 Ordered foams

Figure 3.11 shows the stress-strain relationship for an ordered foam at a range of values of liquid fraction. The stress initially follows the same curve as the dry case. When the Plateau borders touch and the T1 process begins (cf. figure 2.10) the stress strain relationship joins a different curve before returning to the initial curve (reflected in the lines $\tilde{\tau}_{xy} = 0$ and $\epsilon = 1/\sqrt{3}$) when two air-liquid interfaces meet. Above a certain liquid fraction (between 0.05 and 0.06 for zero contact angle) the stress-strain curves all pass through a common intersection point at $(1/\sqrt{3}, 0)$. Above this critical liquid fraction, the foam passes through a configuration like that shown in figure 3.12 (a) at $\epsilon = 1/\sqrt{3}$ giving zero stress. Below the critical liquid fraction, this configuration is not the minimum energy configuration. For $\phi_l = 0.05$, for example, both configurations shown in figure 3.12 have a lower energy, leading to a non-zero stress in this case.

For the wet method, a finite contact angle exists between the air-liquid interfaces separating bubbles and Plateau borders and the air-liquid-air interfaces separating bubbles. As discussed in section 2.6, a zero contact angle causes the numerical method to become unstable and therefore the contact angle is kept small but finite. Figure 3.13 illustrates the effect of a finite contact angle on the stress-strain relationship of an ordered foam. P_α denotes analytic predictions and S_α denotes Surface Evolver simulations, each of contact angle α. The strain (and therefore stress) at which the Plateau borders merge increases with increasing contact angle, as does the strain at which the fourfold Plateau

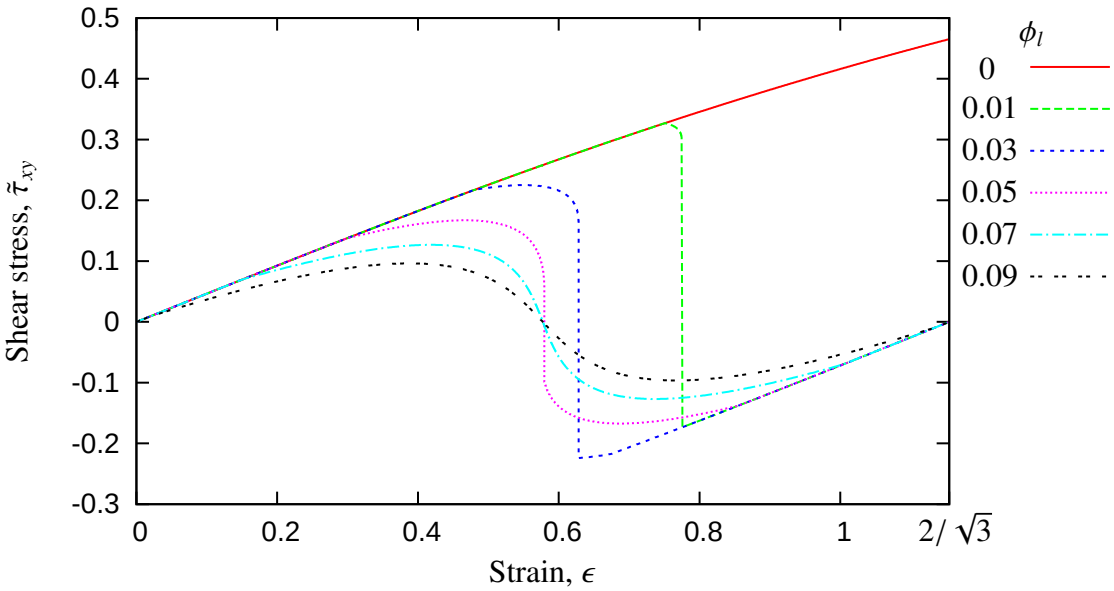

Figure 3.11: Stress *versus* strain curves for an ordered foam for various values of liquid fraction, calculated from the analytic result of Princen [30]. The curves follow the same curve as the perfectly dry foam until the Plateau borders meet, which occurs at lower strains as the liquid fraction is increased.

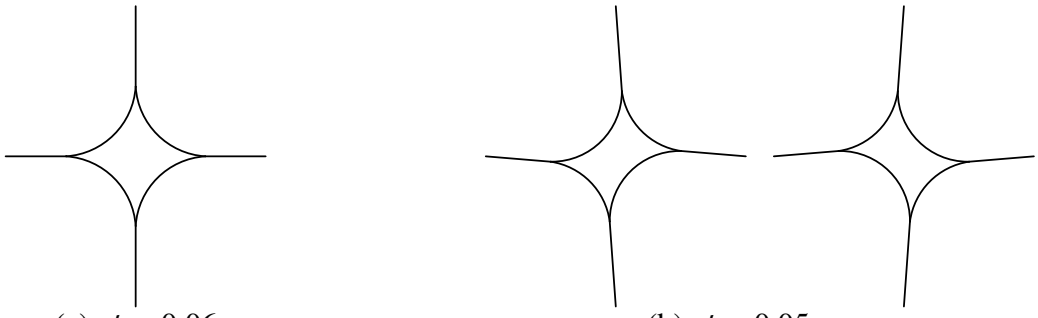

(a) $\phi = 0.06$ (b) $\phi = 0.05$

Figure 3.12: Above a certain liquid fraction, the foam passes continuously through a zero stress configuration at $\epsilon = 1/\sqrt{3}$ like that shown in (a). Below this critical liquid fraction there exist lower energy configurations at $\epsilon = 1/\sqrt{3}$ with a non-zero stress, as shown in (b).

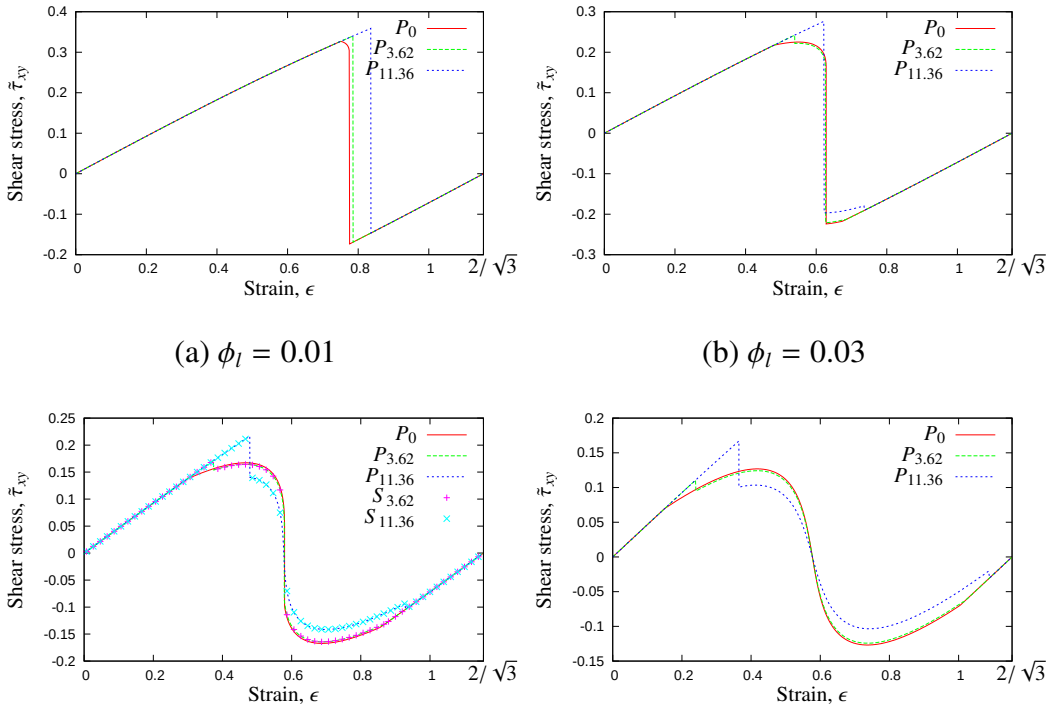

(a) $\phi_l = 0.01$ (b) $\phi_l = 0.03$

(c) $\phi_l = 0.05$ (d) $\phi_l = 0.07$

Figure 3.13: Stress-strain curves for ordered hexagonal foams at different liquid fractions and contact angles, α (denoted as P_α), from the analytic prediction of Princen [30]. For $\phi_l = 0.05$, datapoints from simulations with the wet method, of contact angle α (denoted S_α), are also plotted, showing excellent agreement.

border dissociates back into two threefold Plateau borders.

The effect on the static and dynamic yield stress is shown in figure 3.14. τ_y^s and τ_y^d decrease in each case with increasing ϕ_l. In general, an increased contact angle leads to an increase in static and dynamic yield stress but at small contact angle τ_y^s and τ_y^d can be slightly smaller than for zero contact angle as the liquid fraction is increased.

For zero contact angle the dynamic yield stress goes to zero at roughly $\phi_l = 0.053$. For finite contact angle, the dynamic yield stress does not go to zero but for $\alpha = 3.62$, $\tilde{\tau}_y^d < 0.001$ at liquid fractions greater than $\phi \approx 0.05$.

Simulations of disordered foams with the wet method were performed with a contact angle of $\alpha = 3.62$, which is a good approximation to the case of zero contact angle. For

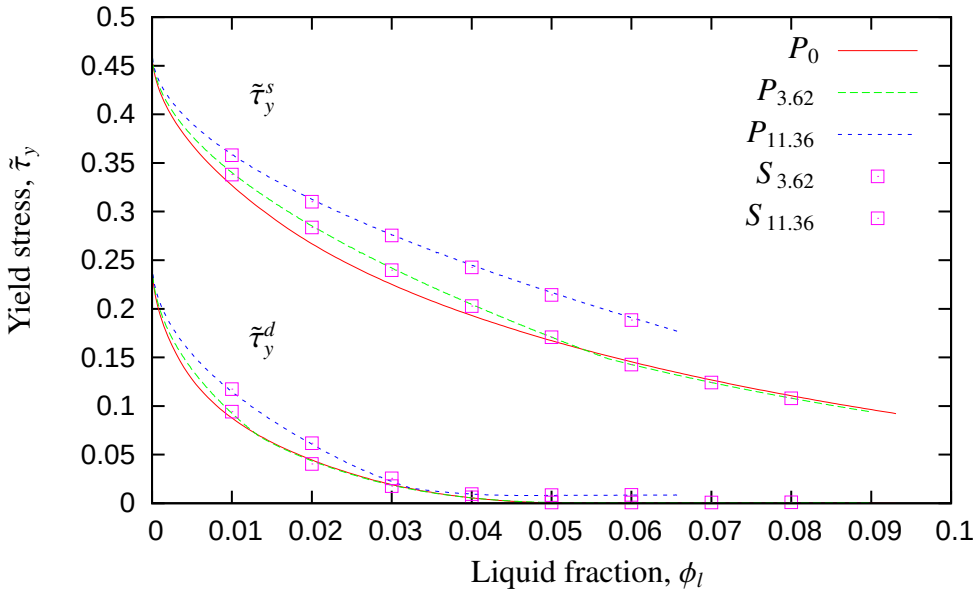

Figure 3.14: The static yield stress, from the analytic prediction of Princen [30], and dynamic yield stress of perfectly ordered two-dimensional foams, extracted by reproducing the stress-strain curves as a function of liquid fraction. Datapoints from simulations with the wet method are also plotted and are in excellent agreement with the analytic prediction. P_α denotes analytic predictions and S_α denotes Surface Evolver simulations, each of contact angle α.

the ordered case, results for dynamic and static yield stress are in excellent agreement with the analytic result (figure 3.14) giving confidence in the method of simulation.

3.3.2.2 Disordered foams

I now consider the effect of varying liquid fraction on the static and dynamic yield stress of disordered two-dimensional foams in linear Couette shear using the methods of simulation described in sections 2.5 and 2.6. Foams of $N_B = 1120$ bubbles were used with the dry method with finite cut-off length. Foams of $N_B = 100$ bubbles were used with the wet method. The static yield stress was measured by taking the maximum shear stress achieved during a simulation, which occurs during the transient. The dynamic yield stress was measured by taking the average shear stress after the transient.

The static yield stress decreases with increasing liquid fraction (figure 3.15 (a)) and

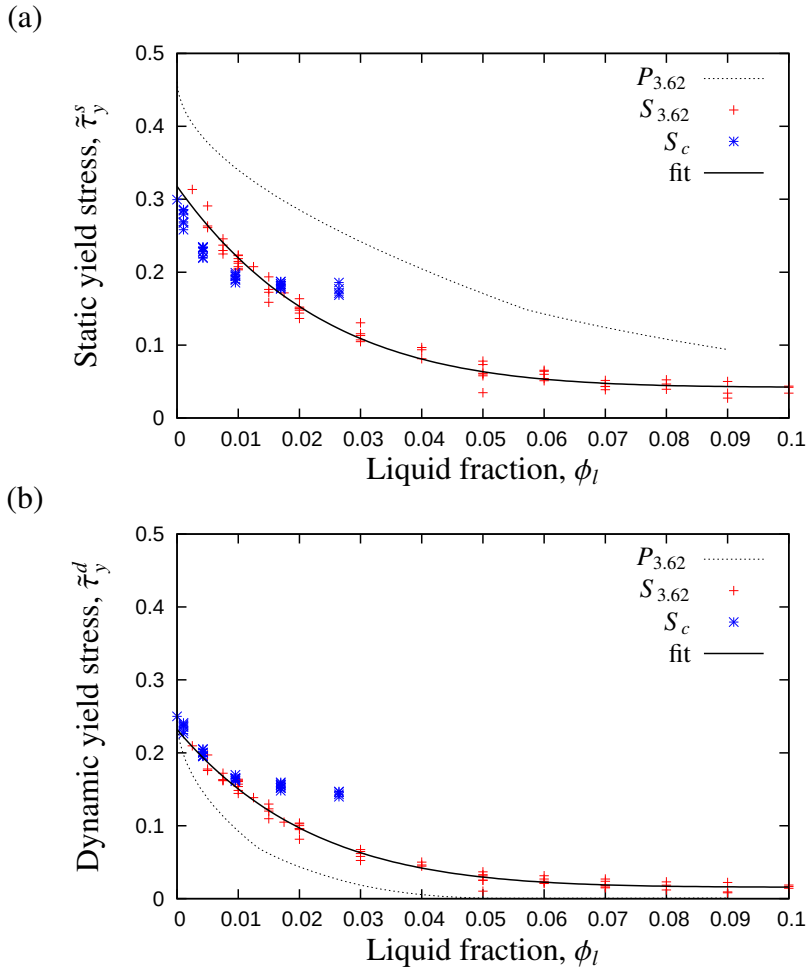

Figure 3.15: The (a) static and (b) dynamic yield stress of disordered two-dimensional foams as a function of liquid fraction for simulations with both the dry method and the wet method. The prediction for ordered foams is plotted for comparison. Data for both methods are in good agreement for liquid fractions up to around $\phi_l \approx 0.01$ and both the static and dynamic yield stress decrease with increasing liquid fraction. The bold lines are fits to equation (3.17). The fit parameters are given in the text.

is lower for disordered foams than for the ordered case. Results from different methods are in good agreement up to a liquid fraction of around 0.01, above which the dry method with cut-off length fails. For a discussion of the reasons the method fails see section 3.4.3.

Figure 3.15 (b) shows the decrease of the dynamic yield stress with increasing liquid fraction. As for the static yield stress, results for both methods are in excellent agreement up to liquid fractions of around 0.01. The dynamic yield stress is higher than in

the ordered case (cf. figure 3.9), and the difference is greater at intermediate values of liquid fraction.

Simulations with the dry method at low liquid fraction in section 3.3.1 suggest that there is a discontinuity in static yield stress between the ordered and disordered cases, but that the dynamic yield stress tends to the ordered value as the area-disorder goes to zero.

Three-dimensional yield stress data are often fitted with the following equation with $b = 2$, a close to one-half and $c = 0$:

$$\tilde{\tau}_y = a(\phi_c - \phi_l)^b + c. \tag{3.17}$$

In two dimensions, $\phi_c \approx 0.16$ and it is also possible to fit a curve of this type to both the static and dynamic yield stress data, but with a very large and with very large error. The static yield stress will not go to zero and also, since a small but finite contact angle is used, $c > 0$ for the dynamic yield stress too, as for the ordered case. For the static yield stress, $a = 74294 \pm 4.82 \times 10^4$, $b = 6.823 \pm 0.35$ and $c = 0.042 \pm 0.0028$. For the dynamic yield stress $a = 6308 \pm 2727$, $b = 5.609 \pm 0.228$ and $c = 0.016 \pm 0.0017$. Although the static and dynamic yield stress can be fitted with an equation of the form of equation (3.17), the magnitude and error of the coefficients suggest that it may not be the most appropriate fit for two-dimensional foams.

Both the static and dynamic yield stress can also be estimated through a weighted average of the static and dynamic yield stress predictions for ordered foams, P^s_α and P^d_α (figure 3.14). No physical justification is given, but the following relationships provide a useful rule of thumb. The static and dynamic yield stress of disordered foams is given to a good approximation by the following combination of Princen's predictions (figure

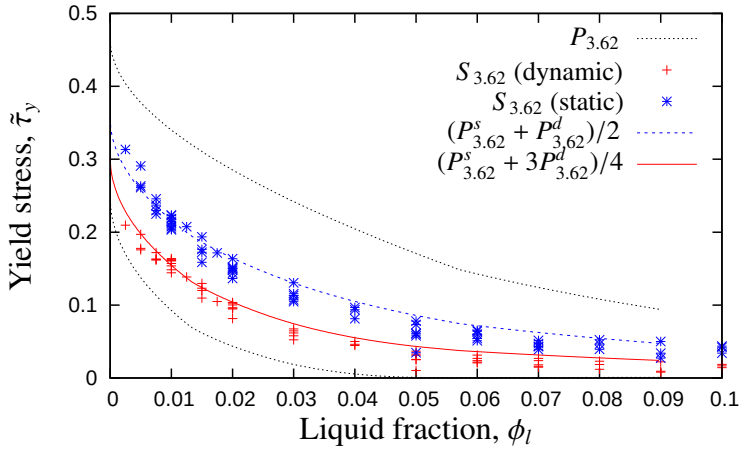

Figure 3.16: The static and dynamic yield stress of disordered two-dimensional foams are given to a good approximation by a weighted average of the predictions of the static and dynamic yield stress of ordered foams.

3.16):

$$\tau_y^s \approx \frac{P_\alpha^s + P_\alpha^d}{2} \tag{3.18}$$

$$\tau_y^d \approx \frac{P_\alpha^s + 3P_\alpha^d}{4}. \tag{3.19}$$

These relationships are a good approximation of the static and dynamic yield stress of disordered two-dimensional foams for contact angles $\alpha = 11.36$ and $\alpha = 3.62$ and are therefore likely to work for a zero contact angle also.

3.4 Discussion

3.4.1 Comparison with experiment

To my knowledge, there are no experimental studies of the effect of liquid fraction on the yield stress of a two-dimensional foam. There are, however, stress *versus* strain relationships published for two-dimensional foams, from which a rough estimation of a non-dimensionalized yield stress can be calculated. From the work of Lauridsen *et al.*

[54] at a liquid fraction of $\phi_l \approx 0.05$ I can estimate the following parameters from the information provided:

$$\tau_y^s = 2.4 \text{ mN m}^{-1} \tag{3.20}$$

$$\tau_y^d = 1.75 \text{ mN m}^{-1} \tag{3.21}$$

$$\langle A \rangle = \pi 0.001^2 = 3.14 \times 10^{-6} \text{ m}^2. \tag{3.22}$$

To calculate $\tilde{\tau}_y^s$ and $\tilde{\tau}_y^d$ from equation (3.4), an estimate for the surface tension, γ, is required. Given that this is a quasi-two-dimensional experiment, γ is a line tension with the dimensions of force. γ depends on the surface tension of the liquid phase, γ_l, which has the usual dimensions for surface tension of force per unit length, and the height, h, of the quasi-two-dimensional foam e.g. the distance between the bounding plates of a Hele-Shaw cell [67]. For a liquid phase with surface tension $\gamma_l = 26.1$ mN m^{-1}, Raufaste *et al.* [67] estimate

$$\gamma/h \approx 110 \text{ mN m}^{-1}, \tag{3.23}$$

and since Lauridsen *et al.* do not report the surface tension of the liquid phase, I shall use the value of Raufaste *et al.* as an estimate in its place. Using the quoted bubble radius as an estimate of the height of the foam in the study of Lauridsen *et al.*,

$$2\gamma \approx 0.11 \text{ mN}. \tag{3.24}$$

A comparison of the experimental values of the static and dynamic yield stress with the corresponding values for a perfectly ordered two-dimensional foam and my simulations of disordered two-dimensional foams for a liquid fraction of $\phi_l = 0.05$ is shown in table 3.1. The values for disordered foams are calculated by taking the average of the yield stress values of the individual simulations at $\phi_l = 0.05$. The dynamic yield

	$\tilde{\tau}_y^s$	$\tilde{\tau}_y^d$
Ordered two-dimensional prediction	0.170857	0.000807
Disordered two-dimensional simulations	0.060911	0.026898
Quasi-two-dimensional experiment	0.038672	0.028198

Table 3.1: Comparison of the static and dynamic yield stress of two-dimensional foams from simulation and experiment.

stress for ordered two-dimensional foams under predicts the experimental value, whilst simulations of disordered two-dimensional foams are in excellent agreement with the experimental observation. The static yield stress is over predicted by both the prediction of ordered foams and the simulations of disordered two-dimensional foams. A possible explanation for the difference is that in the experiment, the foam experiences a pre-shear as a result of inserting the foam into the experimental device, thus reducing the static yield stress.

3.4.2 Comparison with other two-dimensional simulations

The only other study of the variation of the yield stress of a two-dimensional foam with liquid fraction is found in the work of Hutzler *et al.* [21] where a fully periodic foam sample is subjected to extensional shear using the programme PLAT (see section 2.2.1.2). The yield stress is found by fitting a curve of the form

$$\tau = \tau_y \tanh\left(\epsilon/\epsilon_y\right) \tag{3.25}$$

to the data. At high liquid fraction this is difficult and therefore the average stress is used as in my simulations.

Comparison of my data with both wet and dry Surface Evolver methods with the data of Hutzler *et al.* is shown in figure 3.17. The fit to data at low liquid fraction from

the work of Hutzler *et al.* is also plotted and is of the form

$$\tau_y = d - e\phi_l^{1/2}. \tag{3.26}$$

where d and e are constants.

There is good agreement between my data and the data of Hutzler *et al.*, especially at high liquid fraction, although my data appears to be slightly lower than that of Hutzler *et al.* At low liquid fraction there is a steeper decrease of yield stress with liquid fraction in the work of Hutzler *et al.* than I found in my simulations.

The area-disorder of the samples is a possible explanation for the small discrepancy. The area-disorder is not quoted in the study of Hutzler *et al.* but from examination of the figures, is likely to be lower than the area-disorder in my simulations, which was kept to within a small range. The method of shear is another possible explanation for the difference, since I simulated the linear Couette shear of a foam sample between parallel plates and Hutzler *et al.* simulated extensional shear of a fully periodic foam sample. Finally, it may also be the case that it is the method of calculating the yield stress that causes the difference. This may explain why the agreement between the data sets is better at high liquid fraction than as the liquid fraction approaches zero, since at high liquid fraction, Hutzler *et al.* use the average stress as the yield stress in the same manner as I do. The agreement on the whole is very good, with the data of Hutzler *et al.* occurring at the fringes of my data.

3.4.3 Failure of dry method with cut-off length

Plateau borders with three or more sides occur with very low frequency below a liquid fraction of 4%, so the question arises of why the dry method with effective liquid fraction fails at around 1% liquid (figure 3.15). One would expect the occurence of stable

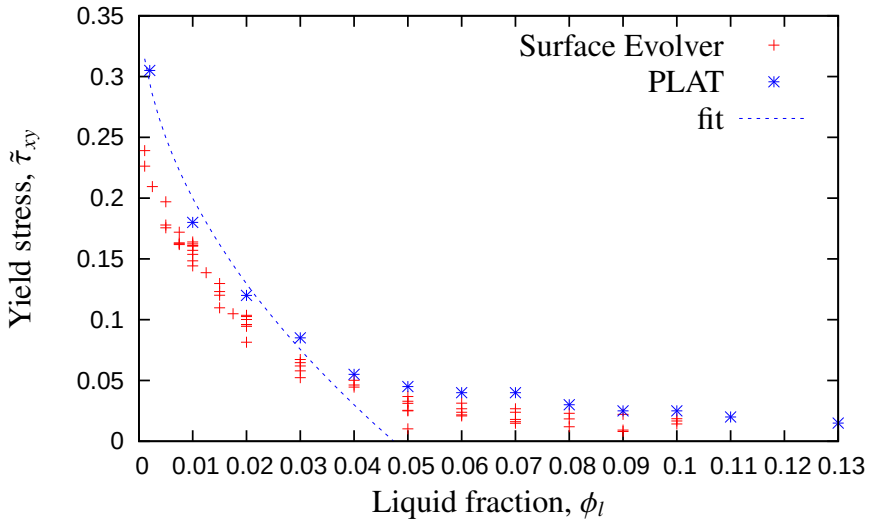

Figure 3.17: Comparison of yield stress *versus* liquid fraction data between my Surface Evolver simulations and PLAT simulations from the work of Hutzler *et al.* [21].

fourfold Plateau borders to be the important factor in the failure of the dry method, but it seems that earlier failure is due to the disordered nature of the foams.

The effective liquid fraction is determined from ordered hexagonal foams. In a disordered foam, small bubbles are surrounded by small edges which often fall below the cut-off length. If the Plateau borders are included explicitly, Plateau borders surrounding small bubbles are smaller than those surrounding big bubbles and therefore the cut-off length should be smaller in these cases. This is illustrated in figure 3.18. Figure 3.18 (a) shows an example of a foam with $\phi_l = 0.02$ and the Plateau borders included explicitly. No threefold Plateau borders have merged. In figure 3.18 (b), the Plateau borders have been removed and the films which fall below the cut-off length for an effective liquid fraction of 2% (using equation (2.5)) have been highlighted in red. Even though no Plateau borders have merged in figure 3.18 (a), when the Plateau borders are removed, several films are smaller than the cut-off length. The result is a deletion of films and creation of fourfold vertices which when popped, returns the film to its original position and no T1 has occurred. The new film remains below the cut-off length

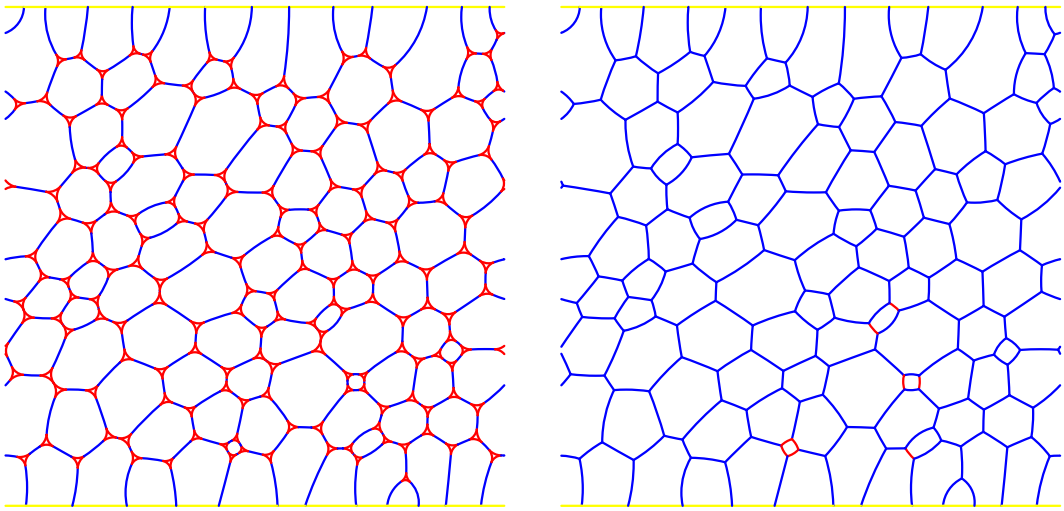

Figure 3.18: (a) A foam with $\phi_l = 0.02$ and the Plateau borders included explicitly. All the Plateau borders are three-sided. (b) The foam from (a) with the Plateau borders removed. Edges which fall below the cut-off length for an effective liquid fraction of 0.02 are highlighted in red. In simulations with the dry method, using an effective liquid fraction, these edges would be deleted to initiate a T1 whereas with the wet method no T1 would occur.

and is repeatedly deleted and popped so that the foam is unable to converge to an equilibrium configuration. Now that the reason for failure is known, it may be possible to adjust the cutoff length according to the area of the surrounding bubbles. Further failure is still expected at the point at which fourfold Plateau borders become stable, but this could also be incorporated into the method by allowing fourfold vertices to persist and represent fourfold Plateau borders. Development of this method would be beneficial since it would be much faster than incorporating the Plateau borders explicitly.

3.5 Summary

Foams are yield stress fluids which exhibit solid-like behaviour at stresses below the yield stress and liquid-like behaviour at stresses above the yield stress. The transition from solid-like to liquid-like behaviour can be seen in oscillatory shear experiments.

For small strain amplitude, the response is purely elastic. For sufficiently large strain amplitudes, the foam is repeatedly required to yield, flow and then return to solid-like behaviour.

The primary harmonics of the stress response to a simulated applied oscillatory shear of a two-dimensional dry foam are in good agreement with experimental data for foams as well as other yield stress fluids such as gels, emulsions and pastes (figure 3.4). Furthermore, the higher harmonics of the stress response are also in good agreement with experimental results for foams (figure 3.5) despite significant differences in the conditions of the studies thus suggesting that there may be some generic foam response independent of container geometry and liquid fraction.

The yield stress has been defined in several ways in the literature and here I concentrated on the definitions of static and dynamic yield stress, both of which decrease with increasing liquid fraction and area-disorder (above a certain level of area-disorder, figures 3.9 and 3.15). For dry foams at low area-disorder, the static yield stress is found to be constant with increasing area-disorder whilst the dynamic yield stress increases with increasing area-disorder.

Whilst the variation of the static and dynamic yield stress of ordered two-dimensional foams with liquid fraction is in qualitative agreement with my results for disordered foams (figure 3.15), values of static yield stress for disordered foams are lower than the value for the ordered case and values of dynamic yield stress are higher in general than the value for the ordered case, highlighting the importance of including disorder when considering the response of real foam systems.

Comparison of yield stress data obtained from dry foam simulations with finite cut-off length and with wet foam simulations shows that the validity of the dry method is limited to liquid fractions below around 1%. The dry method fails since the cut-off length is based on calculations with a perfectly ordered foam. Implementation of

a variable cut-off length based on local area-disorder could extend the range of liquid fractions for which a cut-off length may be used.

In the next chapter I consider the flow of a two-dimensional foam after it has yielded. Previously it has been shown that the topological changes in dry two-dimensional foams localize in space. I consider the effect of liquid fraction and area-disorder on the position and size of the region of localized T1s. The bubble dynamics during localized flow is examined and measures which can identify the region of localized T1s from information about the foam structure are presented.

Chapter 4

Shear localization

4.1 Introduction

Shear localization or shear banding is a common phenomenon arising in non-Newtonian fluids, particularly those with a yield stress. It refers to the existence of two (or more) co-existing regions of fluid flowing in bands at different shear rates (figure 4.1). At its most severe, one region is static (zero shear rate) and this behaviour has been observed in foams: co-existing flowing (liquid-like) and static (solid-like) regions have been observed in experiment [49; 54; 59; 64; 65] and simulation [39–41; 43; 58]. Regions of flow must be accompanied by T1 topological changes and therefore we can also think of shear banding in terms of regions of localized T1s (T1 localization).

Studies of shear localization in three-dimensional foams are relatively few when compared with the two-dimensional foam literature. Experiments by Coussot *et al.* [93] with both emulsions and suspensions, which often exhibit similar properties to foams, find that in the cylindrical Couette and cone and plate geometries the materials show co-existing solid and liquid regions under shear. The liquid region exhibits simple power-law fluid behaviour and more of the material flows as the shear rate is increased. For the suspension, the size of the liquid region decreases with increased jamming, i.e.

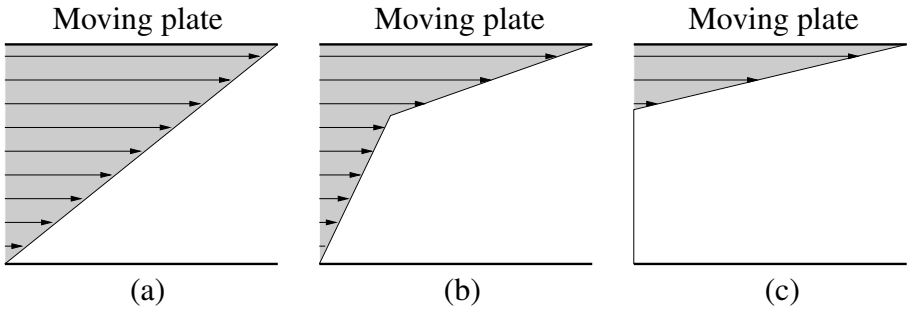

Figure 4.1: Shear localization: (a) The expected flow profile of a Newtonian fluid between parallel plates. For foams with this flow profile I would expect T1s to be distributed evenly throughout the channel. (b) In instances of shear localization, the flow splits into co-existing regions (or bands) of different shear rate. For foams with this flow profile I would expect T1s to occur throughout the channel, with a higher proportion near the moving plate. (c) When shear localization is severe, one region may have zero shear rate. In this scenario I would expect T1s to occur near the top plate only.

with a higher fraction of the suspension consisting of solid particles. Experiments in a cylindrical Couette geometry by Baudez & Coussot [135], both with foams and with polymeric gels, show that there is a critical strain at which there is an abrupt transition from solid-like to liquid-like behaviour. At the critical strain, the material begins to flow with finite shear rate. Rodts *et al.* [94], using a cylindrical Couette geometry, demonstrate with creep experiments, in which a constant stress is applied to a material and the strain is measured as a function of time, that a foam cannot flow steadily below a critical shear rate resulting in shear localization; the size of the liquid region increases with increasing shear rate. If the width of the flowing region is less than around 25 bubble diameters then a continuum assumption for a foam is no longer valid. In a parallel plate geometry, Rouyer *et al.* [29] observe uniform flow for strains much larger than the yield strain before fluctuating velocity profiles are observed, indicating the possible onset of shear localization. Three-dimensional bubble model simulations [28] however do not report any shear localization.

Shear localization in foams has been studied far more extensively in two dimensions than in three dimensions for the reasons discussed in Chapter 1. Results often

seem contradictory but many inconsistencies can now be explained in terms of the differing conditions and control parameters in each study. Some unanswered questions do however remain and I shall address some of these in this chapter. Shear localization in a two-dimensional foam experiment was first brought to the attention of the research community by Debrégeas *et al.* [59] in a cylindrical Couette geometry. The foam was confined between two glass plates ($\mathcal{GG}$) and the inner cylinder was rotated. They found velocity profiles in which the azimuthal velocity decreased exponentially with the radial distance from the inner cylinder. T1 localization was also evident, since the two-dimensional experiment allowed T1 positions to be recorded: they all occurred within 5 bubble widths of the moving cylinder. The velocity profiles were found to be increasingly localized as the liquid fraction was decreased, i.e. as the liquid fraction is decreased the velocity decays at a greater rate as a function of distance from the moving cylinder.

On the other hand, Lauridsen *et al.* [56] used a cylindrical Couette geometry and found velocity profiles consistent with that of a shear-thinning fluid and no shear localization. In this instance however, a bubble raft ($\mathcal{LA}$) was used and the outer cylinder rotated. Further experiments by Lauridsen *et al.* [54], at lower shear rates and lower liquid fraction but using the same geometry, did exhibit shear localization: a solid-like region of foam coexisted with a flowing region. The flowing region again had velocity profiles consistent with those of a shear thinning fluid, but the foam achieved a shear rate equal to the rotation rate of the outer cylinder at a critical radius that was smaller than the radius of the outer cylinder. Above this critical radius, the foam moves elastically and does not flow. Two rates of strain were used, with the critical radius of the smaller shear rate larger than that of the larger shear rate i.e. more of the foam is undergoing shear at slower shear rates, in contrast to the results of Rodts *et al.* [94] in three dimensions.

Shear localization in the cylindrical Couette geometry has also been predicted in simulations. Quasistatic simulations of a dry two-dimensional foam by Cox *et al.* [41] show shear localization near the inner cylinder when the outer cylinder is rotated. Further simulations with the Viscous Froth model [43], incorporating viscous drag from the bounding glass plates of a Hele-Shaw cell ($\mathcal{GG}$), show that as the velocity of the outer cylinder is increased, the localized region moves from the inner cylinder to the outer cylinder.

Theoretical work by Clancy *et al.* [70] explains much of the flow behaviour observed in the cylindrical Couette geometry. They assume a constitutive relation for the stress given by

$$\tau_{r\theta} = \tau_y f(\epsilon/\epsilon_y) + \eta\dot{\epsilon}, \tag{4.1}$$

where $\tau_{r\theta}$ is the shear stress in the cylindrical Couette geometry, ϵ, ϵ_y and $\dot{\epsilon}$ are the strain, yield strain and strain-rate respectively, τ_y is the yield stress, η is the viscosity and f is a function representing the equilibrium relationship between stress and strain. Note that if $f = 1$, the relation reduces to that of the Bingham model [92]. In the cylindrical Couette geometry, a stress balance between the fluid and the drag at the bounding plates gives

$$\frac{\partial \tau_{r\theta}}{\partial r} + \frac{2\tau_{r\theta}}{r} = \beta_d v_\theta \tag{4.2}$$

where r is the radial distance from the centre of the cylinders, v_θ is the azimuthal velocity and β_d is a drag coefficient representing the drag imposed by the bounding plates of a Hele-Shaw cell.

The predicted velocity profiles are a combination of exponential profiles in sheared regions, i.e. those regions with non-zero local strain rate, and constant velocity in non-sheared regions. The decay length of the exponential scales like $(\eta/\beta_d)^{1/2}$ and depends therefore on a competition between the internal dissipation in the system and the ex-

ternal friction. The balance between η and β_d depends on the boundary velocity [136], container geometry, method of confinement and boundary conditions. In some cases, there exists two different sheared regions (one near each wall) and therefore the shear band width is defined as the combined width of the sheared regions. They predict that the shear band width decreases with increasing drag. If the width is bigger than the channel size, the result is no shear localization.

The presence of shear localization when the inner cylinder is rotated (as in Debrégeas *et al.* [59]) is explained in terms of the viscous drag imposed by the bounding plates of the Hele-Shaw cell. The presence of external friction dominates the internal dissipation; the shear band width is smaller than the system size and the velocity profiles are exponential.

They observe a greater range of behaviour when the outer cylinder is rotated, identifying four differing regimes depending on the velocity of the moving plate, channel width and viscous drag. In one regime there is continuous shear across the gap and in another the localization occurs near the inner boundary. There is a regime in which localization occurs at the outer boundary and finally a regime in which localization occurs at both boundaries. The first two regimes account for the results of Lauridsen *et al.* [54; 56], in which localization is observed in one experiment and not in another. The third is consistent with the results of Cox [43] in which localization moves to the outer cylinder as the shear rate is increased. The case in which localization occurs at both boundaries has since been realized by Krishan & Dennin [45]. They found that when the flow is driven by the outer cylinder for a bubble raft ($\mathcal{LA}$), shear localization occurs near the inner boundary, but with a confined bubble raft ($\mathcal{LG}$), a second flowing region appears at the outer boundary as the shear rate is increased.

It seems therefore that external drag is an important factor when considering the shear localization of two-dimensional foams, but we shall see that it is not the only fac-

tor. There are some examples of shear localization in the cylindrical Couette geometry which remain unexplained [41; 43; 137] and these will be discussed later.

In recent years, several experimental studies have been conducted in the linear Couette geometry, although simulations of foam rheology in this geometry date back to Durian [16; 22]. In bubble model simulations of wet foams (see section 2.2.2.3), no shear localization is reported. The first prediction of localized flow in linear Couette shear of foams is found in the work of Jiang *et al.* [39], pre-dating the experimental observations of Debrégeas *et al.* [59] using the cylindrical geometry. Jiang *et al.* [39] used an extended Q-Potts model (see section 2.2.1.3) to simulate both boundary shear and affine (bulk) shear for both ordered monodisperse and disordered polydisperse foam systems. In the case of ordered monodisperse foams, they report T1s localized near both boundaries for boundary shear but a sliding plane of T1s away from the boundary for affine shear. For a disordered polydisperse system they did not observe any shear localization.

Kabla & Debrégeas [40] used the Surface Evolver software with a modified algorithm to simulate linear Couette shear of a dry two-dimensional foam of low area-disorder between jagged boundaries. They found that the T1s localize at either of the boundaries. Cox *et al.* [41] found that the T1s may localize in narrow bands at both boundaries for dry monodisperse foams using the Surface Evolver, in agreement with Jiang *et al.* [39].

Shear localization has only been observed experimentally in the linear Couette geometry in studies where external friction from a bounding plate is present. Wang *et al.* [49] showed that a top plate confining a bubble raft has a significant effect on the flow profiles of the foam. A fairly monodisperse foam was sheared by driving bands at the channel walls rotating in opposite directions. In the absence of a top bounding plate ($\mathcal{LA}$), the profiles were almost linear across the channel, with T1s occurring throughout

the channel, but on inclusion of a bounding plate ($\mathcal{LG}$), T1s became localized near both plates and the velocity decayed rapidly with increasing distance from the moving walls. They also observed that the velocity profiles were independent of the applied shear rate.

Katgert *et al.* [64] also observed shear localization for bubble rafts with a bounding plate. They studied both monodisperse and polydisperse foams and found that the velocity profiles of the monodisperse system were independent of the applied shear rate in agreement with Wang *et al.* [49]. However, for polydisperse foams there *was* a dependence on shear rate. The shear localization becomes more pronounced as the shear rate is increased, as in the cylindrical Couette case [54]. In a further study by Katgert *et al.* [65], varying the liquid fraction by controlling the distance between the bounding plate and the liquid pool, the velocity profiles were found to be increasingly localized as the liquid fraction was increased. This is in apparent contradiction with the results of Debrégeas *et al.* [59] with a Hele-Shaw cell in the cylindrical Couette geometry.

Once more, the theoretical framework developed by Janiaud *et al.* [71] and Clancy *et al.* [70] offers explanations for many of the features described here for linear Couette shear. In this case the model predicts velocity profiles in qualitative agreement with those of Wang *et al.* [49] and Katgert *et al.* [64]. By varying the drag coefficient of the model, both almost-linear velocity profiles and localized velocity profiles can be achieved. An analysis of the dependence of the degree of localization on boundary velocity, consistent with this continuum model, is given by Weaire *et al.* [97; 136].

Simulations by Langlois *et al.* [24] using the bubble model, modified to include the viscous drag from bounding plates, produce velocity profiles in excellent agreement with those of Janiaud *et al.* [71].

It seems that the presence of external friction can account for many observations of shear localization in the literature for linear Couette shear as it did for cylindrical Couette shear. The degree of external friction influences the size of the localized region

[49; 70]. This width of the localized region also depends on the applied shear rate [49; 56; 64]. When the width of the localized region is greater than the channel width, there is no localization and, conversely, when the width of the localization region is less than the channel width this results in coexisting regions of flowing and rigid foam. There are however several cases for which shear localization cannot be explained in terms of drag and shear rate. For example, simulations performed in the quasistatic limit, without viscous dissipation and in which the shear rate is assumed to be much slower than the rate of relaxation of the foam, predict localization in both the cylindrical Couette geometry [41; 43; 137] and the linear Couette geometry [39–41]. What causes the shear localization in these cases? Indeed, what is the relationship between quasistatic simulations and the low shear rate limit of other simulations methods and the theory of Clancy. For the case of the cylindrical Couette geometry, the fact that the stress is higher near the inner cylinder means that some of the foam is above the yield stress and flows, whilst some is not and is static. This explanation does not account for the observed shear localization in linear Couette shear, in which the stress is uniform across the channel. Weaire *et al.* [97] suggest that it is due to the non-monotonic increase of stress with strain at low strain rates, i.e. the existence of a static and dynamic yield stress, which allows for sheared and unsheared regions to coexist. Other obvious candidates affecting the flow of foams are liquid fraction and area-disorder. In this chapter I shall investigate how both parameters affect the shear localization of two-dimensional foams.

4.2 Effect of disorder

To quantify the effect of disorder on the shear localization of foams I shall consider foams in the dry limit, in which I can simulate over a thousand bubbles in order to reduce the possibility that finite size effects might interfere with the results. It is always best

to use as many bubbles as possible whilst keeping simulations tractable. System-wide events still occur even with a large system, but their occurrence becomes more remarkable with increasing system size. Disorder can be characterized in terms of topology using μ_2^n, the second moment of the distribution of the number of sides per bubble, n, or in terms of bubble areas using μ_2^A, the second moment of the distribution of bubble areas, A. Quilliet et al. [69] show that both measures correlate robustly after many shear cycles, but in my simulations, in which the shear is not cycled, the measures still show good correlation both before shearing and after 500 iterations (an applied strain of $\epsilon = 3.91$). Figure 4.2 shows $\sqrt{\mu_2^A}$ *versus* $\sqrt{\mu_2^n}/\langle n \rangle$, enabling comparison with the fit from the work of Quilliet *et al.* [69]. Even though the topological disorder varies as the foam is sheared, there is still an obvious correlation between both measures without any cycling. At low disorder however, the values of topological disorder remain high with respect to the expected value after several shear cycles since it is possible to have disordered monodisperse foams, but the topological disorder has reduced by approximately the same amount in each case under linear Couette shear.

First, I consider the flow of an ordered foam between parallel plates, i.e. hexagonal foams with no area-disorder and no topological disorder. Then I shall consider the effect of varying the area-disorder on the shear localization of a two-dimensional foam. I use the area-disorder rather than topological disorder as a control parameter since it is constant throughout each simulation. I will quantify the effects of varying area-disorder by introducing measures to characterize the position and width of the localized region.

4.2.1 Ordered foams in linear Couette shear

In this section I consider the linear Couette shear of an ordered two-dimensional foam between parallel plates in order to quantify the effect of area-disorder on the shear localization of the foam when disorder is introduced in subsequent sections.

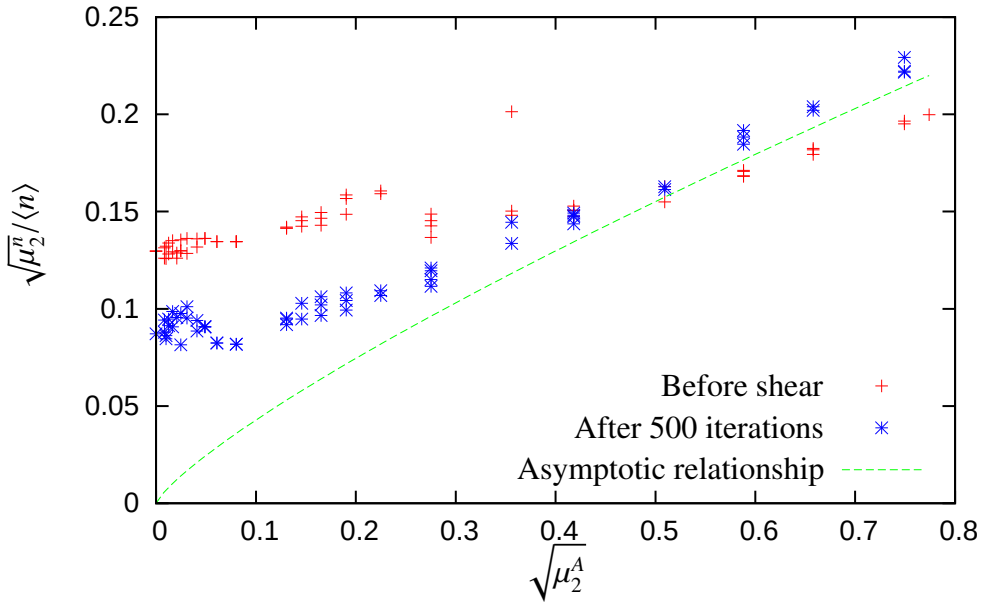

Figure 4.2: Topological disorder and area-disorder correlate robustly after several shear cycles (dashed line) [69]. In my simulations, where the shear is not cycled, a relationship between topological disorder and area-disorder is evident, both before any shear has taken place and after 500 shear steps.

I create an ordered two-dimensional foam consisting of 600 (30×20) bubbles between parallel plates (figure 4.3 (a)), and shear it affinely as described in section 2.7. The effective liquid fraction is $\phi_l = 1 \times 10^{-5}$. If the bubbles at the boundary were replaced with half hexagons of half the area, then the evolution of the structure would be identical to that of a perfectly ordered foam with periodic boundary conditions studied by Princen [30] in which the stress-strain relationship is given in section 3.3.1. Here, in order to preserve perfect ordering in terms of area, the bubbles at the boundary are given the same area as those in the bulk. The only effect that this has is to slightly increase the stress, due to the extra film length of the bubbles at the wall. The ordered foam does not exhibit any shear localization. The displacement profile (figure 4.4 (a)) is linear. Figure 4.4 (b) gives the y-coordinate of each T1 as a function of strain and shows that the T1s occur simultaneously and periodically. When considered in combination with figure 4.4 (c) which shows the (x, y)-coordinates of each T1 during an instant in which

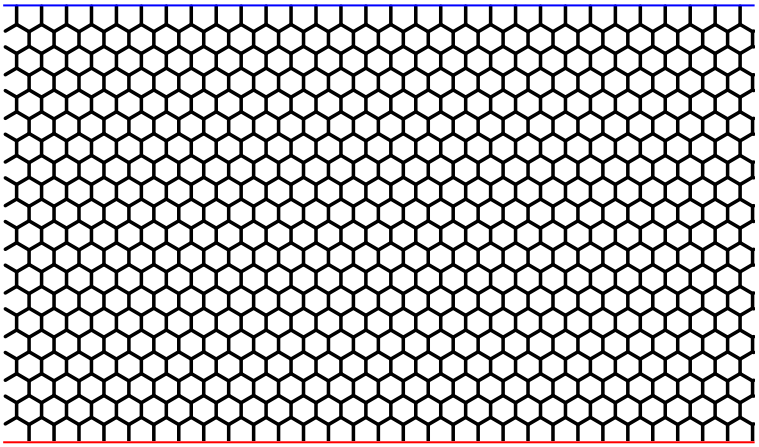

(a)

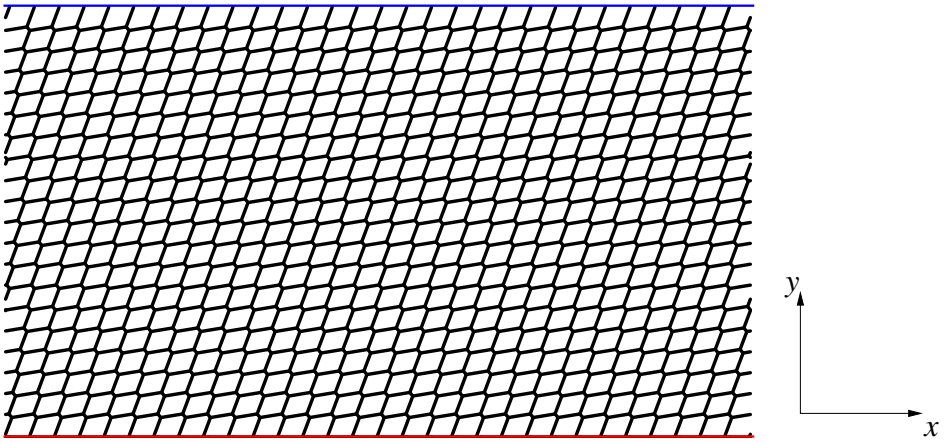

(b)

Figure 4.3: (a) Ordered foam of 600 bubbles between parallel plates. (b) As the foam is sheared affinely, each hexagon has two shrinking edges and all T1s occur simultaneously.

T1s occur, we see that the T1s occur uniformly throughout the foam as each shrinking film falls below the cut-off length at the same time (figure 4.3 (b)).

The absence of shear localization in the ordered case is due to the uniform distribution of T1s. The T1s do not localize and therefore the flow does not localize and shear localization does not occur. In the next section I show that if this precise ordering is disrupted, even by a small amount, then the effect on the flow is significant.

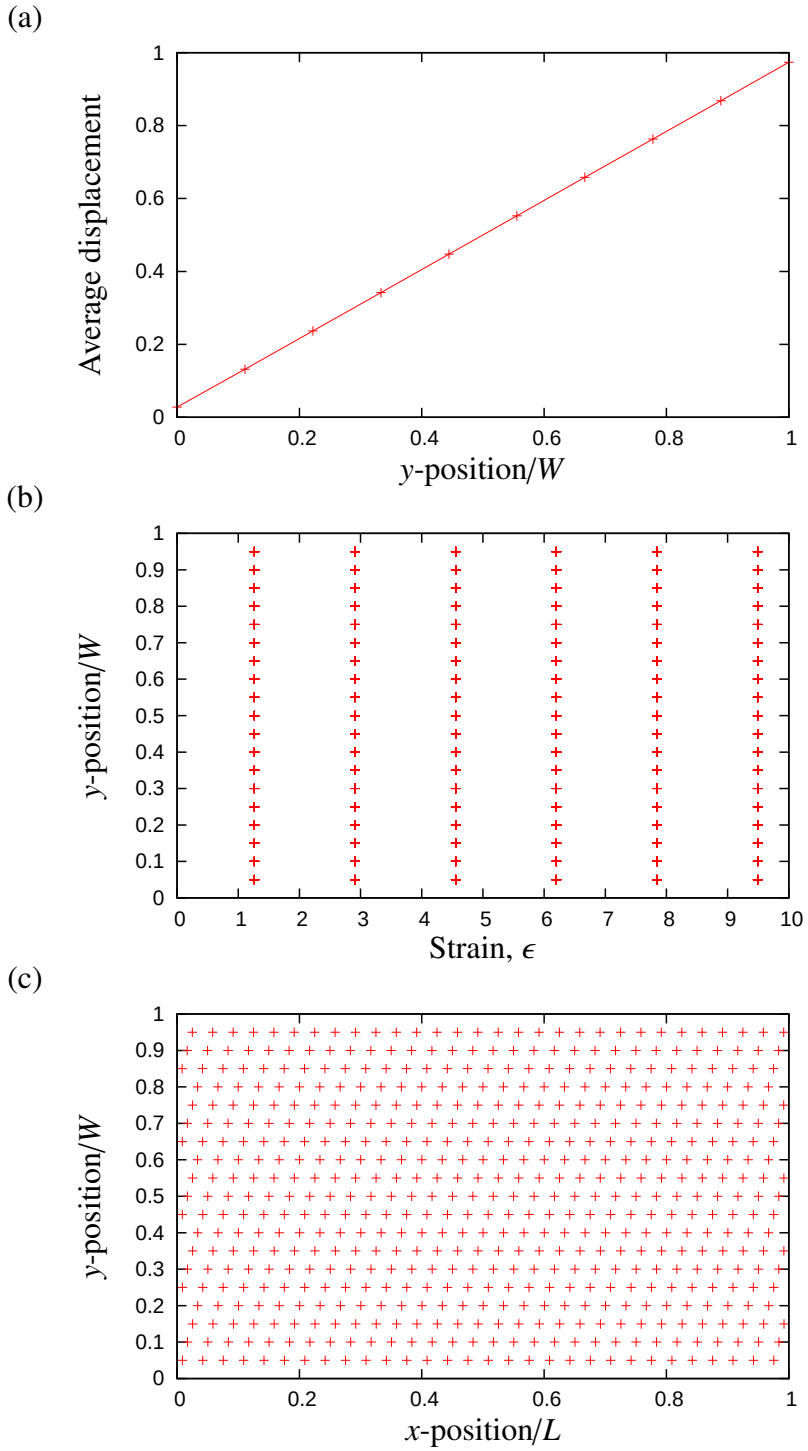

Figure 4.4: Ordered foams: (a) The average bubble displacement per unit strain is almost linear with respect to the distance from the moving wall. (b) T1s occur simultaneously during single system-wide rearrangements. (c) The location of each T1 during a strain increment in which T1s occur. The T1s are distributed uniformly in space.

4.2.2 Disordered foams in linear Couette shear

As discussed earlier, topological disorder and area disorder are related [69] and henceforth I shall only consider the effect of varying the area-disorder on the flow of the foam. I consider foams with $0 < \mu_2^A < 0.8$. Foams of 1120 bubbles are created as described in section 2.5 and examples of foams of different area-disorder are given in figure 2.6. The response of low area-disorder foams to applied strain is dramatically different to that of an ordered foam (section 4.2.1). Initially, a transient is observed in which the T1s occur throughout the foam, with no apparent spatial pattern. They then localize in a narrow band near one of the walls (figure 4.5 (a)). The transient behaviour is equivalent to a *pre-shear* typically applied in experiments, during which the material "forgets" the way in which it was created or inserted into the device.

As the area-disorder increases, the same behaviour is observed but the band of T1s near the wall becomes wider and therefore more of the foam is flowing (figure 4.5 (b)). Figure 4.6 gives the (x, y)-coordinate of each T1 after the transient (above a strain of 2), and shows no apparent spatial preference for T1s in the x direction. For the lowest value of area-disorder shown, $\mu_2^A = 0.0008$ the vast majority of T1s occur between the first and second layer of bubbles - this foam has crystallized i.e. the first two layers of bubbles have hexagonal ordering. For $\mu_2^A = 0.067$, the T1s can still be identified as occurring at the same places as the first two layers of bubbles slide over the others. For $\mu_2^A = 0.0549$, the area-disorder is sufficient to prevent the T1s occurring in the same spots and to allow T1s to spread further into the bulk, but the T1s still remain close to the wall. The increase in the width of the band of T1s can also be seen in figure 4.6 (b).

The displacement profile for very low area-disorder ($\mu_2^A = 0.0008$) shows an abrupt jump in displacement since only a single layer of bubbles is flowing whilst the others remain rigid. As the area-disorder is increased and the band of T1s widens, more layers of bubbles are flowing. The displacement profiles now appear exponential, like those of

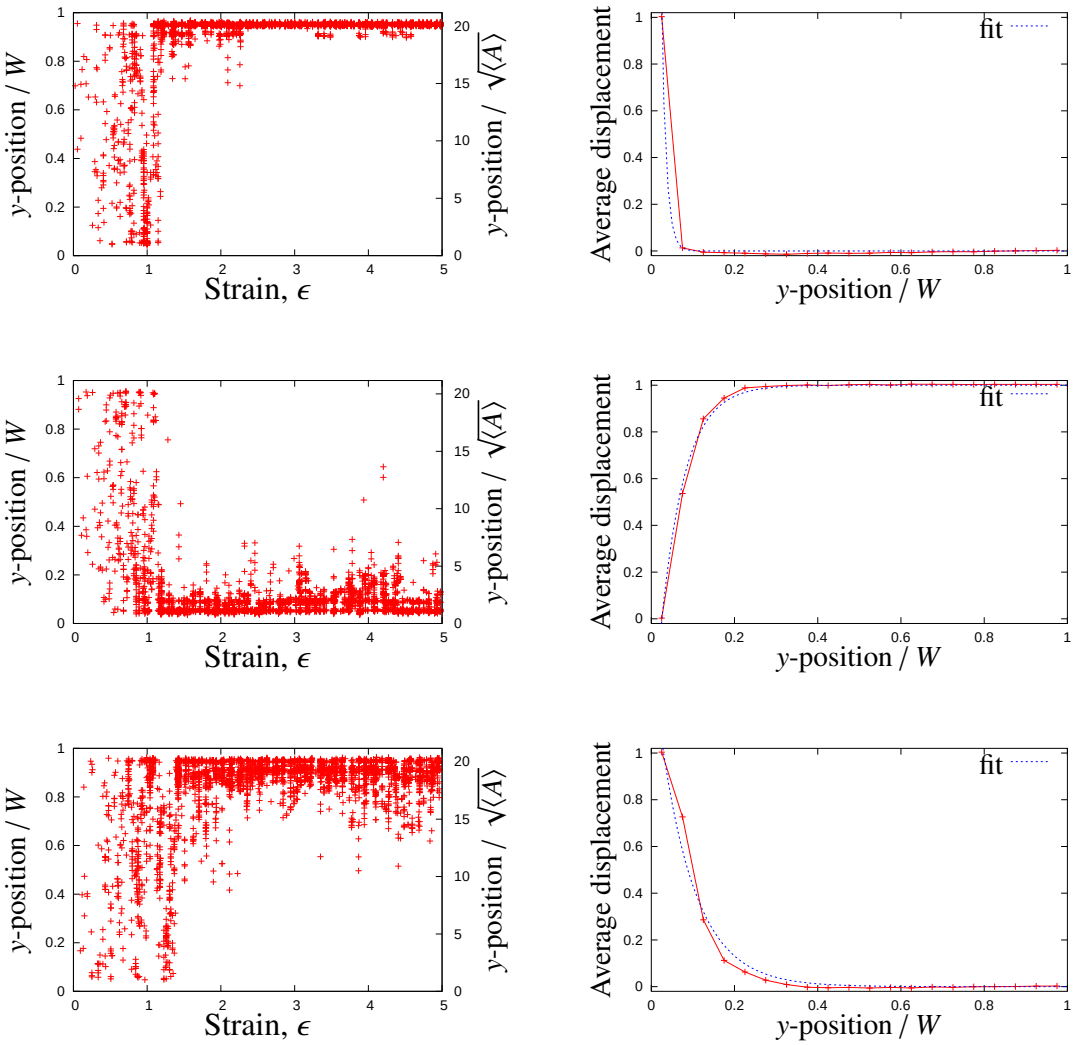

Figure 4.5: T1 localization for foams with low area-disorder. (a) y-position of each T1 versus applied strain and (b) displacement profiles for foams of low area-disorder: $\mu_2^A = 0.0008$ (top), $\mu_2^A = 0.0067$ (middle), $\mu_2^A = 0.0549$ (bottom). After an initial transient, the T1s localize in a band close to either of the walls. The width of this band increases with increasing area-disorder. The blue line is a fit of an exponential curve.

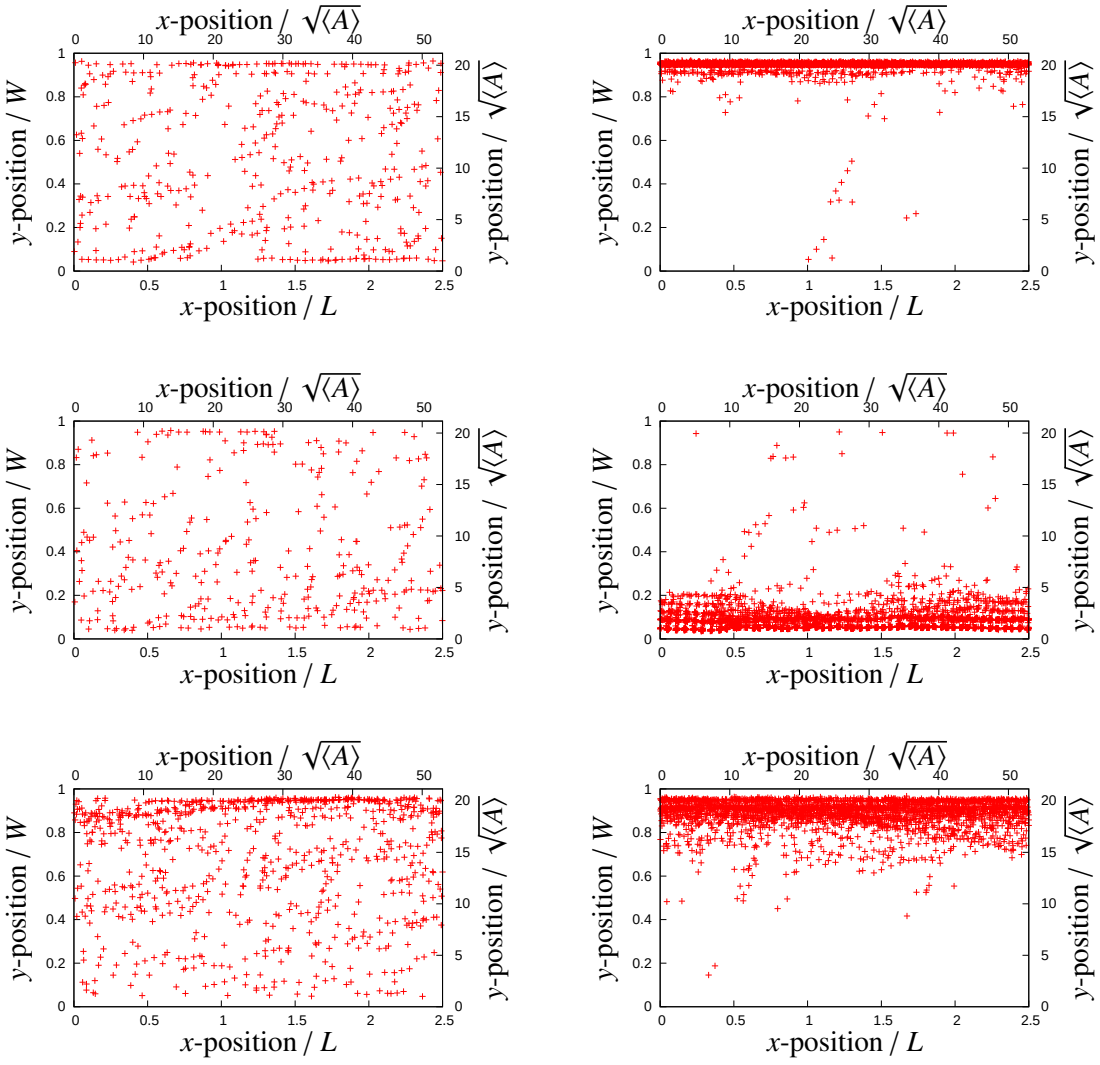

Figure 4.6: (x, y)-coordinate of each T1 for foams of low area-disorder: $\mu_2^A = 0.0008$ (top), $\mu_2^A = 0.0067$ (middle), $\mu_2^A = 0.0549$ (bottom), (a) during the transient regime and (b) after the transient regime. There is no apparent spatial pattern for the T1s during the transient regime, but afterwards most T1s occur in a band.

Kabla & Debrégeas [40] who simulated foams of similar area-disorder.

As the area-disorder is increased further, it becomes evident that T1 localization near one of the walls, along with the associated displacement profiles, are a sample of a range of possible behaviours which can be obtained through variation of area-disorder. With increasing area-disorder, the localized T1s need not be restricted to one of the walls and may choose a different location to localize or, more commonly, whilst the T1s will localize in space for significant intervals of applied strain, the position of the region of localized T1s is not restricted to its original location and is free to move. Figure 4.7 gives two examples of such foams. T1s remain in a given y-interval of the foam for strain intervals as long as one, but then move to a different region. Plotting the (x, y)-coordinates of each T1 for strains greater than 2 (after the transient regime) shows that when averaged over a larger intervals of applied strain, the T1s are far more evenly distributed in space than in foams of lower area-disorder (cf. figure 4.6 (b)).

The effect on the displacement profiles becomes significant. Whilst the displacement profiles averaged over small intervals of applied strain reflect the localized nature of the T1s, displacement profiles averaged over the entire applied strain interval after the transient are not exponential but are almost linear. The whole foam is flowing through a combination of an continued increase in the width of the band of T1s with area-disorder and the effect of a moving localized region. This observation is consistent with those of Jiang et al. [39] who observed regions of localized T1s for ordered foams, but not for disordered foams. I shall now quantify the effect of area-disorder on the position and width of the localized T1s and the effect this has on the flow of the foam.

4.2.3 Position of localized region

I now quantify the effect of area-disorder on the region of localized T1s, and in particular the position and movement of this region *after* the transient regime. I first calculate

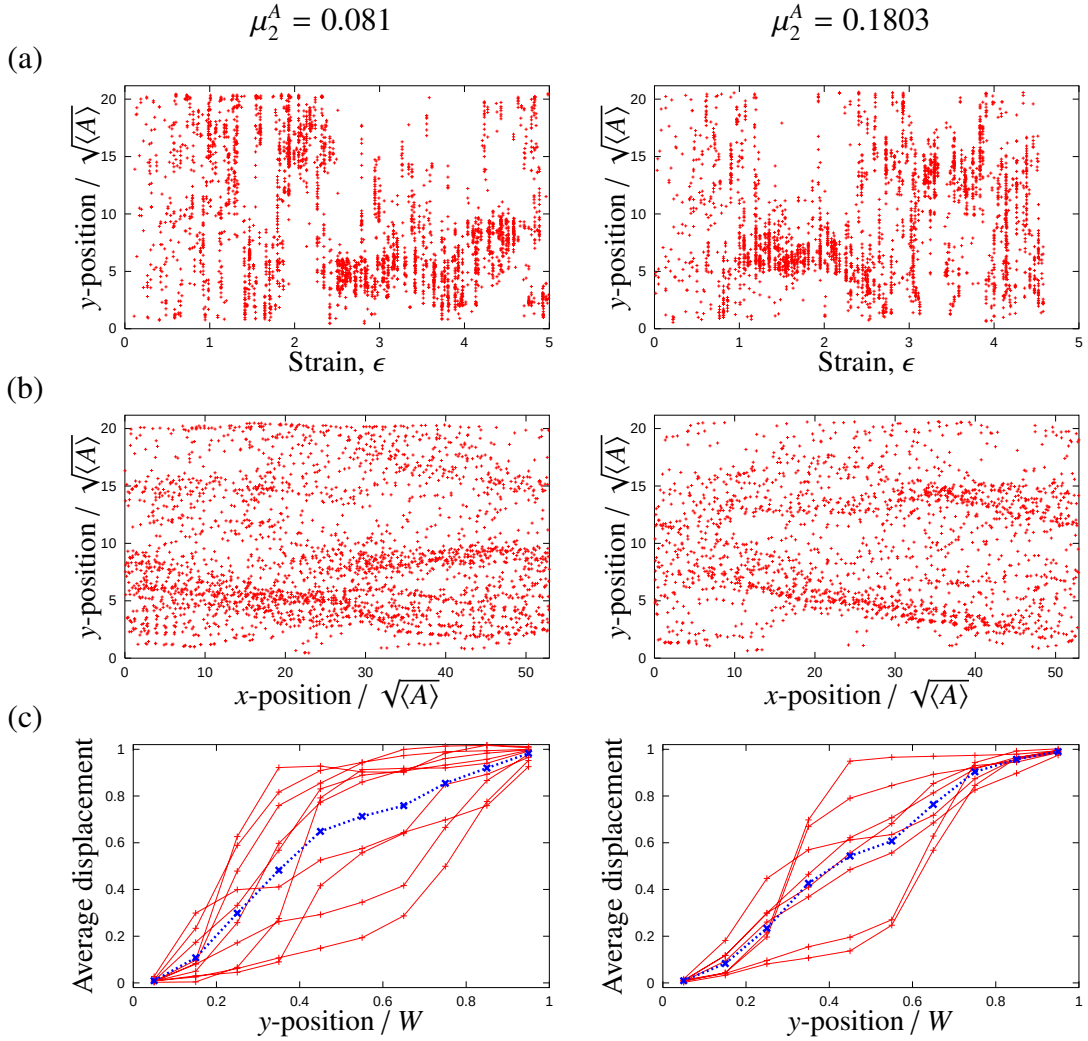

Figure 4.7: (a) The y-position of each T1 *versus* applied strain for foams of moderate area-disorder. (b) (x, y)-coordinate of each T1 for foams of moderate area-disorder after the transient. (c) Displacement of bubbles averaged over strain increments of 0.3 (red) and 3 (blue) for foams of moderate area-disorder. For sufficiently high values of area-disorder, although the T1s remain localized during large increments of applied strain, the region of localized T1s moves around, resulting in a more even distribution of T1s when the entire strain interval of applied strain after the transient is considered. Displacement profiles are localized when averaged over strain increments of 0.3 and almost linear when averaged over a strain increment of 3.

the mean y-coordinate, P_I, of all T1s (each occurring at position y_{T1}) in iteration intervals of size N_I, centred at I i.e. in the interval $B_I = [I - N_I/2, I + N_I/2]$.

$$P_I(N_I) = \frac{1}{N_{T1}} \sum_{y_{T1} \in B_I} y_{T1} \tag{4.3}$$

where N_{T1} is the number of T1s that occur in the interval B_I.

To determine the extent to which the localized region moves around, I then calculate the mean, Y_{T1}, and range, R_{T1}, of P_I over all I (from $I = 200$, after the transient, to the end of the simulation at $I = I_{\max}$) at fixed N_I:

$$Y_{T1} = \frac{1}{I_{\max} - N_I - 200} \sum_{I=200}^{I_{\max}-N_I} P_I(N_I) \tag{4.4}$$

$$R_{T1} = \max_{I \in [200, I_{\max}-N_I]} P_I(N_I) - \min_{I \in [200, I_{\max}-N_I]} P_I(N_I) \tag{4.5}$$

The mean, Y_{T1}, and range, R_{T1}, of the instantaneous positions of the localized region, P_I, for each iteration after the transient will be a good indicator of how much the localized region moves around under applied strain and of whether the localized region is restricted to be near one of the walls. The number of iterations chosen per bin does not have a significant effect on the outcome (data not shown).

As the area-disorder is increased the mean position of the localized region, Y_{T1}, moves away from the walls into the bulk of the foam (figure 4.8 (a)), and the position of the localized region becomes more volatile (figure 4.8 (b)). At low area-disorder the localized region remains within a very small range and R_{T1} is small. As the area-disorder increases so does R_{T1} and so the localized region moves around a lot more. This is consistent with what has been observed in previous sections (figures 4.5 and 4.7): the mobility of the localized region increases the amount of foam where T1s occur, when a larger interval of applied strain is considered. Therefore the stable shear bands that occur at low area-disorder lose their stability as the area-disorder is increased. The

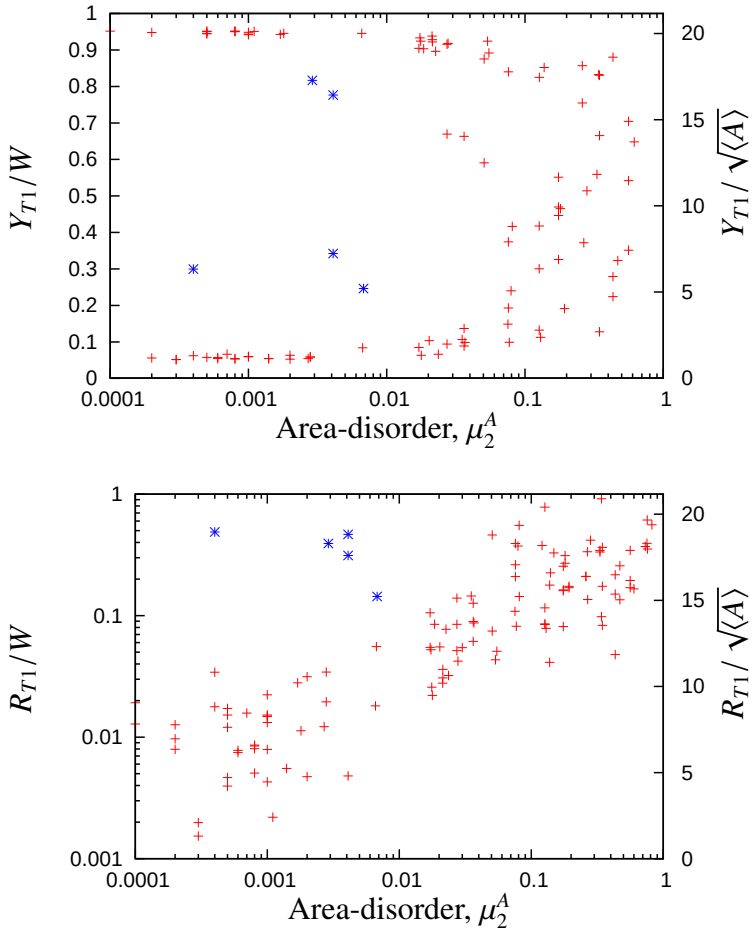

Figure 4.8: (a) The mean position of the localized region, Y_{T1} *versus* area-disorder, μ_2^A. As the area disorder is increased, the localized region can occur away from the walls of the channel. (b) The range of the position of the localized region, R_{T1}, *versus* area-disorder, μ_2^A. The localized region moves to cover an increasing fraction of the channel as the area-disorder is increased. In each case the y-position is normalized by the channel width on the left hand axis and by bubble diameter on the right hand axis.

outlying points on both graphs, coloured blue, are examples of low area-disorder foams in which the shear band became temporarily unstable and the region of localized T1s moved away from the walls of the channel, either briefly or for an extended period. It is not clear why this is the case for foams of such low area-disorder but it seems that a shear band can become unstable even at low area-disorder.

4.2.4 Width of localized region

I now introduce a measure of the width of the localized region, w_{T1}. The standard deviation of the y-positions of the T1s is not used as a measure of width since it is very sensitive to outlying T1s and does not provide an accurate representation of the observed width of the localized region.

I calculate the mean y-coordinate, P_I, of all T1s in the interval $B_I = [I - N_I/2, I + N_I/2]$ as in the previous section, given by equation (4.3). Next, I introduce y-positions, w_u and w_d, to define the interval $Y_I(N_I) = [P_I - w_d, P_I + w_u]$. The fraction of T1s occurring during the interval B_I whose y-coordinate are in $Y_I(N_I)$ is denoted ψ_{T1}. I choose a value for ψ_{T1} and increase w_d and w_u from zero until this value is reached.

If, at any time, w_u or w_d reaches half a typical bubble width from the walls i.e.

$$w_u = W - \frac{1}{2}\sqrt{\langle A \rangle} \quad \text{or} \quad w_d = \frac{1}{2}\sqrt{\langle A \rangle} \tag{4.6}$$

then the interval stops growing at the end which is near the wall and grows on the other side only. The instantaneous width of the localized region, w_I, at iteration I is the size of the interval Y_I and is given by

$$w_I = w_u + w_d \tag{4.7}$$

and the localization width is calculated by averaging all of the w_I:

$$w_{T1} = \frac{1}{I_{\max} - N_I - 200} \sum_{I=200}^{I_{\max}-N_I} w_I. \tag{4.8}$$

w_{T1} has two parameters which affect the resulting width. The number of iterations in a bin, N_I, and the percentage of T1s from each bin required in the y-interval, ψ_{T1}. A suitable choice of parameters is required to accurately represent the true width of the localized region. Figure 4.9 illustrates some combinations of parameters for different foams. An appropriate choice of parameters should not be affected by a moving localized region and provide a good measure of the true width for a range of different foams.

Firstly note that for a foam of relatively low area-disorder, where the localized region does not move around, ψ_{T1} and N_I have a small effect on the measured width. When the area-disorder is higher, more care must be taken in choosing the parameters since the localized region may move around. As the bin size increases, the measured width increases and reaches a plateau for each value of ψ_{T1}, since the bin size is too large to detect regions of localized T1s. In fact, if N_I is large then w_{T1} is roughly equivalent to R_{T1}, the range of the instantaneous positions of the localized region. If the bin size is too small, there will be bins with no T1s, and the measured width will be too small. For the first foam, the localization width is approximately 1-2 typical bubble widths, for the last two foams in figure 4.9 the localization width should represent bands of T1s of approximately 7 and 10 typical bubble widths. The parameters $\psi_{T1} = 0.8$ and $N_I = 50$ result in a good measure of the width of the localized region in each case. Figure 4.10 shows the relationship between localization width and area-disorder using these parameters.

w_{T1} exhibits power law behaviour as functions of disorder. The fit in figure 4.10 is

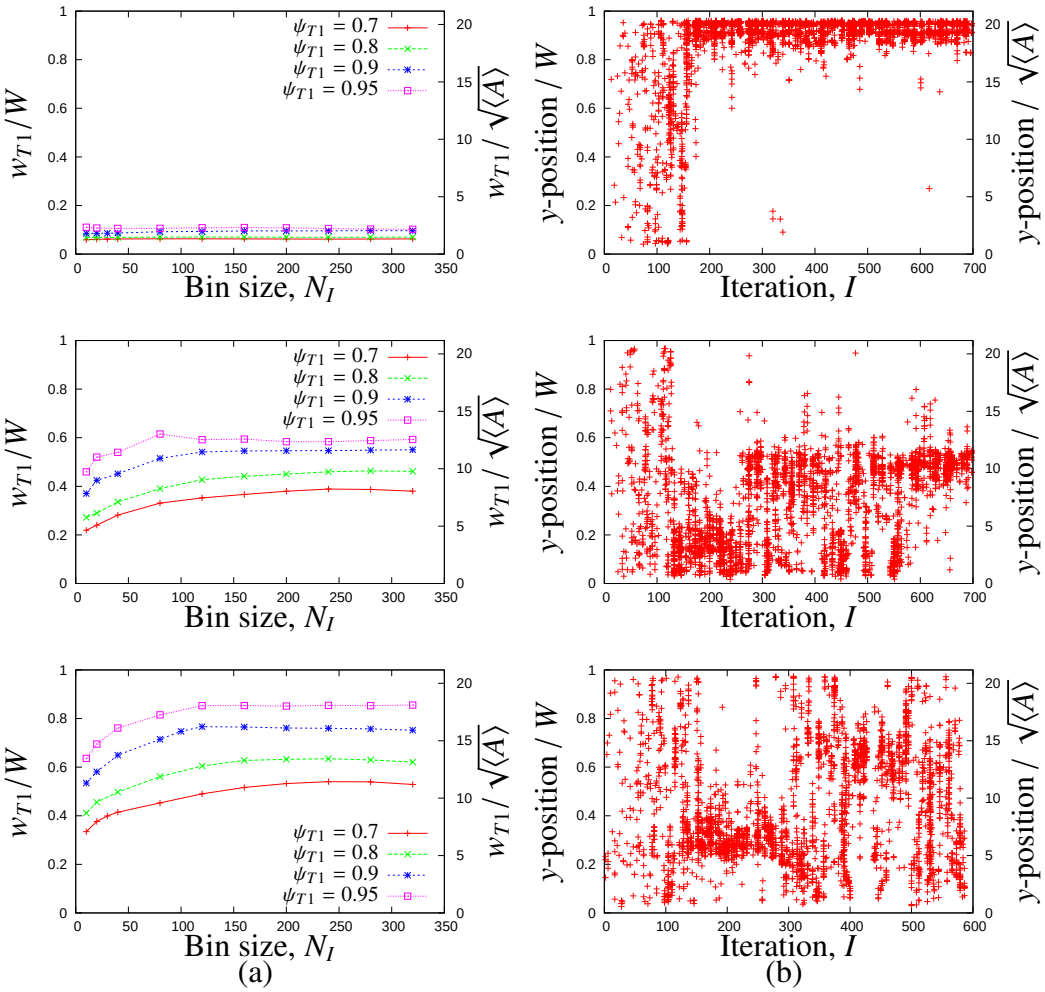

Figure 4.9: (a) The localization width, w_{T1}, *versus* bin size, N_I, for different values of ψ_{T1} for foams in which the y-position of each T1 *versus* iteration number is given in (b).

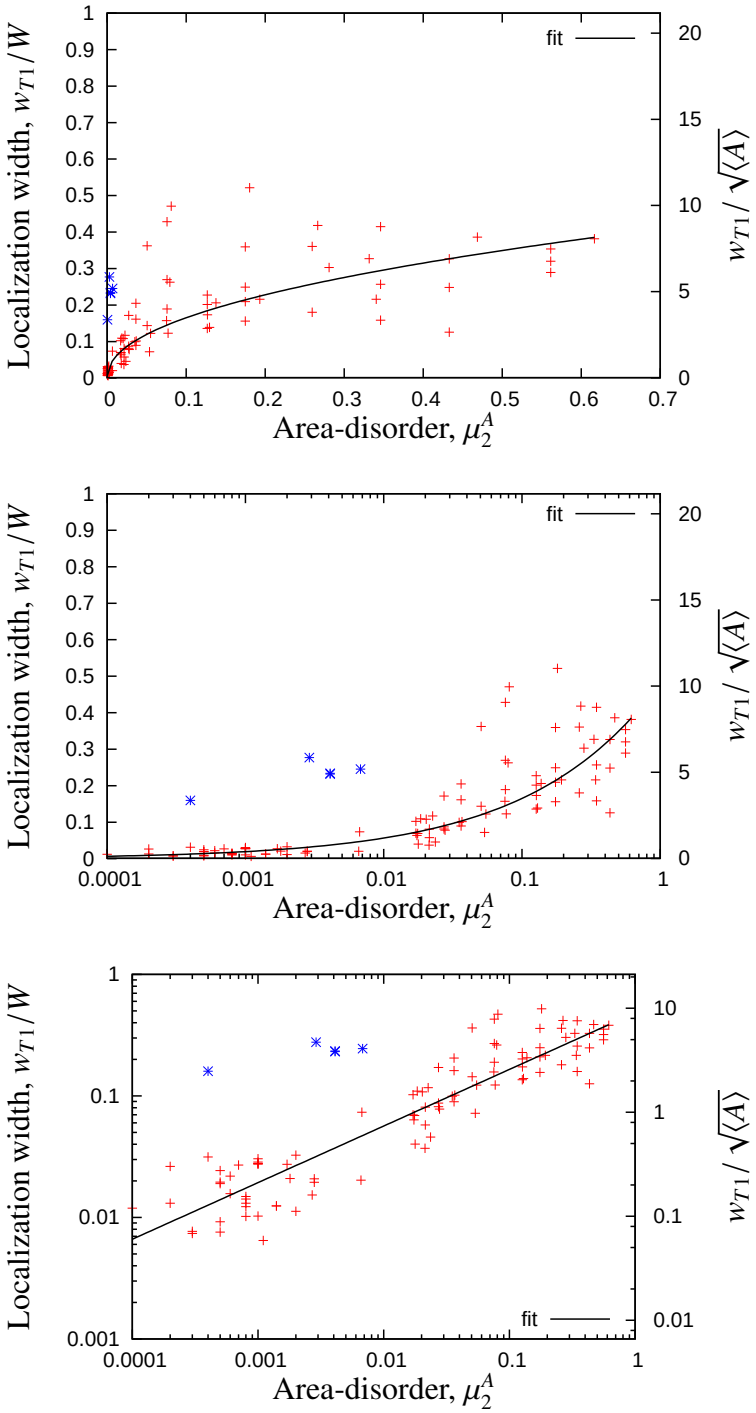

Figure 4.10: The localization width w_{T1} *versus* area-disorder μ_2^A plotted on different axes. The fit is given by equation (4.9). The localization width increases with increasing area-disorder and is approximately proportional to the square root of area-disorder.

given by

$$\frac{w_{T1}}{W} = 1.5(\mu_2^A)^{0.47} \tag{4.9}$$

In terms of typical bubble widths, the localization width is given to a good approximation by

$$\frac{w_{T1}}{\sqrt{\langle A \rangle}} \approx 10\sqrt{\mu_2^A}. \tag{4.10}$$

for the chosen values of ψ_{T1} and N_I. The localized region extends on average up to ten times a typical bubble width, although for foams of high disorder this can sometimes be larger over intervals of applied strain where the localized region is moving, as in the bottom two foams in figure 4.9. The outlying points in blue are low area-disorder foams, in which the region of localized T1s has moved from the wall of the channel, and correspond to the same simulations highlighted in blue in figure 4.8.

4.3 Localized foam structure

I have shown that the flowing region of a dry two-dimensional foam is influenced by the movement of the region of localized T1s to other regions of the foam. It would therefore be useful if it were possible to predict when and where the region of localized T1s would move. To this end, I will highlight the differences in structure between regions of the foam which are in the region of localized T1s and regions which are not, and describe measures which are successful in identifying the localized region given instantaneous information solely about a foam's structure. Perhaps the most obvious measures, the local topological disorder and area-disorder, are not sensitive to the region of localized T1s. Instead, I describe a tensorial measure of local structure and a simple

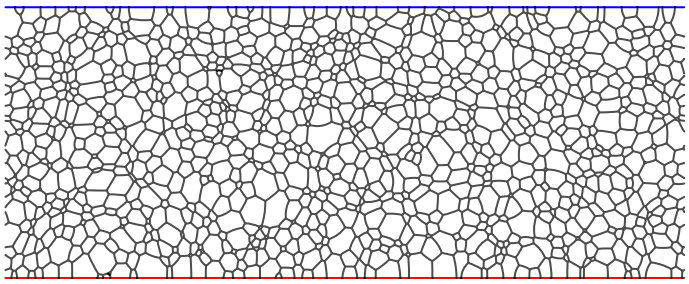

(a)

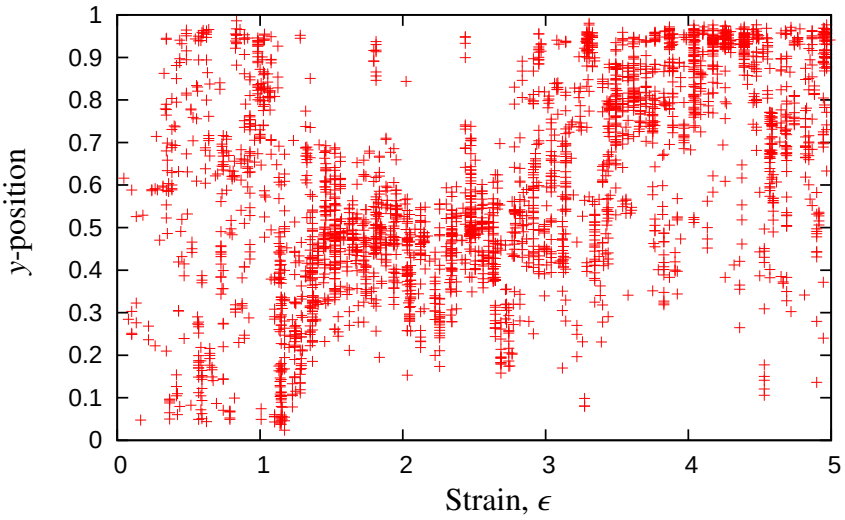

(b)

Figure 4.11: (a) A foam with $\mu_2^A = 0.561$, used to illustrate measures that can identify a localized region. (b) The y-position of each T1 *versus* applied strain for the foam in (a).

one-dimensional measure which can identify the localized region of foam e.g. from a still image. The foam in figure 4.11 (a) will be used throughout to illustrate the ability of each measure to identify the localized region. The foam has area-disorder $\mu_2^A = 0.561$ and was chosen since the localized region moves, providing a sterner test of the measures ability to identify the localized region. The y-position of each T1 *versus* applied strain is given in figure 4.11 (b).

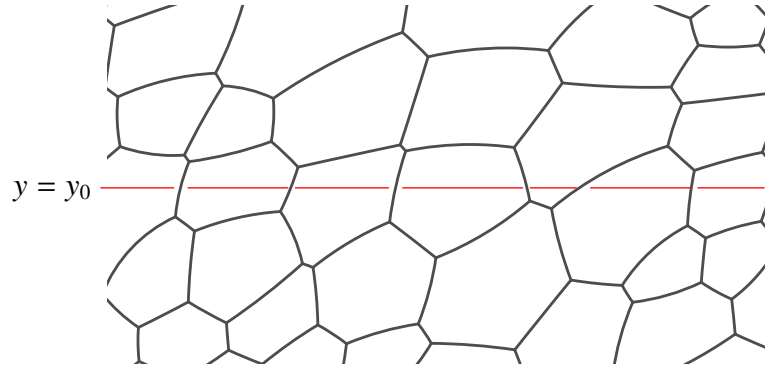

Figure 4.12: Calculating $\mathcal{L}_y$: The average length of the line segments on $y = y_0$ (red) that cover each bubble is calculated for each $y \in [0, W]$.

4.3.1 One-dimensional measures

I describe simple one-dimensional measures which may be sensitive to the region of localized T1s.

1. The local area-disorder, $\mu_2^{A,\mathrm{loc}}$, measured in horizontal strips of the foam.

2. The local topological disorder, $\mu_2^{n,\mathrm{loc}}$, measured in horizontal strips of the foam.

3. The average area of the bubbles where the y-coordinate of their centre is within a horizontal strip of the foam, $\langle A \rangle^{\mathrm{loc}}$.

4. The average length, $\mathcal{L}_y$, of the horizontal line $y = y_0$ that is covered by each bubble, and is calculated for each $y \in [0, W]$ (figure 4.12), sometimes referred to as the linear intercept method [138].

Figure 4.13 shows each measure at three different strains for the foam where the y-position of each T1 versus strain is plotted in figure 4.11 (b). The only measure to correctly identify the localized region is $\mathcal{L}_y$, i.e. it is the only measure that has a pronounced peak in the appropriate range of y. For $\epsilon = 0$, $\mathcal{L}_y$ has no pattern. At strains beyond the transient regime, $\mathcal{L}_y$ is maximized in the localized region. For $\epsilon = 1.5$, $\mathcal{L}_y$ is maximized in the centre of the channel at $y/W = 0.5$, coinciding with the region of

localized T1s. For $\epsilon = 3.125$, $\mathcal{L}_y$ is maximized in the top of the channel at $y/W = 0.78$, with further peaks at the centre of the channel, reflecting the uncertainty in the position of the localized region during a time of transition from the centre of the channel to the top. For $\epsilon = 4$, $\mathcal{L}_y$ is maximized in the top of the channel at $y/W = 0.92$ and the localized region has now settled at the top of the channel. In figure 4.14 I superimpose $\mathcal{L}_y^{\max}$ the y-position at which $\mathcal{L}_y$ reaches a maximum at the corresponding strain, onto the y-position of the T1s versus applied strain. Although $\mathcal{L}_y$ is very noisy, it consistently identifies the region in which the T1s have localized. The other measures in figure 4.13 either have peaks in regions where there are no T1s or are missing peaks in regions where the T1s are localized.

4.3.2 Texture tensor

In the previous section I showed that a one-dimensional measure of a foam's structure can identify regions of localized T1s and regions of no T1s from a single image. The Texture tensor [139; 140] is a tensorial measure of the foam structure and may provide more information regarding which features of the foam structure allows identification of the region of localized T1s. The Texture tensor, $\mathbf{M}$, is calculated from a foam structure and quantifies the local deformation of the foam. It is a symmetric tensor given, in two dimensions, by

$$\mathbf{M} = \begin{pmatrix} M_{xx} & M_{xy} \\ M_{yx} & M_{yy} \end{pmatrix} = \langle \mathbf{l} \otimes \mathbf{l} \rangle = \begin{pmatrix} \langle l_x^2 \rangle & \langle l_x l_y \rangle \\ \langle l_x l_y \rangle & \langle l_y^2 \rangle \end{pmatrix} \tag{4.11}$$

where $\mathbf{l}$ denotes the link joining neighbouring bubble centres. l_x and l_y are the components of $\mathbf{l}$ in the x and y directions respectively, $\otimes$ denotes a tensor product and $\langle . \rangle$ denotes an average over a representative area of foam. $\mathbf{M}$ can be diagonalized and the largest eigenvalue of $\mathbf{M}$, λ_1, gives the degree of stretching and the corresponding eigen-

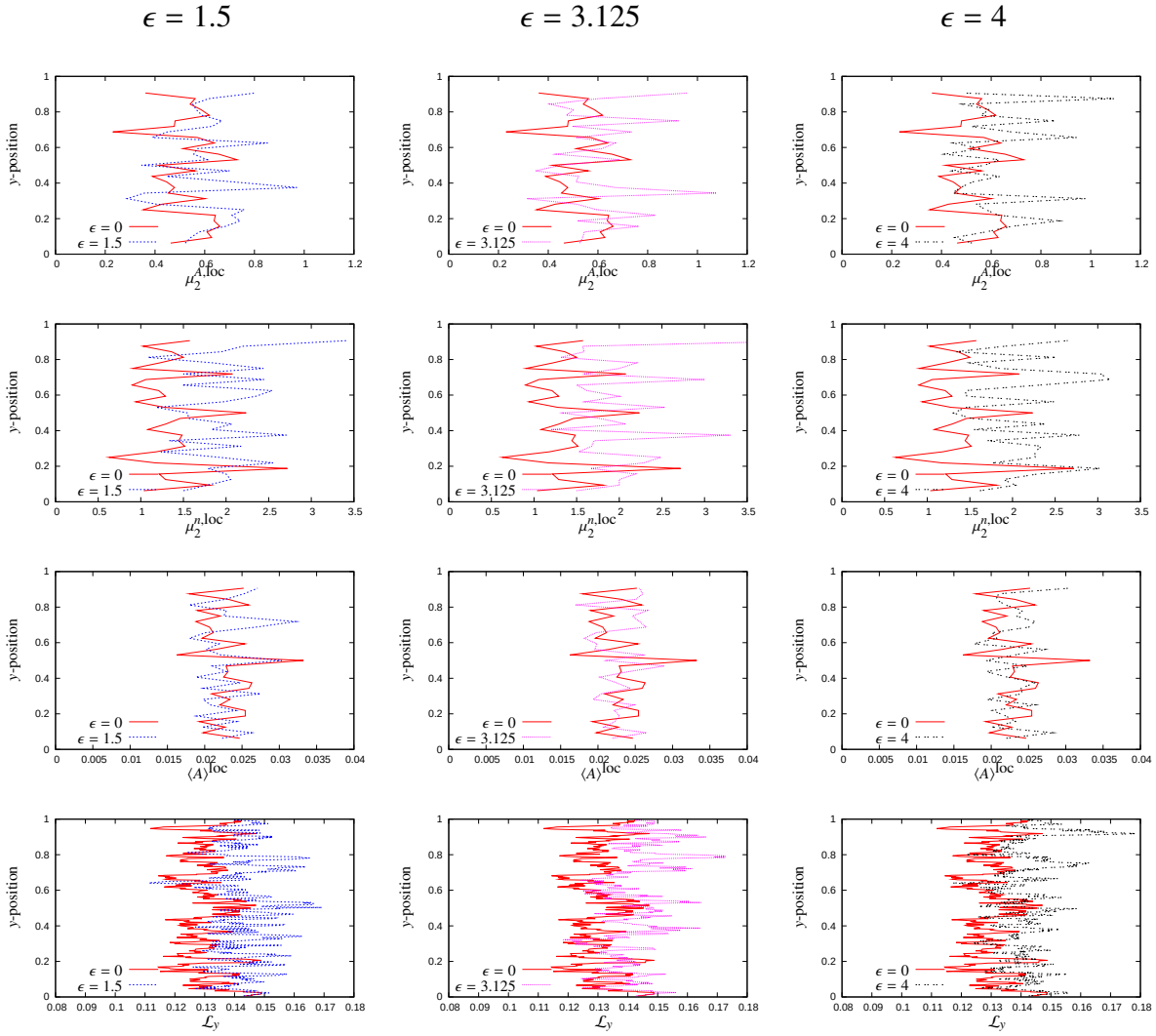

Figure 4.13: One dimensional measures as a function of y-position at different strains for the foam in figure 4.11. The one-dimensional measure $\mathcal{L}_y$ is sensitive to the region of localized T1s whilst more obvious measures are not, i.e. it is the only measure that has a pronounced peak in the appropriate range of y (see text and cf. figure 4.11 (b)).

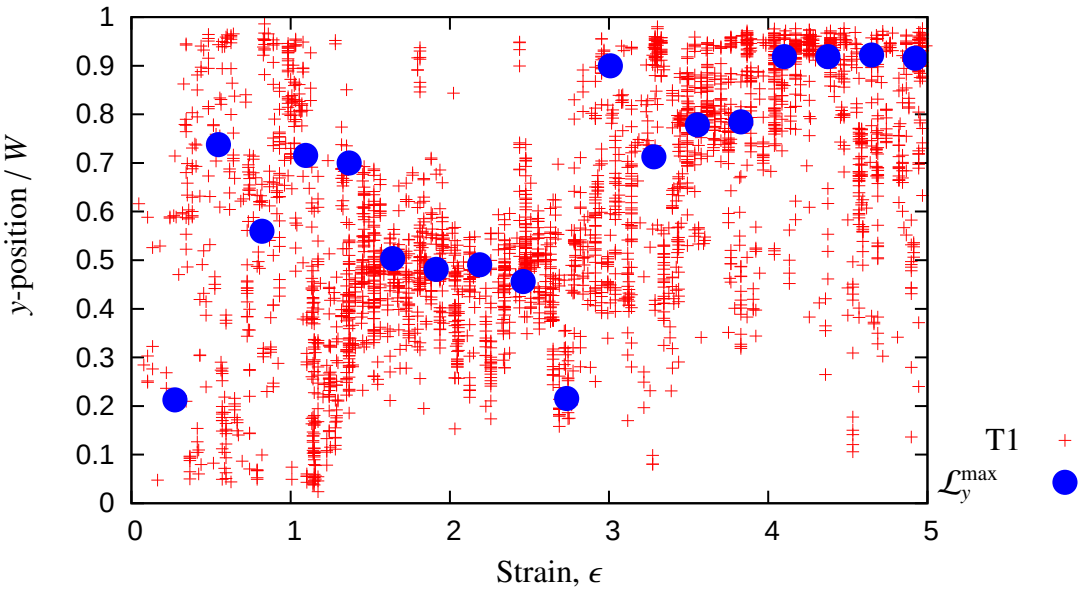

Figure 4.14: The y-position of each T1 versus applied strain for a foam with $\mu_2^A = 0.561$ (figure 4.11). The maxima of one-dimensional measure $\mathcal{L}_y$, superimposed as blue dots at strain intervals of 0.27, consistently identities the region of localized T1s.

vector, $\mathbf{e_1}$, points in the direction in which bubbles are being stretched. The eigenvector, $\mathbf{e}_2$, of the other eigenvalue, λ_2, will be perpendicular to $\mathbf{e}_1$. The angle that the direction of stretching makes with the direction of shear, θ_T, is a measure of the *orientation* of the bubbles. I choose to use arrows to represent the Texture tensor: they point in the direction of the eigenvectors with length proportional to the eigenvalues. The Texture tensor can also be represented as an ellipse with major and minor axes of magnitude proportional to the eigenvalues of $\mathbf{M}$ (figure 4.15).

Figure 4.16 gives the y-position of each T1 versus strain for a 1120 bubble dry foam with μ_2^A =0.561 (as in figure 4.11) and the Texture tensor calculated at strain intervals of one and averaged over 20 horizontal strips of the foam. At zero strain the foam is undeformed, both eigenvalues are roughly equal and eigenvectors are mostly in the x or y directions implying little bubble orientation or deformation. As the foam is strained, bubbles re-orient, indicated by the direction of the arrows, and the arrows stretch further in the regions where the foam is most strained, causing T1s to occur. At $\epsilon = 3$, the foam

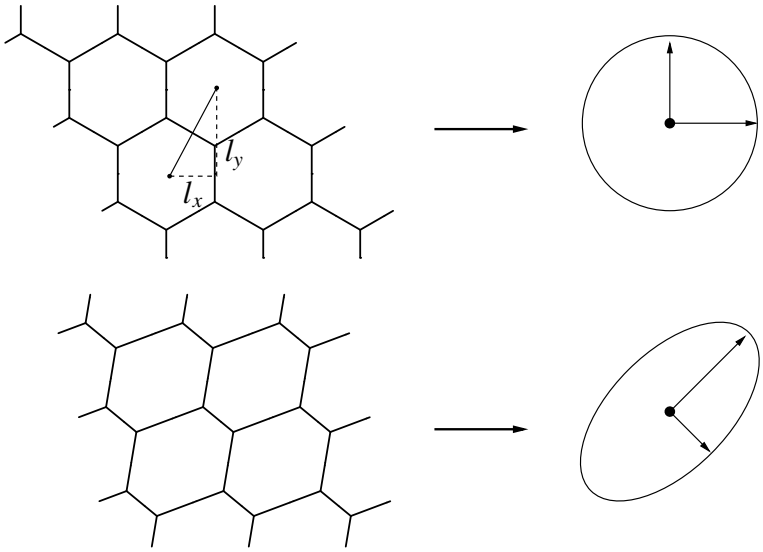

Figure 4.15: The Texture tensor is calculated from the x and y components, l_x and l_y, of all bubble centre-to-centre links within a chosen region of a foam, and can be represented as an ellipse, or by two perpendicular arrows. The largest arrow points in the direction of the largest eigenvector of $\mathbf{M}$ and indicates the direction in which the foam is being stretched, and the orientation of the bubbles.

is in a transitional period where the region of T1s is moving and this uncertainty in T1 position is reflected in the Texture tensor. In cases where the regions of T1s are not well defined it can be difficult to pick out these regions just by looking at the texture tensor.

I plot each individual component of the Texture tensor, along with the eigenvalues, for a better understanding of which features of the Texture tensor cause it to identify the localized regions. Figure 4.17 gives the components of $\mathbf{M}$ as a function of y-position. M_{xx} and M_{yy}, which are measures of stretching in the x and y directions respectively, have similar starting values. As the foam is strained, M_{xx} increases whilst M_{yy} decreases. The average values of M_{xx} and M_{yy} stay the same after the transient, but show fluctuations across the channel. M_{xy} is a measure of the local shear strain, and starts at zero and increases to a value which is constant on average but fluctuates across the channel. As the foam is strained, M_{xx} and M_{xy} are maximized in the localized region. At $\epsilon = 3$, where the region of localized T1s is moving, there are two peaks for M_{xx} as a function of y-position. There seems to be no relationship between M_{yy} and the localized

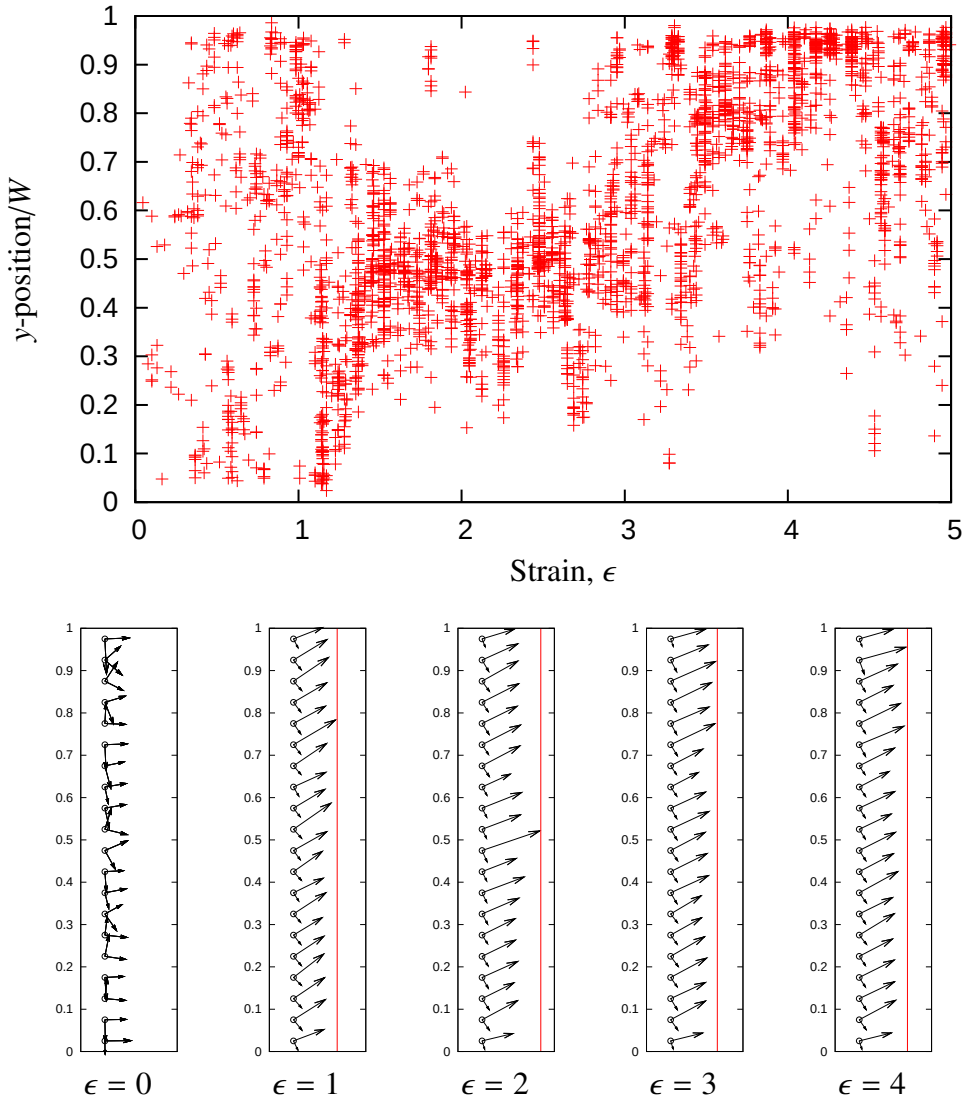

Figure 4.16: The Texture tensor is sensitive to the region of localized T1s. The Texture tensor is calculated for horizontal strips in the foam shown in figure 4.11 (a) at different strains. The y-position of each T1 *versus* strain is repeated here for easy comparison with the Texture tensor. When measured for the undeformed foam ($\epsilon = 0$), there is no apparent pattern, but for other applied strains, the Texture tensor picks out regions of T1s. The case $\epsilon = 3$ occurs during a transitional period where the region of localized T1s is moving and this uncertainty is reflected in the Texture tensor.

region. Therefore it is the component of centre-to-centre links in the direction of shear which is sensitive to the region of localized T1s, which contributes to both M_{xx} and M_{xy}.

M_{xy} is a measure of local strain [141], the shear modulus can therefore be approximated by

$$G = \left.\frac{\mathrm{d}\tau_{xy}}{\mathrm{d}\epsilon}\right|_{\epsilon=0} \approx \frac{\tau_{xy}}{M_{xy}}. \tag{4.12}$$

Since M_{xy} is maximized in the localized region and in the linear Couette geometry the shear stress should be homogeneous throughout the channel, G will be minimized in the localized region, indicating that localization arises as a consequence of a localized structural "weakness" in the foam. If the localization is thought of in terms of the foam fracturing, this picture is consistent with other elastoplastic materials, where a crack or weakness in the material propagates and results in fracture. The fact that the localized region can move to another region of the foam suggests that a foam can recover from this failure.

Figure 4.17 also gives the eigenvalues of the Texture tensor as a function of y-position. Initially there is no pattern to the profile, but at subsequent strains, λ_1 is maximized in the region of localized T1s. λ_2 shows a weaker, if any, correlation with the localized region. Of the two eigenvalues, it is λ_1 that identifies the region of localization and this can be seen in figure 4.16 where the arrows are longest in the localized region. The bubbles are therefore more stretched in the localized region. The direction in which they are stretched is given by θ_T, the angle that the eigenvector corresponding to the largest eigenvalue makes with the direction of shear. In figure 4.17, this orientation is plotted as a function of y-position. Initially, since the foam is not under any applied strain, the eigenvalues are of similar magnitude. The direction of stretching has little relevance in this case since the bubbles are largely unstrained and therefore the orientation of the bubbles loses its significance [141]. θ_T at $\epsilon = 0$ is not plotted in figure 4.17 since it fluctuates greatly and obscures the data for θ_T at other strains. As the foam

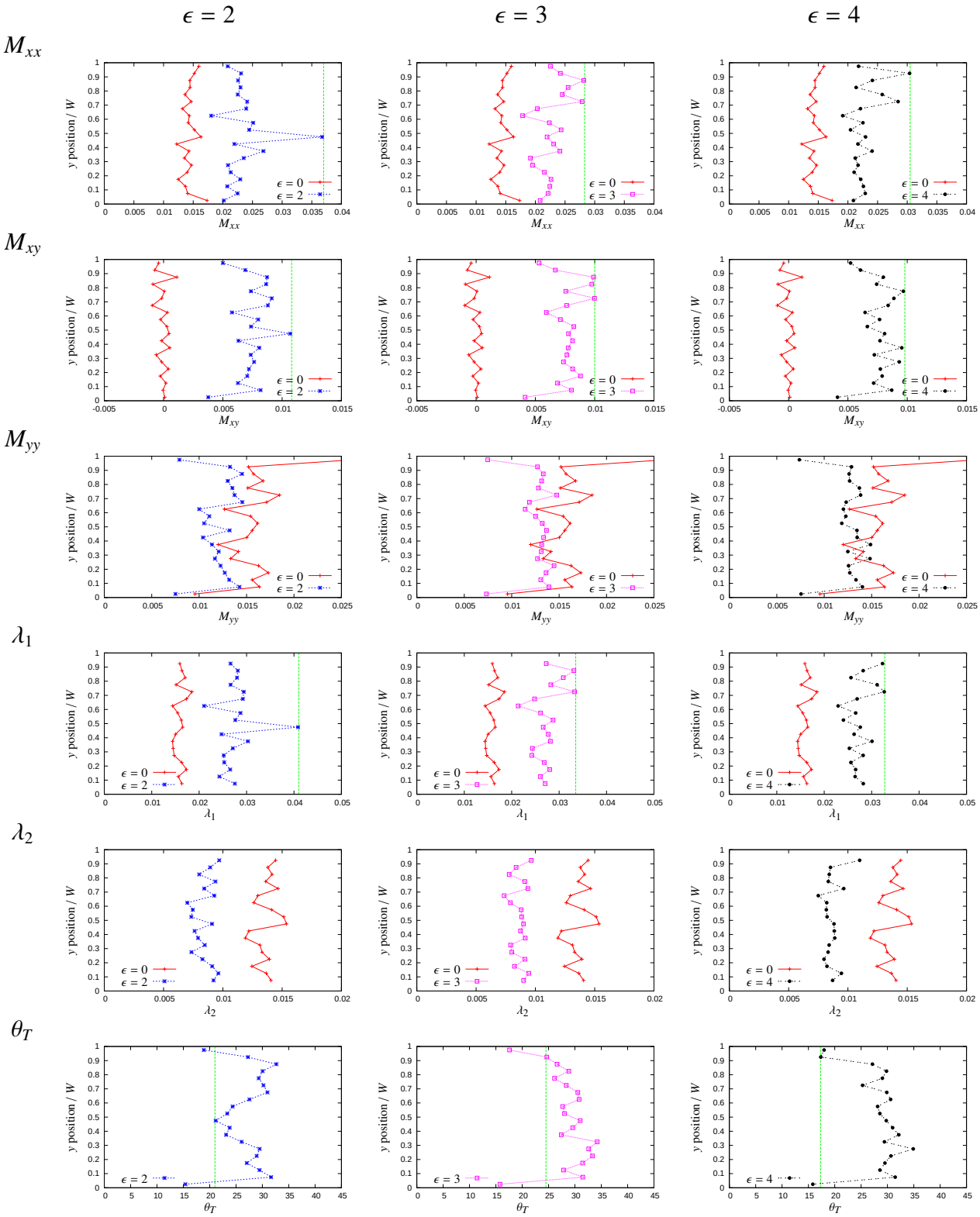

Figure 4.17: The individual components of the Texture tensor, eigenvalues and orientation as a function of y-position for the same foam as in figure 4.16 compared with their values at $\epsilon = 0$. The average value of M_{xx}, M_{xy} and M_{yy} doesn't change, but fluctuates. λ_1, M_{xx} and M_{xy} are sensitive to the region of localized T1s in that they have peaks corresponding to the localized regions whilst the θ_T is minimized in the same region.

is strained, the bubble orientation is smallest in the region of localized T1s, provided that the points at the boundary, which are fixed at about 15° to 20°, are not considered.

4.4 Bubble dynamics during flow localization

Thus far in this chapter I have shown that for quasistatic shear of dry foams, the T1s become localized in space, and that the position and size of the localized region depends on the area-disorder of the foam. In this section I consider the movement of the bubbles as the foam is sheared. Having seen that area-disorder has a significant impact on the position and spatial distribution of T1s and hence the flow of dry two-dimensional foams, I shall turn my attention to the behaviour of the individual bubbles during the flow. To do so I shall examine instantaneous displacement vector plots.

Figure 4.19 gives the instantaneous displacement fields at different strains during the transient flow of the linear Couette shear of the 1120 bubble foam shown in figure 4.11. The arrows represent the displacement of the bubble centres during a strain increment of $\delta\epsilon = 0.0078$ where the magnitude of the vectors has been multiplied by four. At low strains there are no T1s and most strain increments result in affine displacement of the bubbles, as in figure 4.19 (a). Even a single T1, as in figure 4.19 (b), has little impact on the overall flow field. As the applied strain increases, there is a smaller proportion of strain increments in which no T1s occur and the displacement fields are like those shown in figure 4.19 (c) and (d), where T1s occur in spatial clusters, forming what are known as quadrupolar macroscopic rearrangements (figure 4.18) [142]. The effects of the T1s are felt across the channel so that the presence of the channel wall has an impact on the rearrangement dynamics (figure 4.19 (d)). The extent of this impact is considered later in this section.

Figure 4.20 gives the instantaneous displacement fields at different strains during

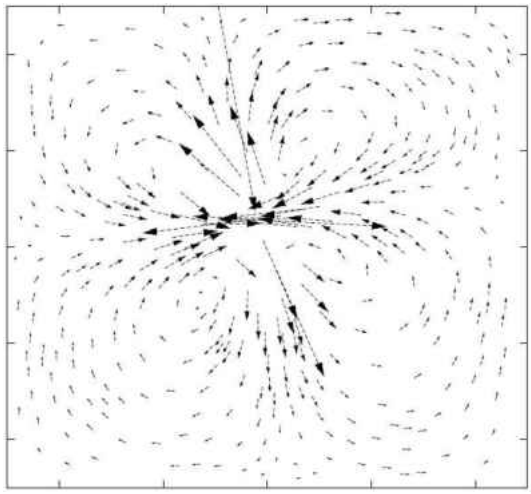

Figure 4.18: Displacement field during a quadrupolar macroscopic rearrangement, courtesy of Cox *et al.* [142]

the flow of the foam after the transient regime, i.e. during the period of localized flow. A greater proportion of strain increments now include T1 rearrangements, although there are still periods of affine displacement in which no T1s occur. The flow of the bubbles after the transient regime becomes highly non-linear and rich flow behaviour is observed. This was not observed by Kabla *et al.* [58] who found that the T1s localize only near the wall after the transient. The bubbles undergo collective large-scale swirling motions involving more T1s than in the transient regime. These form vortices (figure 4.20 (a)) where the T1s have localized away from the walls, as well as large quadrupolar rearrangements (figure 4.20 (b)) involving many T1s. Figure 4.20 (c) shows the displacement field during an interval in which a localized region is moving from the centre to the upper wall and figure 4.20 (d) shows the displacement field during localized flow at the upper wall. Figures 4.20 (a) and (d) occur as combinations of the smaller quadrupolar rearrangements aligning, resulting in a fracture with large movement of bubbles. In figure 4.20 (d), which is similar to the displacement profiles of Kabla *et al.* [58], the fracture occurs near the wall and therefore vortices do not appear.

(a) $\epsilon = 0.04$

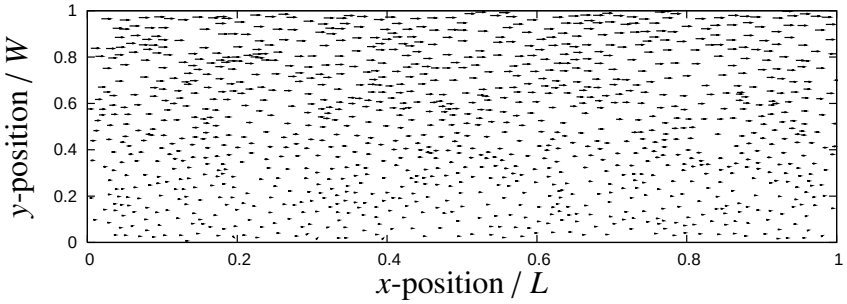

(b) $\epsilon = 0.05$

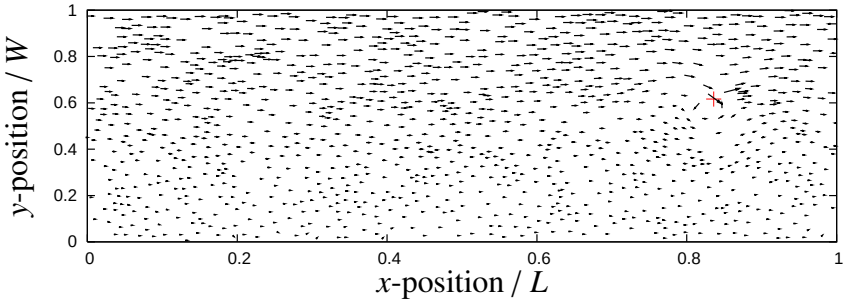

(c) $\epsilon = 0.10$

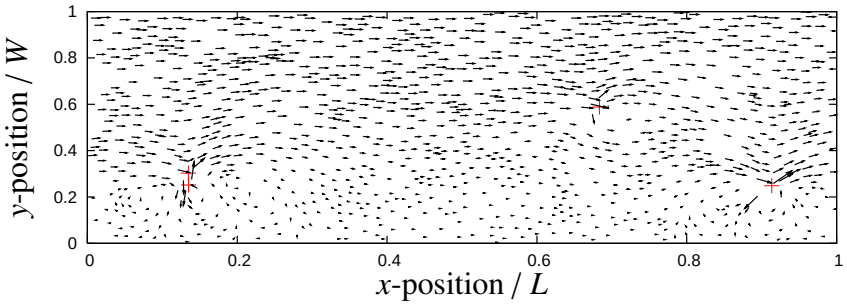

(d) $\epsilon = 0.34$

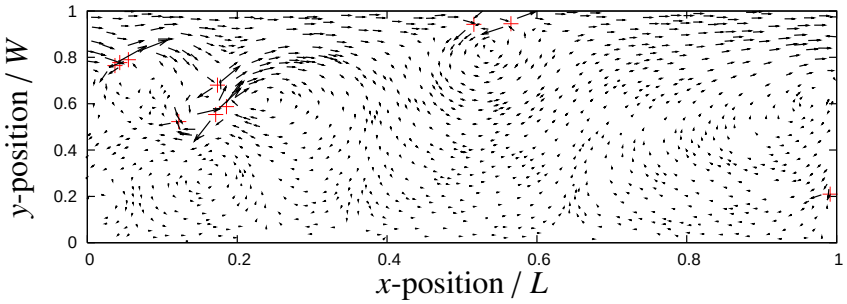

Figure 4.19: Displacement fields for the foam of 1120 bubbles, whose T1 positions are given in figure 4.14, during the transient regime. The position of the T1s are marked with red plusses. Most steps during the transient have no T1s and the displacement is affine like that shown in (a). A single T1 like that shown in (b) at (0.82,0.6) has little effect on the displacement field. As the end of the transient is approached, more T1s are involved in each macroscopic rearrangement and quadrupolar rearrangements can be identified in (c) and (d).

(a) $\epsilon = 1.52$

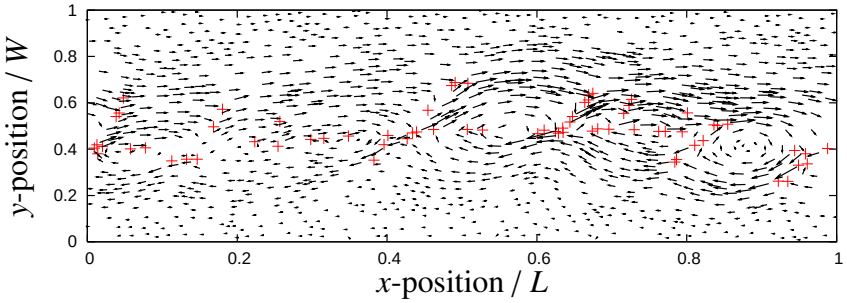

(b) $\epsilon = 2.91$

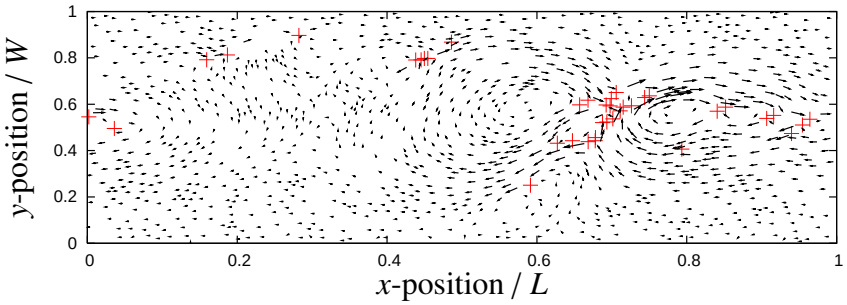

(c) $\epsilon = 3.04$

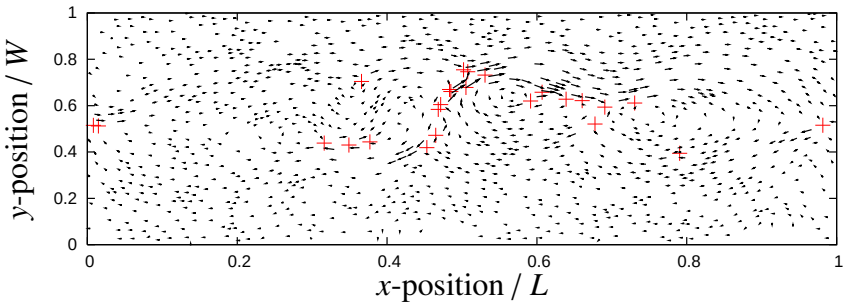

(d) $\epsilon = 3.49$

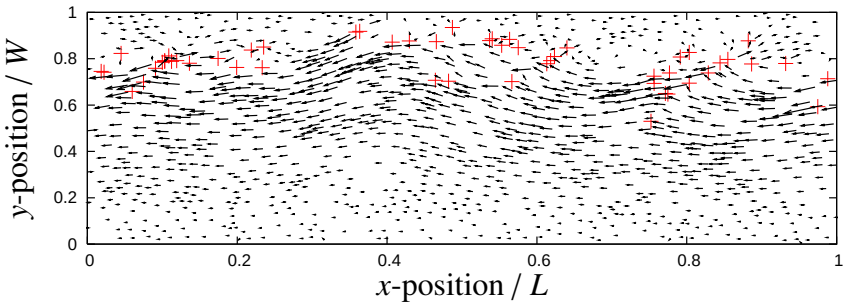

Figure 4.20: Displacement fields for the foam of 1120 bubbles, whose T1 positions are given in figure 4.14, after the transient regime. The positions of the T1s are marked with red plusses. After the transient, macroscopic rearrangements involve many more T1s, forming large quadrupolar rearrangements which combine to form swirling vortices. Localization must occur away from the walls for the vortices to occur, as in (a). When the localization is near one of the walls, as in (d), the displacement field is like those observed by Kabla *et al.* [58].

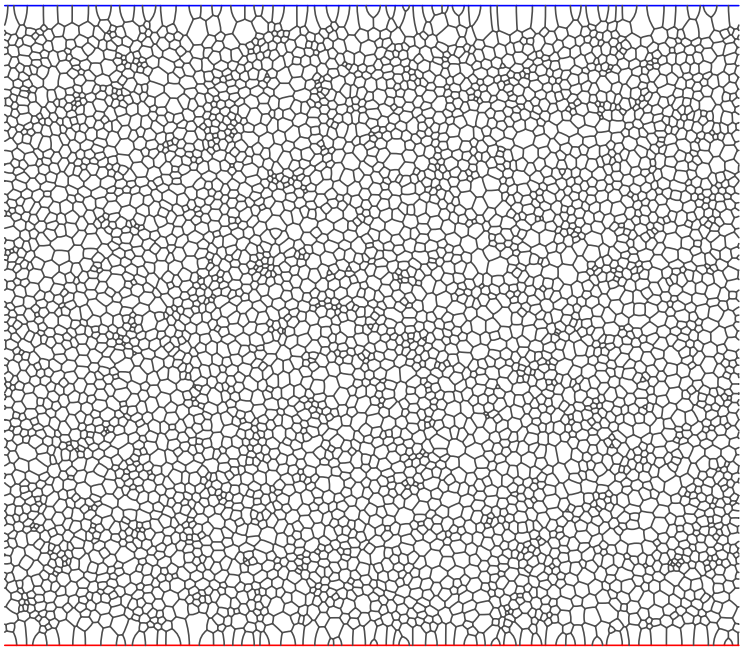

Figure 4.21: A dry foam consisting of 5000 bubbles with area-disorder $\mu_2^A = 0.32$. Time constraints limit the number of foams of this size that can be simulated.

In order to establish to what extent the effects we see are obstructed by the walls of the channel, I performed a simulation with 5000 bubbles and area-disorder $\mu_2^A = 0.32$ (figure 4.21). Only one such simulation was performed due to the huge amount of computational time ($\sim$ 3 months) required to simulate the shear of so many bubbles up to a strain of 3. The liquid fraction was set at $\phi_l = 0.005$ in order that the transient regime be reached at lower strain and therefore shorter computational time.

The y-position of each T1 *versus* applied strain is given in figure 4.22 (a) for this large foam. The transient behaviour is the same as for previous simulations, in that the T1s occur with no apparent pattern. Thereafter, the T1s localize in space away from the walls for large intervals of applied strain (greater than 1) and the position of the localized region moves, consistent with observations of smaller foam systems. There is a stationary region close to the non-moving bottom wall, extending for about 15 typical bubble widths (figure 4.22 (b)), and a similar plug flow region next to the moving wall. These are interpolated with a linear displacement profile (figure 4.22 (c)).

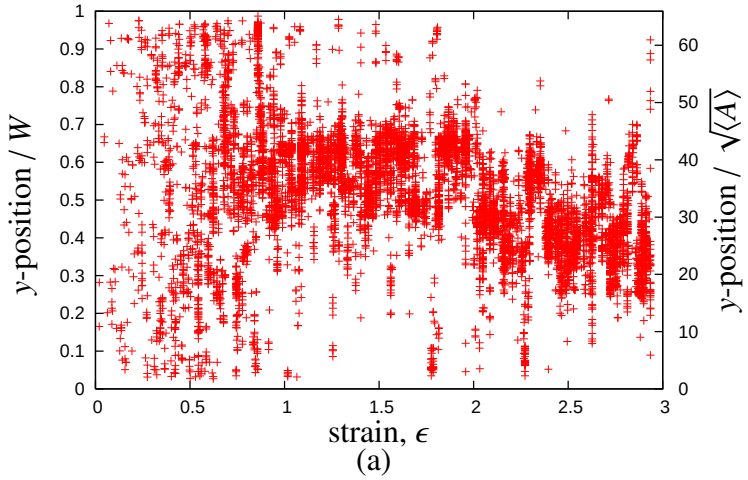

(a)

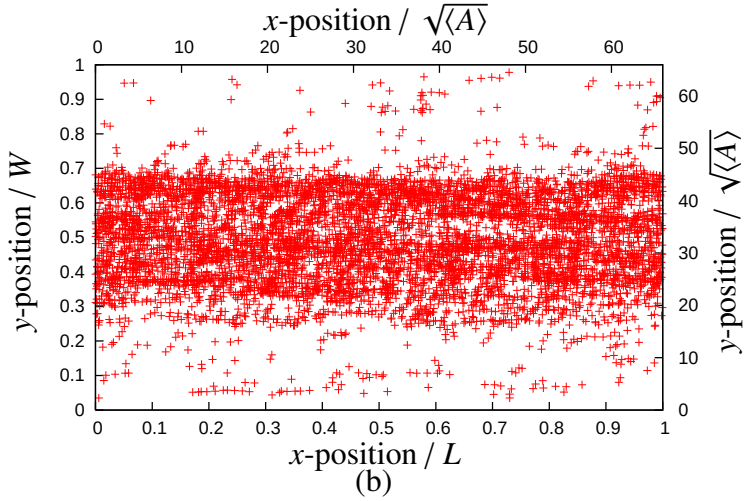

(b)

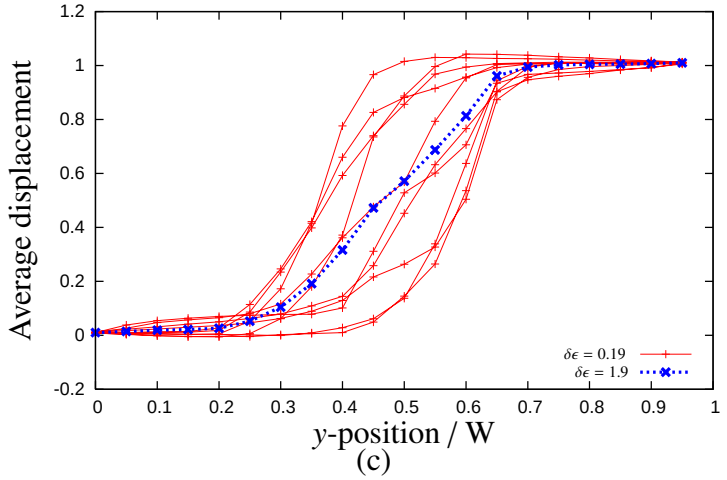

(c)

Figure 4.22: (a) y-position of each T1 versus applied strain for the 5000 bubble foam. The T1s localize away from walls and the position of the localized region moves. (b) (x, y)-position of each T1 after the transient for the 5000 bubble foam. There is an absence of T1s at the walls since the foam has localized near the middle. (c) Displacement profile of the 5000 bubble foam averaged over strain increments of 0.19 and 1.9.

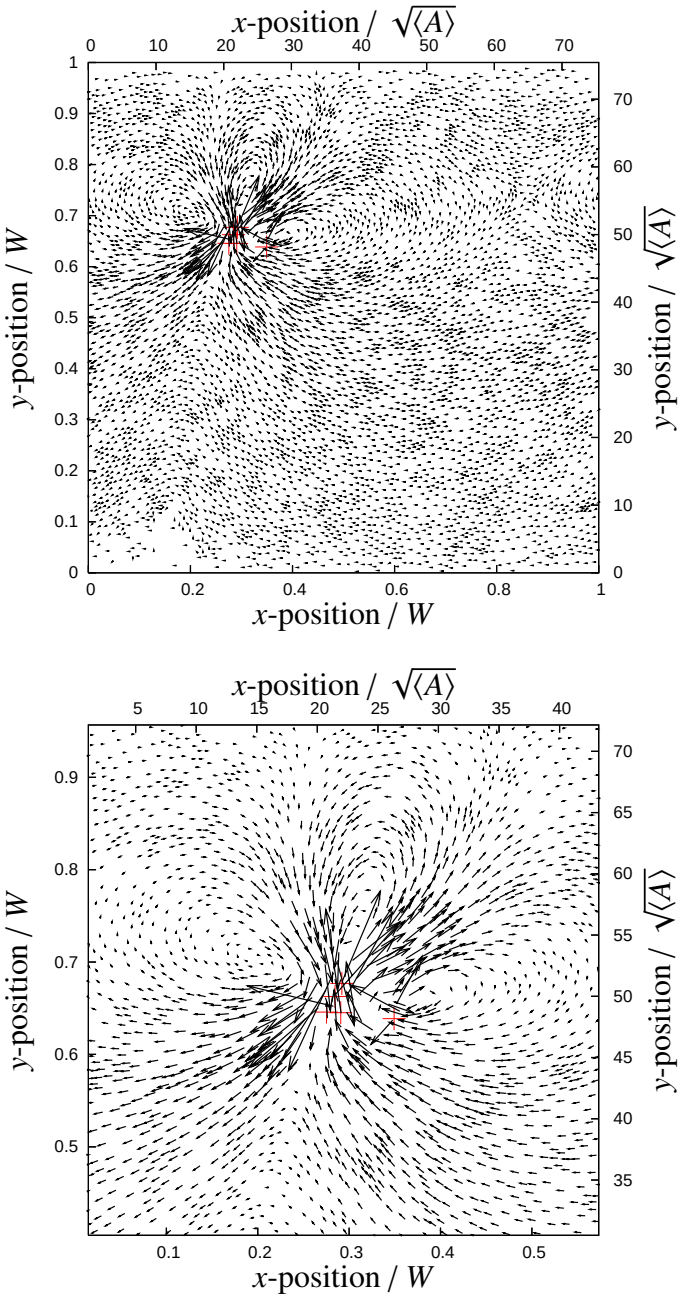

Figure 4.23: (a) Non-affine displacement field for the 5000 bubble foam during a strain step with a few T1s. The position of the T1s are marked with red plusses. The T1s cause a quadrupolar rearrangement which extends far into the bulk. (b) Closer view of the rearrangement.

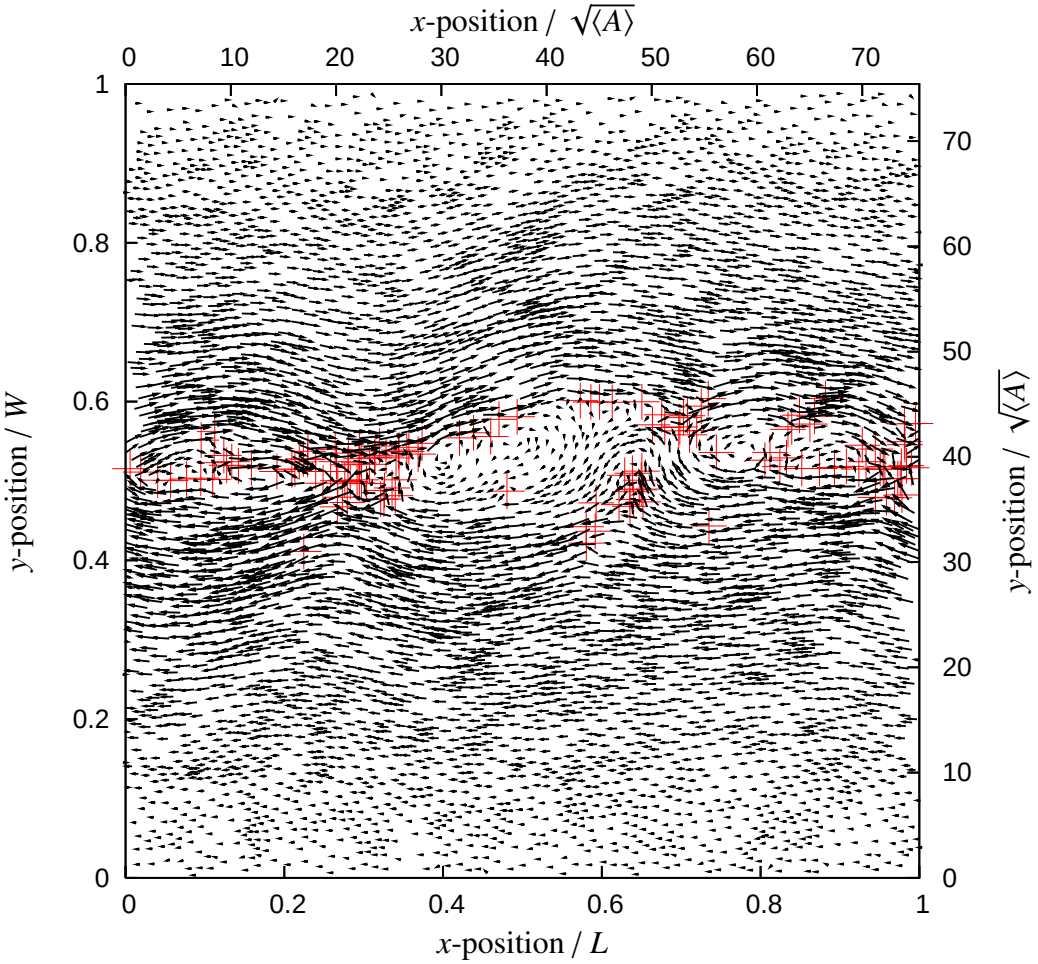

Figure 4.24: Non-affine displacement field for the 5000 bubble foam during a strain step with many T1s ($\epsilon = 1.43$). The position of the T1s are marked with red plusses. The T1s cause large vortex-like rearrangements which align along the direction of shear, and impact almost the whole foam.

Figure 4.23 gives instantaneous displacement fields during T1 events. The effect of a single T1 on the otherwise affine displacement field is minimal, as in the 1120-bubble case. The effect is small, with only a few bubbles affected. Figure 4.23 (a) shows how the effect of a combination of relatively few T1 events extends far into the foam. In contrast to the displacement fields for the 1120 bubble foam, the non-affine displacement field is plotted i.e. the expected affine displacement of each bubble in the absence of any T1s is subtracted from the actual displacement to show only the deviation from the linear displacement field. The T1s combine to create a large quadrupolar rearrangement which affects approximately 15 bubbles in each direction. Figure 4.24 shows an example of the non-affine displacement field of a larger rearrangement where vortices align and the foam fractures, affecting approximately 30 bubbles above and below. This behaviour is reminiscent of that seen at particle scale in Lennard-Jones glasses [143; 144] where interaction between particles is governed by a pairwise potential. Elastic interactions between bubbles in two dimensions are represented to a good approximation by a pairwise harmonic potential dependent on the bubble radii [145] which may account for why, for a dry foam at least, bubbles can behave like particles.

4.5 Effect of liquid fraction

The liquid fraction of a foam is one of the most important parameters affecting its rheology, and as I have shown in Chapter 3, the effect of varying liquid fraction on the yield stress of two-dimensional foams is dramatic. In this section I consider the effect of varying liquid fraction on the shear localization of two-dimensional foams. To do so I use the simulation method for wet foams described in section 2.6, and simulate the linear Couette shear of two-dimensional wet foams consisting of 100 bubbles between parallel walls (as shown in figure 2.9). Previously in this chapter I showed that area-

disorder has an effect on the shear localization of foams, and so for the purposes of investigating the effect of varying liquid fraction I keep the area-disorder to within a small range, $0.095 < \mu_2^A < 0.13$. I vary the liquid fraction in the range $0 < \phi_l < 0.1$, and measure the width of the region of localized region of T1s, w_{T1}, in the same manner as described in section 4.2. Here the T1 position is taken to be the point at which two Plateau borders merge (figure 2.10). If during a single strain step, Plateau borders repeatedly merge and separate, then a separate T1 is recorded each time the Plateau borders merge. This will not have a significant effect on the overall result, since the situation arises infrequently and only at high liquid fraction. Some simulations were performed with 200 bubbles to increase confidence in the validity of the results.

Figures 4.25 and 4.26 show the y-position of each T1 *versus* applied strain for different liquid fractions. For $\phi_l = 0.01$ the T1s are localized in space and the position of the localized region is mobile. From the simulations performed with dry foams, this is to be expected for this value of area-disorder ($\mu_2^A = 0.1269$, cf figure 4.8). For $\phi_l = 0.02$, the T1s remain localized in space, but the localized region is wider. For $\phi_l = 0.05$, regions of T1s are wider and it becomes more difficult to identify a localized region. For $\phi_l = 0.09$, no regions of localized T1s can be identified.

Figures 4.27 and 4.28 show the displacement profiles for different liquid fractions, for the same foams as in figures 4.25 and 4.26. At low liquid fractions a similar picture is seen to that encountered for dry foams earlier in the chapter (figure 4.27): displacement profiles, averaged over strain intervals of 1, are localized, exhibiting areas where the foam is not flowing. The effect is reduced when the displacement is averaged over larger intervals of applied strain due to the moving localized region. At higher liquid fraction (figure 4.28) displacement profiles deviate less from a linear profile when averaged over applied strain intervals of both $\delta\epsilon = 1$ and $\delta\epsilon = 4$. Once the liquid fraction is sufficient for the T1s to fill the majority of the channel, the displacement profiles become very

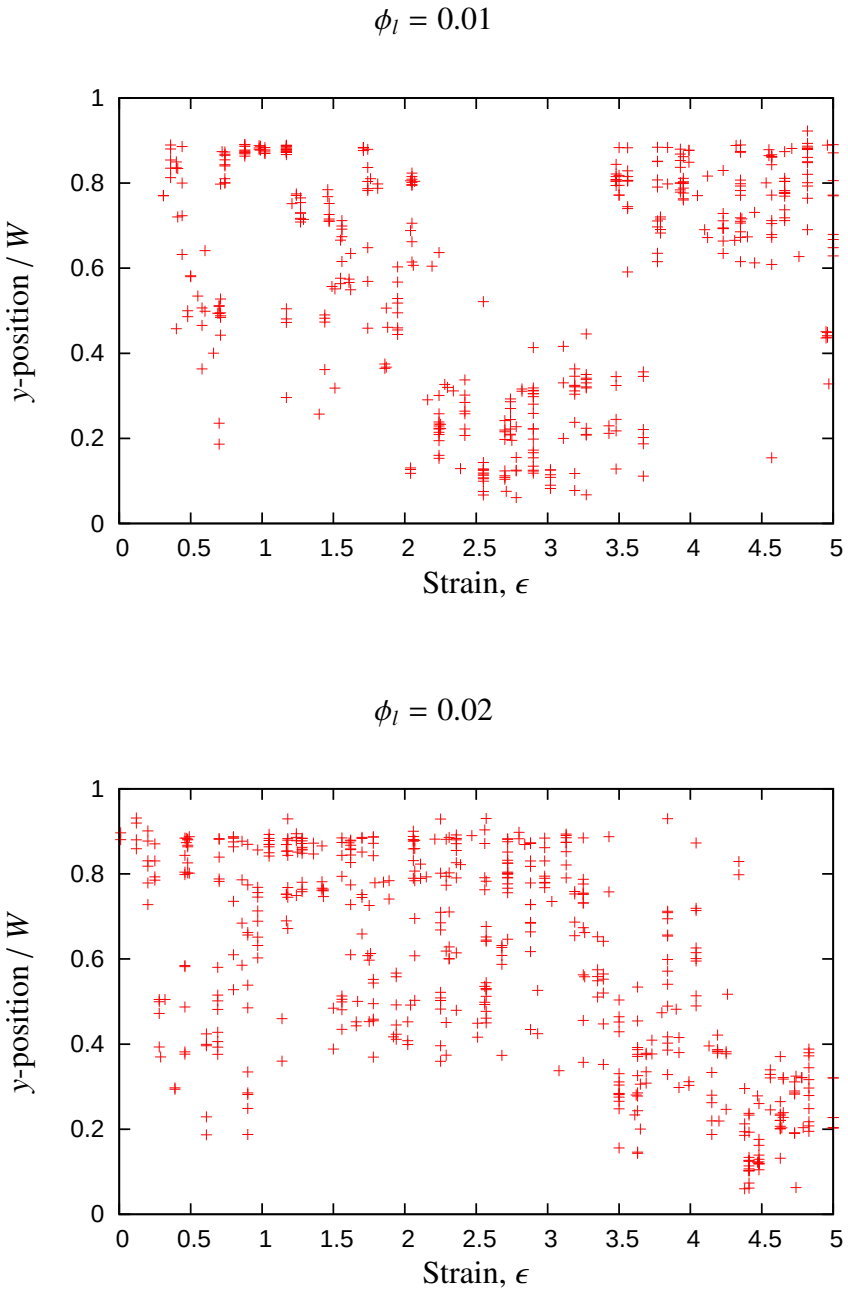

Figure 4.25: y-position of each T1 *versus* applied strain for foams with liquid fractions $\phi_l = 0.01$ and $\phi_l = 0.02$. For $\phi_l = 0.01$, the T1s are localized in space, whilst a localized region for $\phi_l = 0.02$ also moves and is wider than that for $\phi_l = 0.01$.

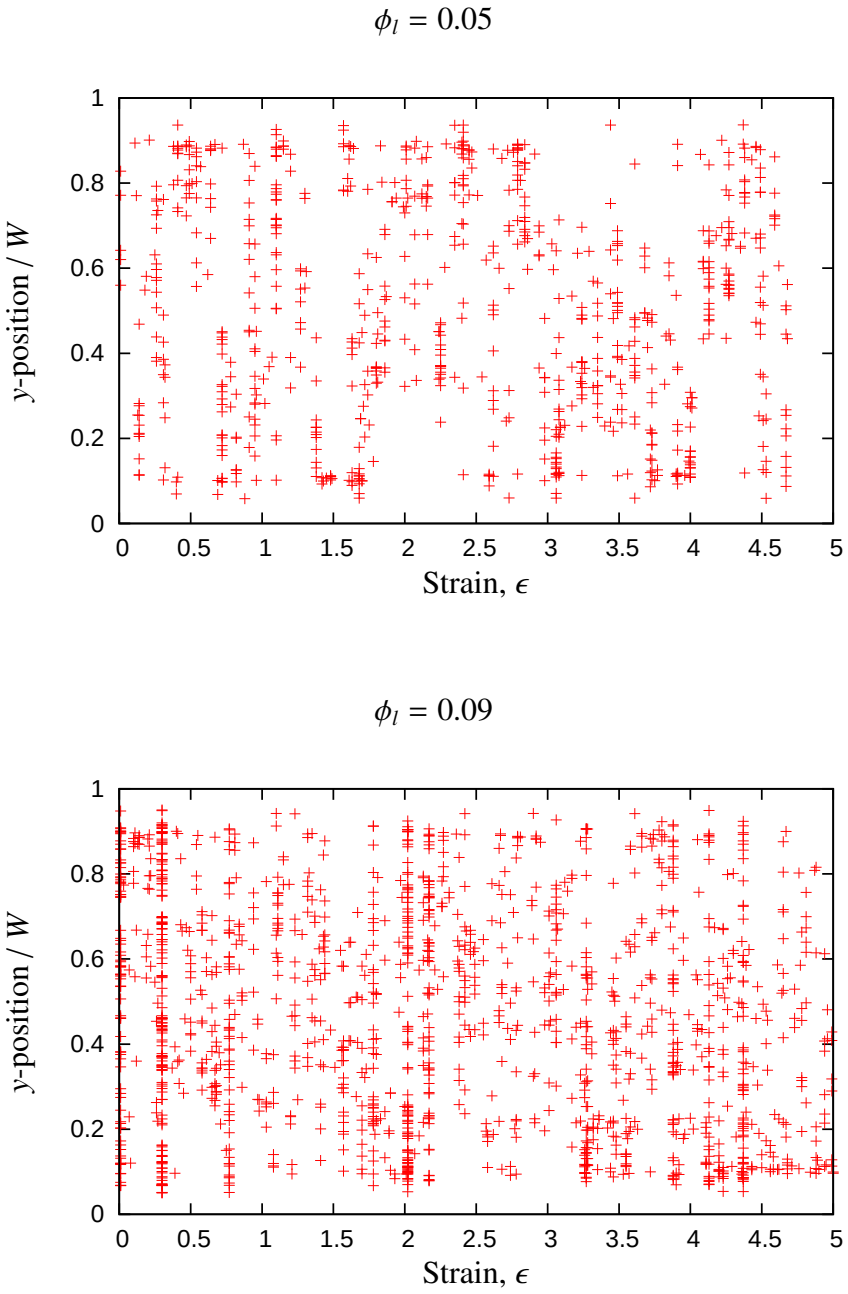

Figure 4.26: y-position of each T1 *versus* applied strain for foams with liquid fractions $\phi_l = 0.05$ and $\phi_l = 0.09$. For these liquid fractions, the T1s span the majority of the channel. There may be evidence of intermittent T1 localization at $\phi_l = 0.05$.

similar.

I quantify the position and width of the localized region in the same manner as in sections 4.2.3 and 4.2.4. The mean position of the localized region, Y_{T1}, *versus* liquid fraction is plotted in figure 4.29 (a). At low liquid fraction, the mean position of the localized regions is away from the walls and scattered since the localized region is moving. As the liquid fraction increases, the mean position settles in the centre of the channel as the width of the localized region grows to fill the channel.

The range of the position of the instantaneous localized region, R_{T1}, is plotted in figure 4.29 (b) against liquid fraction. The scatter at low liquid fraction indicates that the localized region can move in a region which is anywhere between 2 and 7 typical bubble widths in size. As the liquid fraction increases the movement of the localized region decreases. Since the width of the localized region is growing with increasing liquid fraction and T1s fill a greater proportion of the channel, the position of the localized region is less free to move.

The width of the localized region is given in figure 4.30, with the choice of $N_I = 50$ and $\psi_{T1} = 0.8$, the same values used for dry foams in section 4.2.4. The predicted localization width for foams in the dry limit from equation (4.10) is also plotted in figure 4.30 (b), with $\mu_2^A = 0.1$, and is in good agreement with data from the wet foam simulations. The localization width, w_{T1}, increases with increasing liquid fraction. The localization width plateaus at approximately $\phi_l = 0.05$ coinciding with the liquid fraction at which the mean position of the localized region settles at the centre of the channel (figure 4.29 (a)) as T1s fill the channel (cf. figure 4.26).

Note that since the channel consists of approximately 10 by 10 bubbles, there will be very few T1s whose y-position is within one typical bubble with of the walls ($\sqrt{\langle A \rangle} = 0.1$), allowing T1s to fill a maximum of approximately 0.8 times the channel width, W. With $\psi_{T1} = 0.8$, the localization width is unlikely to exceed $0.8 \times \psi_{T1} = 0.64$, although

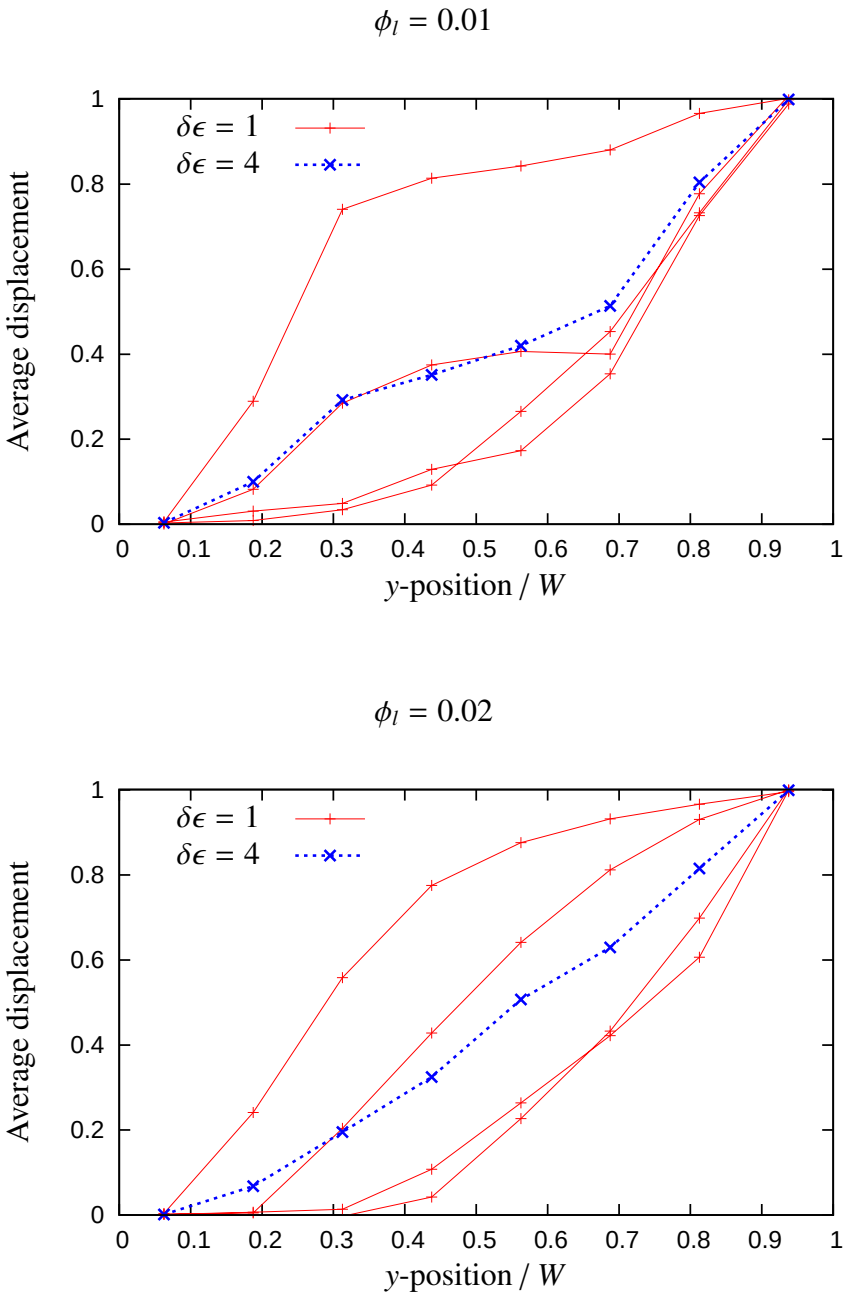

Figure 4.27: Displacement profiles for foams with $\phi_l = 0.01$ and $\phi_l = 0.02$ for $\epsilon > 1$. When averaged over small strain intervals the displacement profiles are non-linear, but when averaged over larger strain intervals, a moving localized region leads to a smoother displacement profile which deviates less from a linear profile.

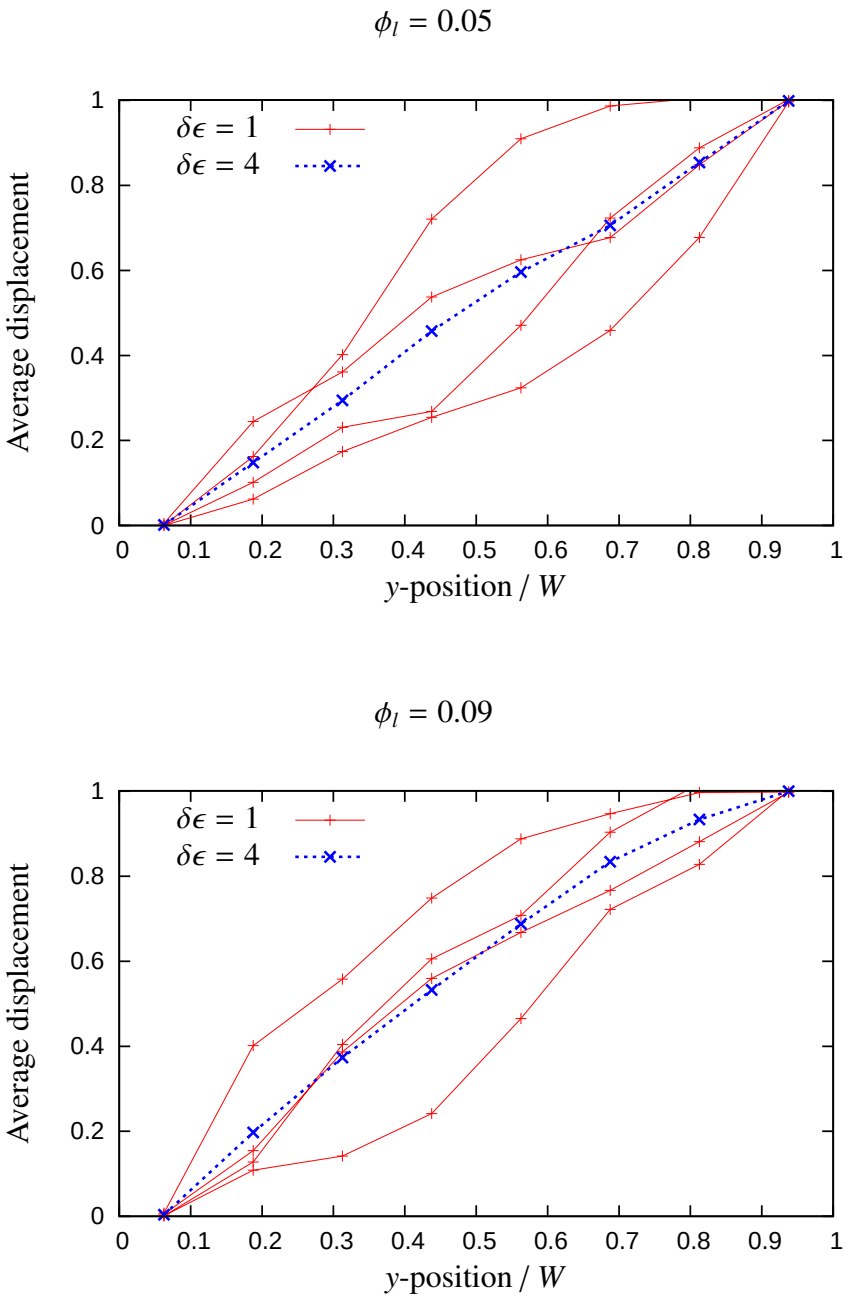

Figure 4.28: Displacement profiles for foams with $\phi_l = 0.05$ and $\phi_l = 0.09$ for $\epsilon > 1$. The profiles are smoother deviate less from a linear profile than dryer foams when averaged over both small and large strain intervals.

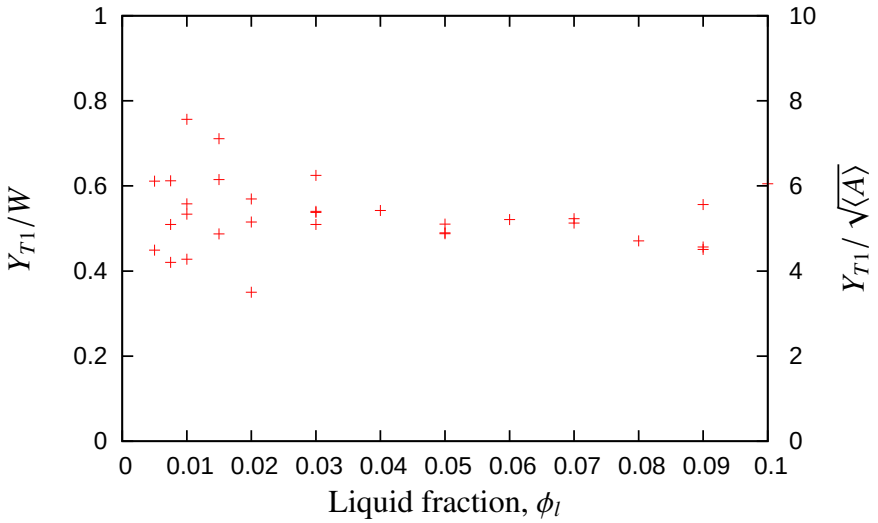

(a)

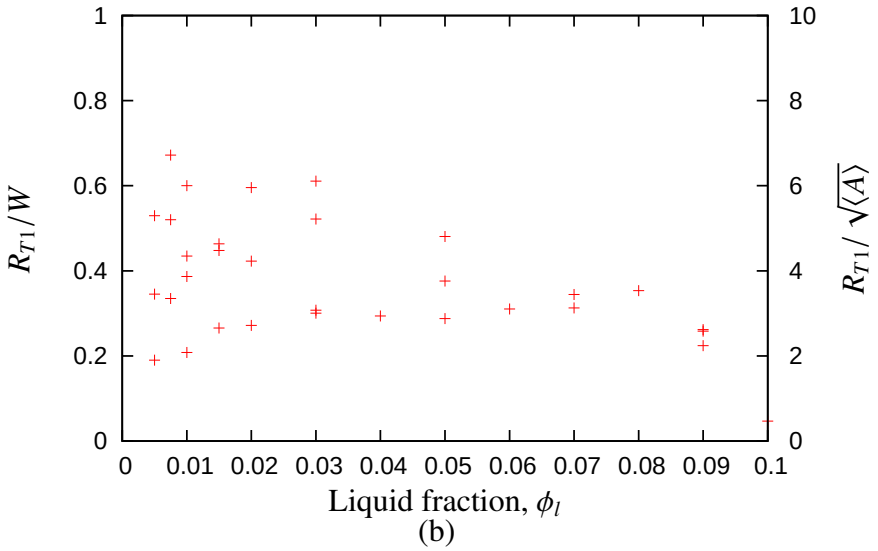

(b)

Figure 4.29: (a) The mean y position of the localized region, Y_{T1}, *versus* liquid fraction, ϕ_l. (b) The range of the positions of the localized region, R_{T1}, *versus* liquid fraction, ϕ_l.

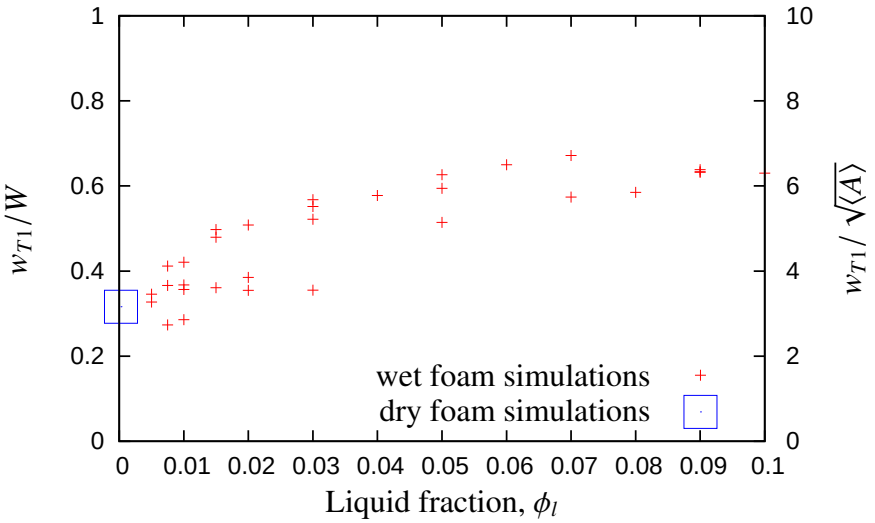

Figure 4.30: The localization width, w_{T1}, with $\psi_{T1} = 0.8$ and $N_I = 50$ as for the dry case for wet foams with area-disorder $0.095 < \mu_2^A < 0.128$. The prediction from dry foam simulations ($\phi_l = 2.6 \times 10^{-4}$) using equation (4.10) with $\mu_2^A = 0.1$ is also plotted. w_{T1} increases with increasing liquid fraction.

one could conceive special cases where it would be possible. Therefore as w_{T1} reaches a plateau at approximately 0.6, this is interpreted as the T1s filling the channel and is consistent with what is observed in figure 4.26.

It is to be expected that for wider channels, the localization width would not plateau but continue to increase. It was not possible to test this hypothesis due to the restrictions on the number of bubbles that can be simulated at high liquid fraction.

Referring back to the displacement profiles in figures 4.27 and 4.28, the displacement profiles are almost linear when averaged over large intervals of applied strain. At low liquid fraction this arises from a small localized region which moves around. As the liquid fraction increases, the almost linear profile occurs as a result of the localized region filling the channel. The liquid fraction therefore has a significant effect on the localized region and through this, the flow of the foam.

These results are consistent with the observations of Debrégeas *et al.* [59] with a Hele-Shaw cell ($\mathcal{GG}$) but seem to contradict those of Katgert *et al.* [65] with a confined

bubble raft ($\mathcal{LG}$). In the latter case, the only means of controlling the liquid fraction is to vary the distance between the bounding plate and the liquid pool. Subsequently, the bubbles change shape, becoming more stretched at low liquid fractions and having a flat pancake-like shape at high liquid fraction. It may be the shape of the bubbles, as opposed to the volume fraction of liquid, which sets the degree of localization in this case.

4.6 Summary

T1 localization has been observed in some studies but not in others. The presence of external friction accounts for many instances in which the T1 localization is observed in quasi-two-dimensional experiments, with some exceptions, but it does not account for T1 localization observed in quasistatic simulation of dry foams.

The position and size of the localized region depends on both the liquid fraction and area-disorder of the foam, which could further explain why T1 localization occurs in some studies but not in others. The width of the localized region increases approximately linearly with increasing liquid fraction (figure 4.30) and as the square root of area-disorder (equation (4.10), figure 4.10), resulting in a greater amount of flowing foam. At low liquid fraction the degree to which the position of the localized region moves around increases as the area-disorder is increased (figure 4.8), allowing different regions of foam to flow in turn. The overall effect is an increase in flowing foam. If the liquid fraction and area-disorder are sufficient, the localized region fills the channel and no localized flow is observed (figure 4.28).

It is plausible therefore that T1 localization occurs when there is some restriction on the free flow of bubbles, as is the case when external friction is present or when using the cylindrical Couette geometry, since part of the foam is at a stress above the yield

stress whilst the remainder is at a stress below the yield stress. To these conditions I would now include that localization may occur when the foam is very dry or very ordered.

I also note that the behaviour of foams at low area-disorder differs significantly from the ordered case, reinforcing the claim in Chapter 3 that the inclusion of disorder is essential when considering real foam systems. The importance of considering disordered systems can also be seen when looking at bubble dynamics. During localized flow the bubbles undergo large scale vortex-like motion (figure 4.20 (d)), similar to what is observed in Lennard Jones glasses, but which only appears when the localized region is away from the walls, which requires a certain amount of area-disorder.

The region of localized T1s in a dry two-dimensional foam can be identified from information solely about the foam structure using either a tensorial measure of foam structure or a simple one-dimensional measure, both of which can be calculated from a single still image. The next step after identification of the localized region is to be able to predict to which region of the foam the localized region will move.

In the next chapter I consider the local bubble configuration during a T1 and whether the individual T1 events at small scale can be related to the phenomena of yielding and T1 localization at the longer length scales considered in this and the previous chapter.

Chapter 5

T1 orientation

5.1 Introduction

I have thus far shown that the phenomena of foam yielding and T1 localization depend on the liquid fraction and area-disorder of the foam. These large scale phenomena are the manifestation of the combination of many local structural rearrangements at the bubble scale, i.e. T1s, a fundamental process in the flow of foams. In this chapter, I relate yielding and localization to the topological changes at the bubble scale by considering the local bubble configuration during a T1 process.

Recall that in a dry two-dimensional foam, a T1 occurs when a film shrinks to zero length, resulting in a fourfold Plateau border which immediately dissociates into two threefold Plateau borders joined by a film roughly perpendicular to the one which has disappeared (figure 1.4). As the liquid fraction is increased, fourfold Plateau borders become stable and may remain as fourfold Plateau borders for finite intervals of applied strain before dissociating back into threefold Plateau borders. (figure 2.10).

To maintain a consistent description of a T1 for both wet and dry foams, it is better to think in terms of nearest neighbours, i.e. two bubbles that share a common film [46; 141]. A T1 process involves the rearrangement of four bubbles, two of which

are nearest neighbours beforehand, and another two which become nearest neighbours after the event. Following Graner *et al.* [141], nearest neighbours are defined to be those that have a film in common, and a line joining their centres defines a link. A T1 is initiated and a link disappears when Plateau borders merge and the film between them disappears. When Plateau borders separate, a new film and a new link are created. The local bubble configuration during a T1 can be characterized by its orientations (θ_d, θ_c), defined as the angles that the disappearing and created links (respectively) make with the direction of shear. Examples of T1s and their orientations are given in figure 5.1.

For higher liquid fraction, five or more sided Plateau borders may be formed, e.g. when a fourfold Plateau border and a threefold Plateau border merge to create a fivefold Plateau border. In the same manner as when fourfold Plateau borders are formed, θ_d is measured when the Plateau borders merge and a link disappears and θ_c is measured when a Plateau border of five or more sides dissociates back into two Plateau borders with fewer sides and a new link is created.

T1 orientations have been measured experimentally in a bubble raft by Wang *et al* [46] (figure 5.2 (i)). They found that the distributions of θ_d and θ_c had peaks at 45° and 130° respectively, suggesting more-likely local geometries for bubbles separating and coming together. The distribution of θ_d was broader than that of θ_c. At low shear rates the distributions were smooth and bell-shaped with secondary peaks. As the shear rate was increased, the distributions became more spiked and the secondary peaks disappeared. The location of the primary peaks appeared to decrease slightly as the shear rate is increased, in agreement with simulations of Cox of ordered two-dimensional foams using the Viscous Froth model [146].

In figure 5.2 (ii) I give an example of the orientations of T1s in simulations of dry two-dimensional foams. The distributions of θ_d and θ_c have peaks in the region of 30° and 140° respectively and the distribution of θ_c is broader than that of θ_d.

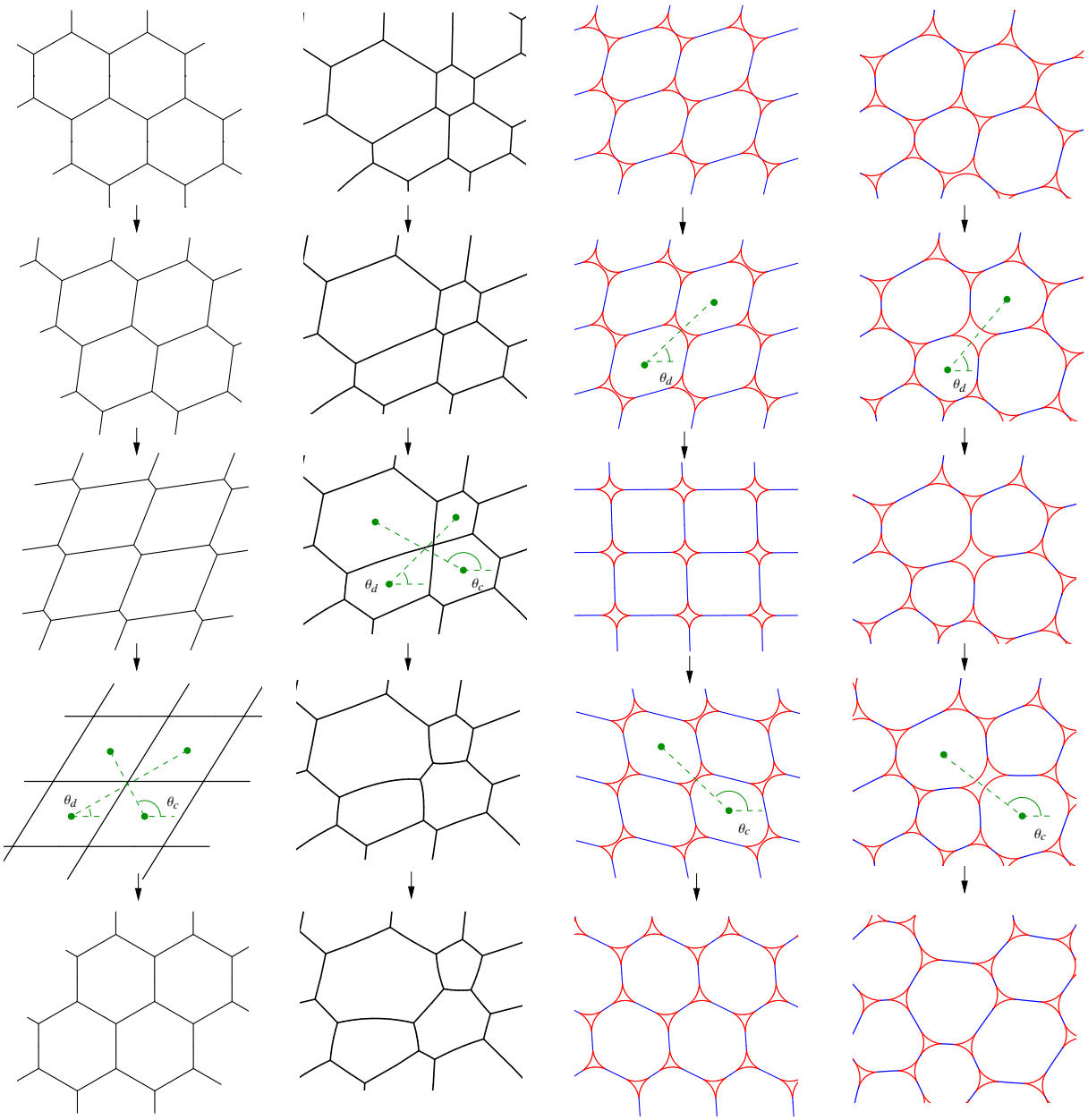

Figure 5.1: Examples of T1s and their orientations θ_d, θ_c. The evolution of the structures proceeds from top to bottom in each case. (a) Ordered dry foam, (b) disordered dry foam, (c) ordered wet foam and (d) disordered wet foam. The orientations are calculated at the instants at which two threefold Plateau borders merge (θ_d) and at which a fourfold Plateau border dissociates into two threefold Plateau borders (θ_c). For dry foams this occurs at the same instant.

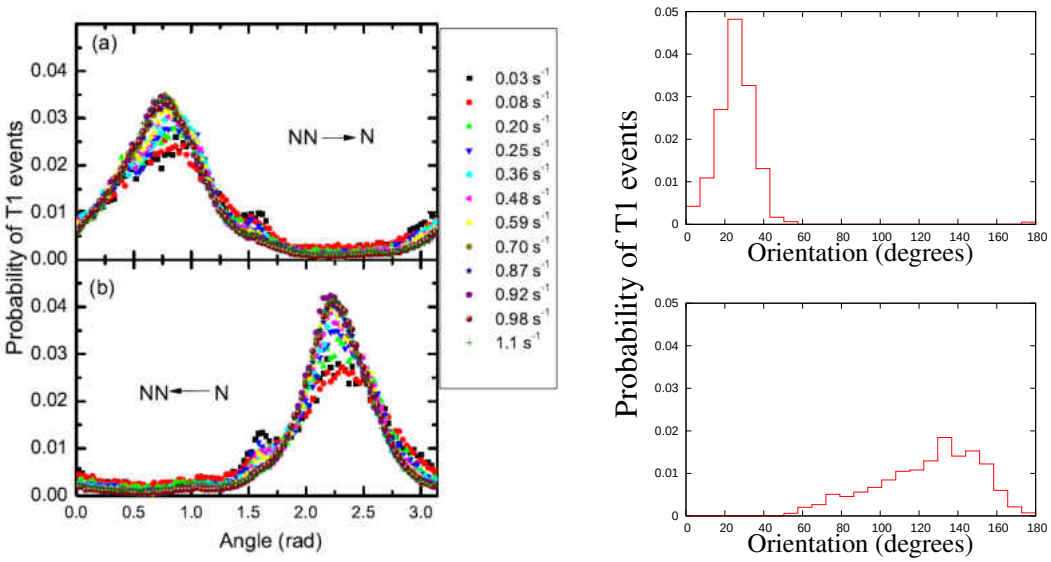

(i) (ii)

Figure 5.2: (i) Previous results of Wang *et al.* [46] for the orientation of T1s in a bubble raft. (ii) Example of the distribution of T1 orientations from my simulations of a dry two-dimensional foams which will be discussed later. In each case the distribution of θ_d is shown in the upper figure and the distribution of θ_c in the lower figure.

The orientation of the new film created after a T1 has been measured from two-dimensional simulations of a coarsening foam under a constant applied stress by Vincent-Bonnieu *et al.* [147]. The orientation of the new film was found to be related to the macroscopic strain step occurring as a result of the individual T1. The orientation of the new film is not the same as either θ_d or θ_c, but is likely to be related to both in some way for dry foams.

In this chapter I investigate the effect of liquid fraction and area-disorder on the distributions of the T1 orientations and show that the distributions of Wang *et al.* and data from dry foam simulations are consistent with the variation of the distributions of T1 orientation with liquid fraction and area-disorder. I also relate T1 orientation to foam yielding and T1 localization, showing a non-trivial link between the individual T1

events and the foam response to applied strain at larger length scales. The orientation of the disappearing link, θ_d, is a measure of local strain at the instant a T1 occurs. A high value of θ_d indicates a low local strain and *vice-versa*. The yielding and flow of a foam requires that many T1s occur and the distribution of the orientation of the T1s is related to mesoscopic phenomena involving collections of bubbles, such as T1 localization, and macroscopic phenomena such as foam yielding and flow.

5.2 Reference case: Ordered foam

I begin by considering the T1 orientations of a fully-ordered hexagonal foam (figure 5.1 (a) and (c)). To calculate the orientations, all that is required are the strains at which (i) two threefold Plateau borders merge, ϵ_d, and (ii) the fourfold Plateau border separates, ϵ_c. These values can be obtained from the analysis of Princen [30], described in Chapter 3. Then

$$\tan\theta_d = \frac{1}{\epsilon_d + 1/\sqrt{3}}, \tag{5.1}$$

$$\tan\theta_c = \frac{1}{\epsilon_c - \sqrt{3}}. \tag{5.2}$$

Figure 5.3 shows the variation of θ_d and θ_c with liquid fraction for different contact angles. As in previous chapters, the effect of a finite contact angle is considered since simulations of disordered wet foams are performed with contact angle $\alpha = 3.62$. The same notation is used as in Chapter 3 to distinguish between analytic predictions, P_α, and Surface Evolver simulations, S_α, of different contact angle, α.

For a perfectly dry hexagonal foam, the T1 occurs at $\epsilon = 2/\sqrt{3}$, resulting in $\theta_d = 30^\circ$ and $\theta_c = 120^\circ$. θ_d increases as the liquid fraction increases since the strain at which the T1 occurs decreases with increasing liquid fraction.

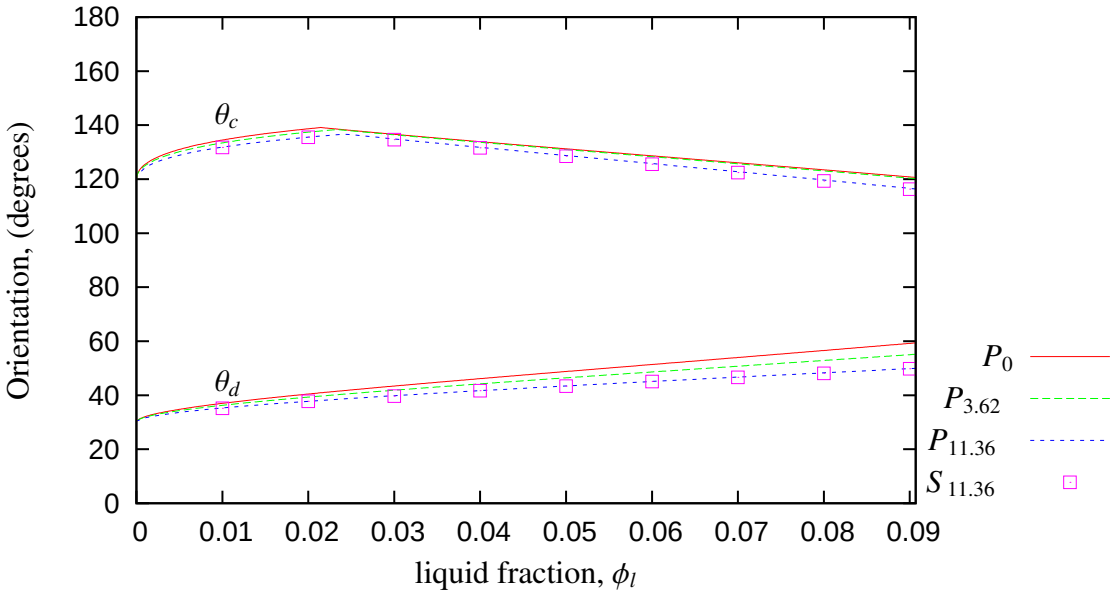

Figure 5.3: The T1 orientations θ_d, θ_c in an ordered hexagonal foam *versus* liquid fraction. P_α denotes analytic predictions and S_α denotes Surface Evolver simulations, each of contact angle α. θ_d increases monotonically with increasing liquid fraction whilst θ_c exhibits a change in behaviour at the point at which a fourfold Plateau border becomes stable over a finite interval of applied strain.

θ_c exhibits more complex behaviour as a function of liquid fraction. It initially increases from 120° with increasing liquid fraction. At $\phi_l \approx 0.02$, the behaviour changes and θ_c decreases as the liquid fraction increases. The change in behaviour is related to the stability of a fourfold Plateau border. At low liquid fractions, fourfold Plateau borders are unstable and immediately dissociate back into two threefold Plateau borders. θ_d and θ_c are therefore measured at the same strain, and since the T1 occurs at decreasing strains as the liquid fraction increases, this results in an increase in θ_c. Once the liquid fraction is sufficiently high that a fourfold Plateau remains stable for a finite strain interval, the behaviour changes. θ_c is measured at the strain at which the fourfold Plateau border dissociates into two threefold Plateau borders and this occurs at increasing strain as the liquid fraction increases, resulting in a decrease in θ_c as the liquid fraction is increased.

The effect of a finite contact angle is to increase θ_d and decrease θ_c, since an in-

creased contact angle results in both threefold Plateau borders merging and fourfold Plateau borders separating at higher strains. The effect is greater on θ_d, but a contact angle of $\alpha = 3.62$ remains a good approximation to the zero contact angle case.

Simulations in the Surface Evolver with the wet method described in section 2.6 reproduce the analytic result for finite contact angles; therefore it can be used with confidence to extend the study to disordered foams.

5.3 Effect of area-disorder on T1 orientation in dry foams

Having looked at the predicted orientation of T1 events for ordered foams over a range of liquid fractions, I consider what effect the introduction of area-disorder has on the T1 orientation. In order to obtain good statistical averages, I consider foams in the dry limit $\phi_l = 2.6 \times 10^{-4}$ where simulations with over a thousand bubbles can be performed. The orientations of each T1 *versus* applied strain are shown in figure 5.4 for a foam with $\mu_2^A = 0.2809$. After an initial transient up to a strain of order one, as for the stress in Chapter 3, the orientations remain within a certain range and therefore I consider the orientations of T1s after a strain of 2 only, to ensure that any transient behaviour is omitted.

The evolution of the distribution of θ_d with area-disorder is shown in figure 5.5. For an ordered foam, such a graph would appear as a delta function. With increasing area-disorder the distribution broadens.

θ_d is well-fitted by a normal distribution of mean λ_d and standard deviation σ_d. The probability density function (PDF) is given by

$$f_d(\theta_d) = \frac{1}{\sqrt{2\pi}\sigma_d} \exp\left(\frac{(\theta_d - \lambda_d)^2}{2\sigma_d^2}\right). \tag{5.3}$$

To produce the histograms the interval was divided into 25 bins, giving a bin size of

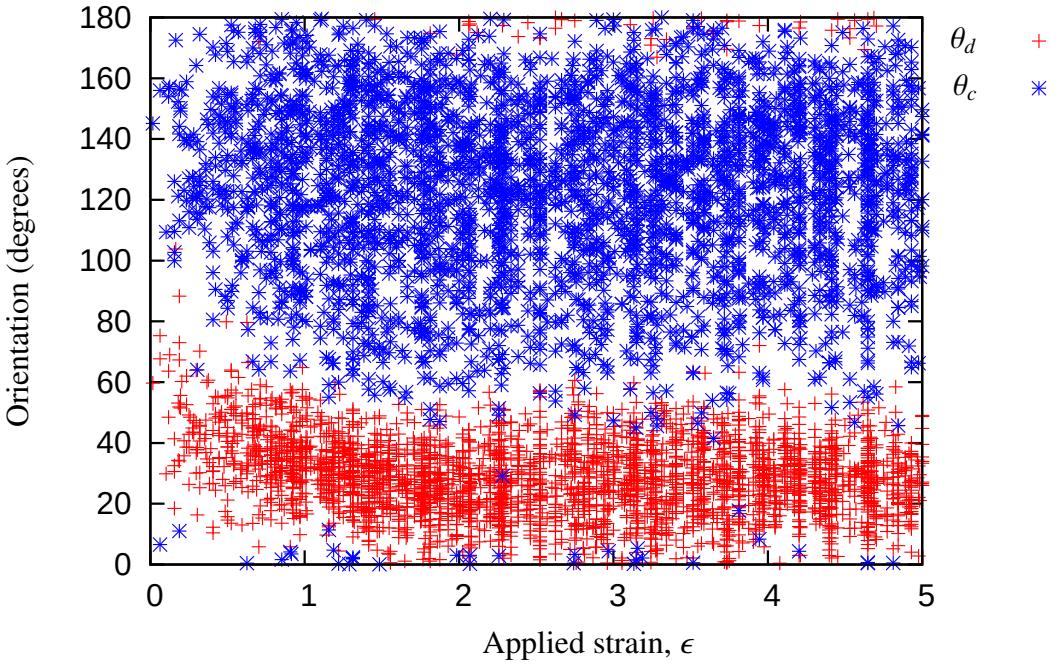

Figure 5.4: The orientation of each T1 *versus* applied strain. After an initial transient, the orientations remain within a certain range. Note that θ_d is sometimes negative, shown as values close to 180°.

7.2° which was found to have sufficient detail to capture the shape of the distribution and large enough that the distribution does not appear noisy.

The mean and width of the fitted distributions are given in figure 5.6 (a) and (b). λ_d appears to decrease initially with increasing area-disorder and then increase slightly with increasing area disorder. At low area-disorder the orientation approaches the value for the ordered case ($\theta_d \approx 31°$ at $\phi_l = 2.6 \times 10^{-4}$ from figure 5.3). σ_d increases with power law behaviour as the area-disorder is increased, implying that the width would reduce to zero as the area-disorder tends to zero. Simulations of monodisperse foams do however have finite values of σ_d (data not shown) and this must be attributed to the foam being topologically disordered. The mean and width of the distribution of the disappearing link are plotted together in figure 5.6 (c). The variation in the mean of the distribution is small relative to the width of the distribution, especially at high area-disorder.

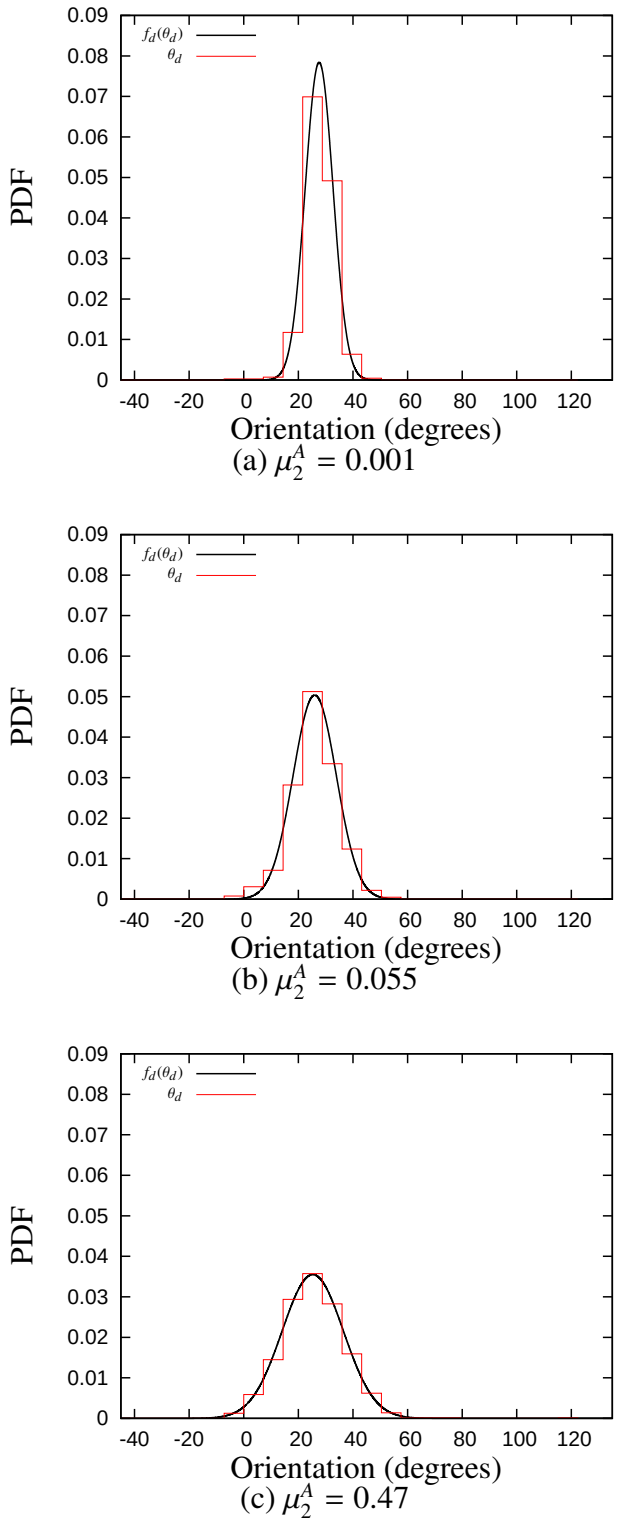

Figure 5.5: The distribution of the orientation of the disappearing link, θ_d, for different values of area-disorder, μ_2^A. The distribution of θ_d is well-fitted by a normal distribution. The steps are histograms of the data and the bold line is the PDF of the fitted normal distribution. As the area-disorder increases, a greater variation in orientation is observed and the distribution broadens.

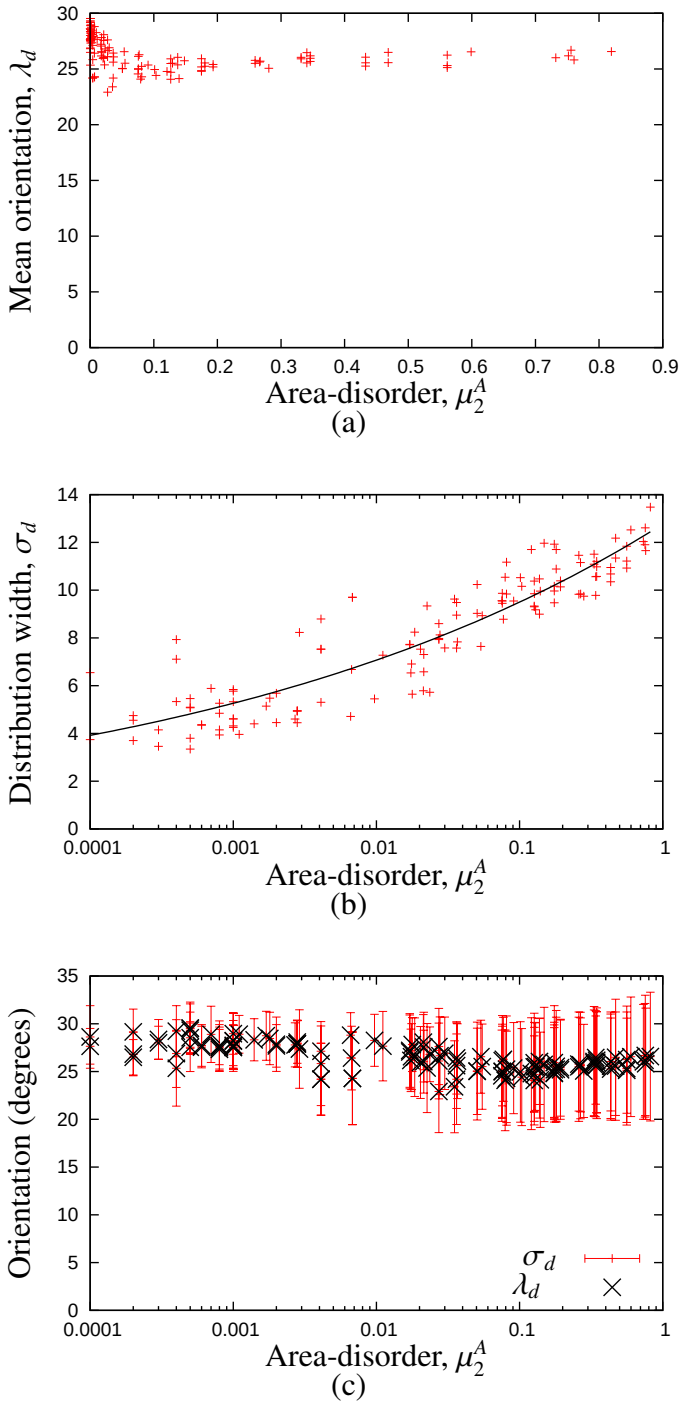

Figure 5.6: The variation of (a) the mean, λ_d, and (b) width, σ_d, of the distributions fitted to the orientation of the disappearing link, θ_d, with area-disorder, μ_2^A. Above a certain values of area-disorder, λ_d increases with increasing area-disorder. As the area-disorder decreases, λ_d approaches the value for the ordered case ($\theta_d \approx 31^\circ$ at $\phi_l = 2.6 \times 10^{-4}$). σ_d increases with increasing area-disorder. The solid line is a power law fit to the data. λ_d and σ_d are plotted together in (c). The mean is shown as crosses and the width of the distribution by the red bars.

The outlying points at low area-disorder correspond to simulations in which the localized region jumps from the wall to the centre of the channel, leading to an increased localization width (cf. section 4.2.4). This suggests a link between T1 *localization* and T1 orientation, which is discussed later in section 5.5.2.

The evolution of the distribution of θ_c with area-disorder is shown in figure 5.7. The distribution appears to have two modes, with the low θ_c mode growing in prominence as the area-disorder is increased. The distribution is well-fitted by a bimodal normal distribution with PDF

$$f_c(\theta_c) = pf_{c1}(\theta_c) + (1-p)f_{c2}(\theta_c) \tag{5.4}$$

where

$$f_{ci}(\theta_c) = \frac{1}{\sqrt{2\pi}\sigma_{ci}}\exp\left(\frac{(\theta_c - \lambda_{ci})^2}{2\sigma_{ci}^2}\right), i = 1, 2 \tag{5.5}$$

are normal PDFs with mean λ_{ci} and standard deviation σ_{ci} (of the same form as PDF (5.3) for θ_d) and p is a mixing parameter. $i = 1$ denotes the distribution with smallest mean and $i = 2$ the distribution with the largest mean.

Figure 5.8 shows the variation of the distribution parameters with area-disorder. At low area-disorder both means, $\lambda_{c1}, \lambda_{c2}$, are similar. As the area-disorder increases, one mean grows while the other is reduced. The opposite happens to the widths of the distributions, σ_{c1}, σ_{c2}: the distribution of the high θ_c mode has a low width, but this width increases slightly with increasing area-disorder until it is of the same order as the width of distribution of the low θ_c mode. The distribution of the low θ_c mode starts off very wide and the spread of the data is greater than for the high θ_c mode, but as the mean decreases, the spread of the points decreases until it is of the same order as the spread of the data for the width of the high θ_c mode. The mixing parameter p also increases with increasing area-disorder, i.e. at low disorder, the high θ_c mode dominates the overall distribution, but as the area-disorder increases, the low θ_c mode becomes more

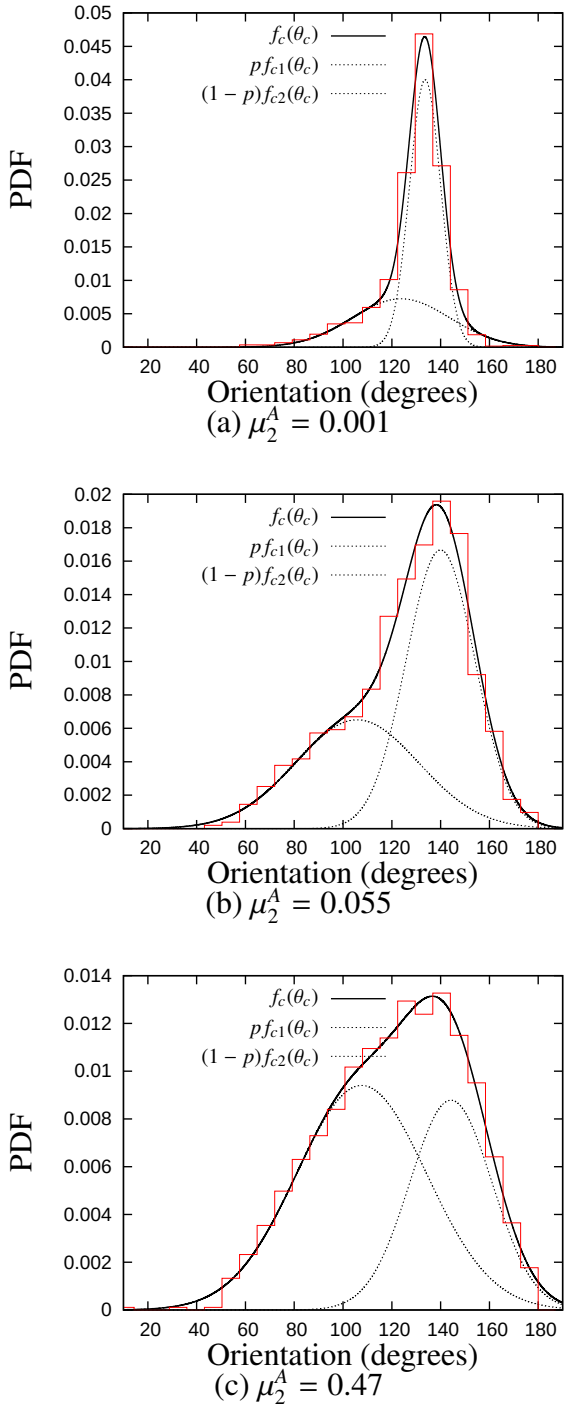

Figure 5.7: The distribution of the orientation of the created link, θ_c, for different values of area-disorder, μ_2^A. The steps are histograms of the data, the dotted lines are the fit functions and the bold line is a weighted sum. The distributions are well-fitted by a bimodal normal distribution, suggesting different underlying causes for T1s. At low area-disorder, the high θ_c mode dominates the distribution. As the area-disorder increases, the low θ_c mode grows in prominence.

prominent and at high disorder is of equal or greater prominence than the high θ_c mode (figure 5.7). The increase of p is linear in $\ln\mu_2^A$. The solid line in figure 5.7 (c) is given by

$$p = 0.053\ln\mu_2^A + 0.63. \tag{5.6}$$

The effect on the mean, λ_c, and width, σ_c, of the overall distribution is as follows. The mean starts in the region $\lambda_c \approx 130°$ at low area-disorder and decreases with increasing disorder as the mixing parameter increases (note that for ordered foams, $\theta_c \approx 123°$ at $\phi_l = 2.6 \times 10^{-4}$). The width, σ_c, starts low at low area-disorder and increases as the mixing parameter increases with increasing area-disorder.

A bimodal distribution suggests different underlying causes leading to T1s. The peaks indicate that when a T1 occurs, certain local configurations of bubbles are more likely than others. The cause of these specific configurations is not yet known. Some hypotheses have however been ruled out. I find that the proximity of the walls and the number of sides of the four bubbles involved in the T1 do not have an effect on its orientation (data not shown).

5.4 Effect of liquid fraction on T1 orientation in disordered foams

To study the effect of varying liquid fraction on the orientation of T1 events in disordered foams, I use the "wet method" described in section 2.6 and the area-disorder is kept within the range $0.09 < \mu_2^A < 0.13$. Simulations are restricted to 100 bubbles in order that they can be completed in reasonable time (1-4 weeks depending on liquid fraction). With fewer bubbles, the statistics will not be as good as for the dry simulations performed in the previous section, and it is not possible to adequately fit a

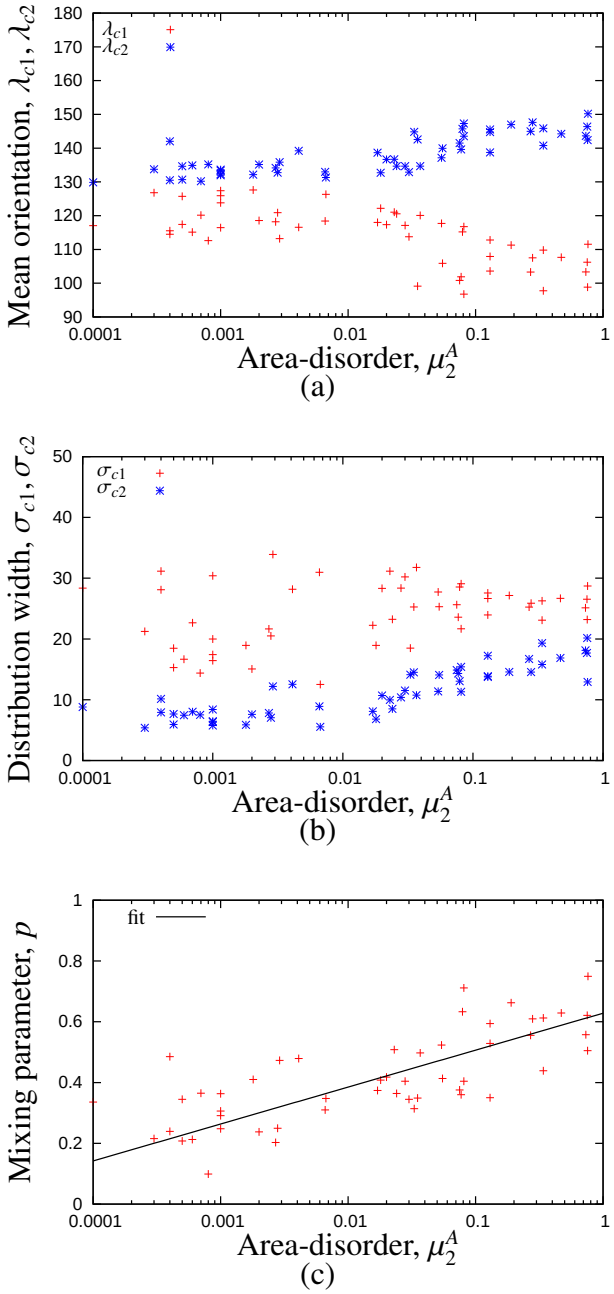

Figure 5.8: (a) The mean of each normal distribution, $\lambda_{c1}, \lambda_{c2}$, contributing to the overall distribution of θ_c against area-disorder μ_2^A. At low-area-disorder, the means are similar, but one mean grows and the other is reduced as the area-disorder is increased. (b) The width of each normal distribution, σ_{c1}, σ_{c2}, contributing to the overall distribution of θ_c against area-disorder μ_2^A. At low area-disorder, the width of the distribution of the low θ_c mode is greater and shows more variation than that of the low θ_c mode. As the area-disorder is increased, both widths have similar magnitude and spread. (c) The mixing parameter, p, against area-disorder μ_2^A. The mixing parameter determines the influence of each normal distribution on the overall distribution of θ_c, and increases with increasing area-disorder as the low θ_c mode grows in prominence.

distribution to the data. However, the sample mean, $\langle . \rangle$, and standard deviation, SD(.), of the orientations θ_d and θ_c will indicate the behaviour as a function of liquid fraction.

Recall that for a perfectly ordered foam, the orientation of the disappearing link, θ_d, increases with increasing liquid fraction, whilst the orientation of the created link, θ_c, decreases with increasing liquid fraction after an initial increase at low liquid fraction (figure 5.3). The evolution of the distributions of θ_d and θ_c with liquid fraction, ϕ_l, is shown in figures 5.9 and 5.10. Although the statistical information is not as good as was obtained from simulations in the dry limit, a similar distribution of θ_d, with a single sharp peak, is observed at low liquid fraction ($\phi_l = 0.0075$) as was found for foams in the dry limit (cf. figure 5.5). As the liquid fraction is increased the distributions broaden and, at $\phi_l = 0.04$, resemble those found by Wang *et al.* [46] (cf. figure 5.2 (i)). At low shear rate the distributions of θ_d of Wang *et al.* reach a maximum value of approximately 0.25 at 45°, and are similar in shape, position and width to the distribution I see in figure 5.9 (b) obtained from disordered wet foam simulations. A detailed comparison of my results with the study of Wang *et al.* is found in section 5.5.1.

At low liquid fraction, the distribution of θ_c appears to have two modes (figure 5.10 (a)), as in the dry limit (cf. figure 5.7). As the liquid fraction increases, the distributions broaden and the statistics are not good enough to identify multiple modes if they exist. If more than one mode did exist, this would mean that at high ϕ_l there are further preferred local arrangements of bubbles when T1s occur. Perhaps a more likely outcome is that as the rigidity-loss transition [36] is approached, the distribution becomes uniform with all orientations equally likely.

With increasing liquid fraction the distributions of both θ_d and θ_c span the entire 180° interval. As a result, additional care must be taken in calculating the sample mean and variance. The chosen 180° interval over which the data is represented will influence

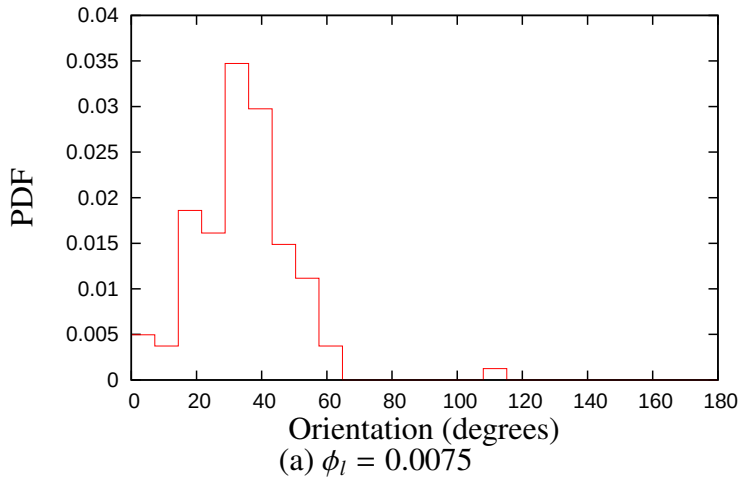

(a) $\phi_l = 0.0075$

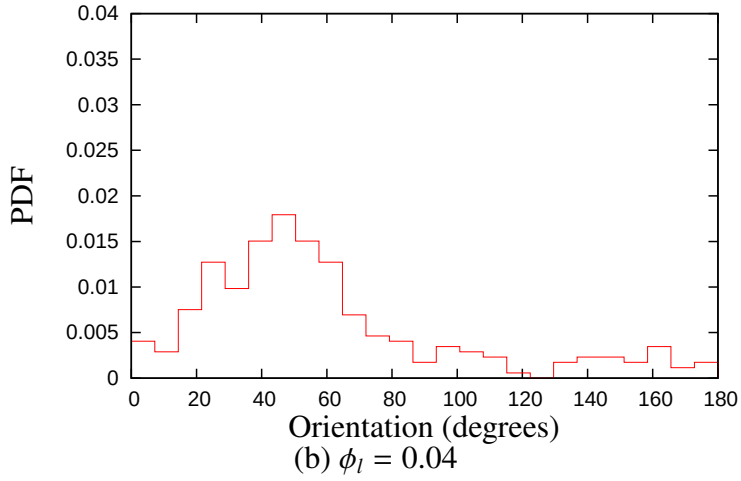

(b) $\phi_l = 0.04$

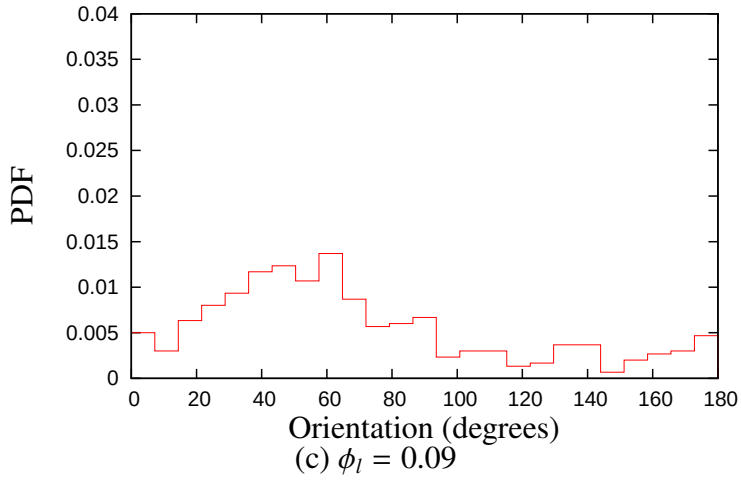

(c) $\phi_l = 0.09$

Figure 5.9: The evolution of the distribution of the disappearing link, θ_d, with liquid fraction. (a) At low liquid fraction the distribution has a single sharp peak, as for foams in the dry limit (cf. figure 5.5). (b)-(c) As the liquid fraction increases, the peak becomes less pronounced and the distribution broadens and spans the entire interval so that every orientation is present.

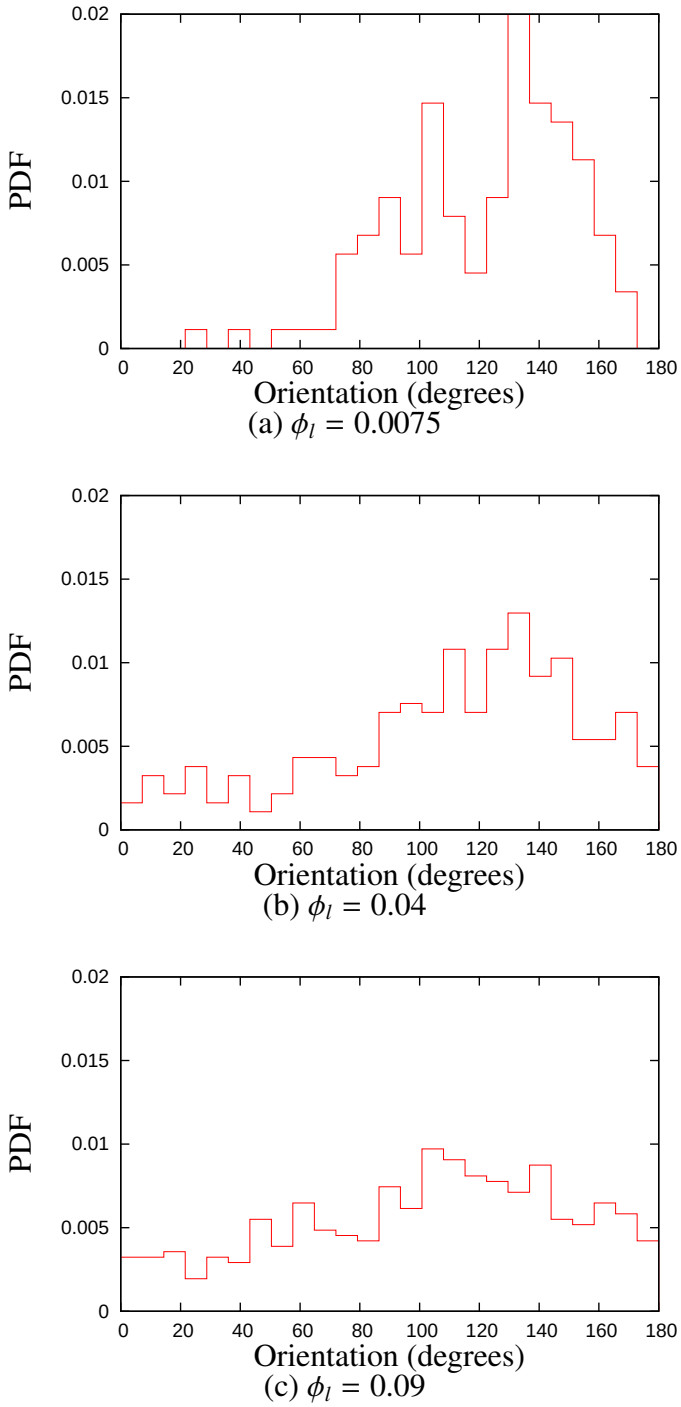

Figure 5.10: The evolution of the distribution of the created link, θ_c, with liquid fraction. (a) At low liquid fraction the distribution appears to have two modes similar to those found for foams in the dry limit (cf. figure 5.7). (b)-(c) As the liquid fraction increases, the peak becomes less pronounced and the distribution broadens and spans the entire interval. Multiple modes, if they exist, are harder to identify.

the usual method of calculating the mean and variance of N datapoints:

$$\langle x \rangle = \frac{1}{N} \sum_{j=1}^{N} x_j \tag{5.7}$$

$$\mathrm{Var}(x) = \frac{1}{N} \sum_{j=1}^{N} \left(x_j - \langle x \rangle \right)^2 . \tag{5.8}$$

For example, representing the data with the peak in the middle of the interval will yield different values of mean and variance than if the data was represented such that the peak was at the lower end of the interval. Thus, I calculate a *circular* mean and variance which are independent of the choice of interval. Following Mardia [148], I proceed as follows: For each simulation, let θ_i, $i = 1 \ldots N_\theta$, denote the orientation of the links after the transient. Each orientation is multiplied by a factor of two so that the data for each simulation is 360° periodic, and each datapoint is considered as a point on the perimeter of the unit circle. Let θ'_i denote the new datapoints. Then

$$\theta'_i = 2\theta_i. \tag{5.9}$$

The mean, $\langle \theta' \rangle$, can then be calculated from

$$R\cos\langle \theta' \rangle = C \quad \text{and} \quad R\sin\langle \theta' \rangle = S \tag{5.10}$$

where

$$C = \frac{1}{N_\theta} \sum_{i=1}^{N_\theta} \cos\theta'_i \tag{5.11}$$

$$S = \frac{1}{N_\theta} \sum_{i=1}^{N_\theta} \sin\theta'_i \tag{5.12}$$

$$R = \sqrt{C^2 + S^2}. \tag{5.13}$$

Thus, for $-90^\circ < \tan^{-1}(S/C) < 90^\circ$, θ' can be calculated as follows:

$$\theta' = \begin{cases} \tan^{-1}\left(\frac{S}{C}\right) & \text{if } S > 0 \text{ and } C > 0 \\ \tan^{-1}\left(\frac{S}{C}\right) + 180^\circ & \text{if } C < 0 \\ \tan^{-1}\left(\frac{S}{C}\right) + 360^\circ & \text{if } S < 0 \text{ and } C > 0 \end{cases} \tag{5.14}$$

The sample mean and standard deviation of the original T1 orientations are then given as

$$\langle\theta\rangle = \frac{\langle\theta'\rangle}{2} \tag{5.15}$$

$$\mathrm{SD}(\theta) = \frac{\sqrt{-2\ln R}}{2}. \tag{5.16}$$

Note now that the sample mean and standard deviation are used instead of the mean and width of the fitted distributions used in section 5.3 where there was enough information to fit a statistical distribution.

Figure 5.11 shows the variation in the mean and standard deviation of the orientation of the disappearing link, $\langle\theta_d\rangle$ and $\mathrm{SD}(\theta_d)$, with liquid fraction. $\langle\theta_d\rangle$ increases with increasing liquid fraction and may reach a plateau at around 45° - more data with $\phi_l > 0.1$ is required to verify this, which is beyond the scope of my present simulations given the computational time required. The difference between the ordered and disordered case is not great and in this instance the ordered case provides a reasonably good approximation of disordered foam response. An increase in $\langle\theta_d\rangle$ with liquid fraction indicates that T1s are initiated at lower applied strain as the liquid fraction increases. $\mathrm{SD}(\theta_d)$ also increases with increasing liquid fraction. T1s occur with a wider range of orientations, with the likelihood of one particular orientation being diminished.

The variation in the mean and standard deviation of the orientation of the created link, $\langle\theta_c\rangle$ and $\mathrm{SD}(\theta_c)$, with liquid fraction is shown in figure 5.12. In contrast with the

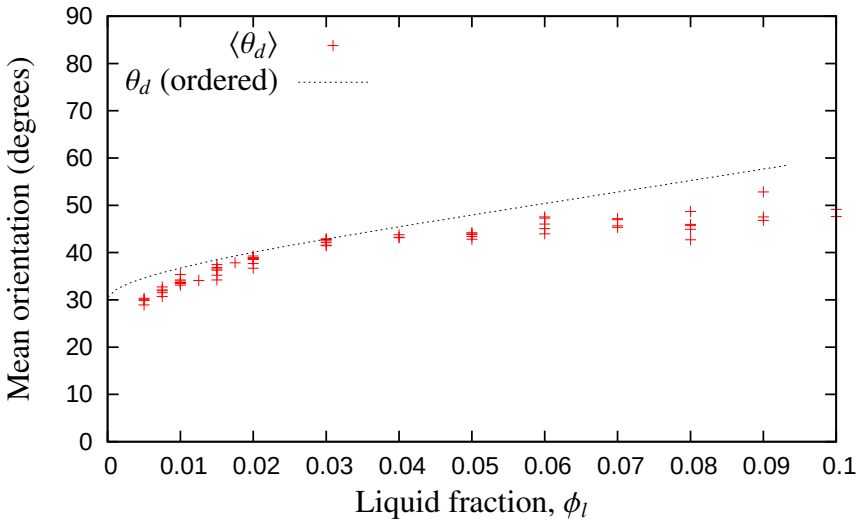

(a)

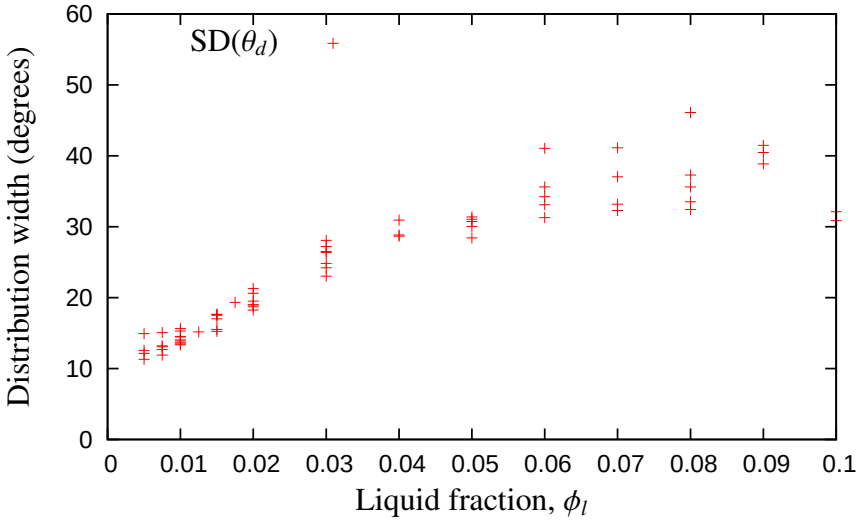

(b)

Figure 5.11: (a) The mean orientation of the disappearing link, $\langle\theta_d\rangle$, increases with increasing liquid fraction. The dashed line is the prediction for ordered foams. (b) The standard deviation of the orientation of the disappearing link, SD(θ_d), increases with increasing liquid fraction.

ordered case, $\langle\theta_c\rangle$ is constant at low liquid fraction, and may show a slight decrease at high liquid fraction. There is no discontinuity in behaviour associated with the stability of a fourfold Plateau border as in the ordered case, indicating that in this respect the ordered foam, in which all T1s occur simultaneously, does not provide a good picture of a disordered wet foam. Since only the mean orientation is considered, these conclusions could be misleading if the distribution is bimodal, as in the dry limit.

SD(θ_c) increases with increasing liquid fraction. The distribution broadens with increasing liquid fraction until all orientations are possible.

5.5 Discussion

5.5.1 Comparison with experiment

Having described the dependence of T1 orientation on liquid fraction and area-disorder, I consider to what extent the results are consistent with the experimental study by Wang *et al.* [46].

I begin by highlighting the differences between my simulations and the experiments of Wang *et al.* [46]. My simulations are performed in the quasistatic limit with liquid fraction in the range $0 < \phi_l \leq 0.1$ and area-disorder in the range $0.00016 \leq \mu_2^A \leq 0.8$. In the work of Wang *et al.*, experiments are performed with monodisperse foams. The liquid fraction is not specified. It is likely to be greater than 0.05 but it is hard to define an effective liquid fraction in such an experiment [74]. The authors do not consider any of their results to be in the quasistatic limit.

The main difference between the experimental results with those from simulations in the dry limit presented at the beginning of the chapter (figure 5.1) is the position of the peak of the distributions of the disappearing link. The mean depends primarily on liquid fraction and, to a lesser extent, area-disorder. As the liquid fraction increases,

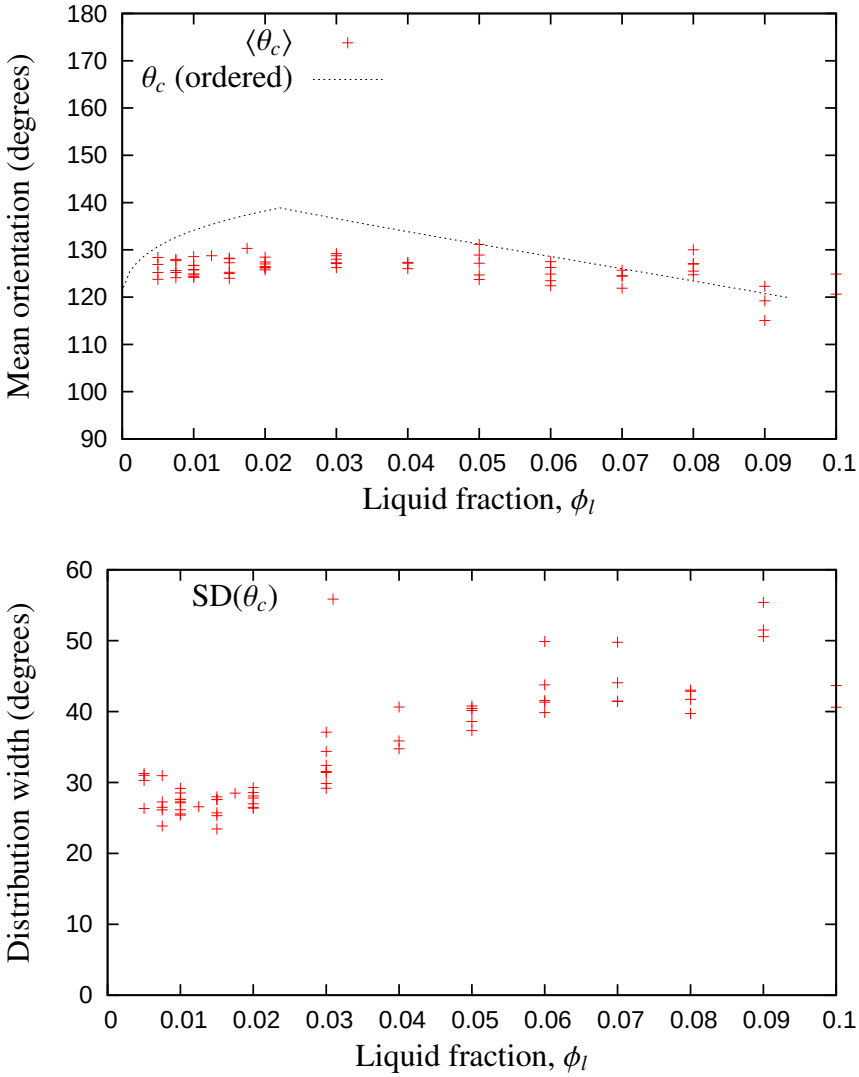

Figure 5.12: (a) The mean orientation of the created link, $\langle\theta_c\rangle$, is constant over a large range of liquid fraction and decreases slightly at high liquid fraction. In contrast to the ordered case, there is no discontinuity in the behaviour associated with the stability of a fourfold Plateau border. (b) The standard deviation of the orientation of the created link, SD(θ_c), increases with increasing liquid fraction.

the mean orientation (and therefore the peak of the distribution) also increases (figure 5.11), to a value comparable to that observed by Wang *et al.* when the liquid fraction exceeds $\phi_l \approx 0.05$.

The mean orientation of the created link does not change with liquid fraction but does depend on area-disorder. The peak of the distribution for low area-disorder foams (equal to the largest mean of the bimodal distribution) is approximately 130° in agreement with the low area-disorder experiments of Wang *et al.*

Whilst I cannot reproduce the exact conditions of the experimental study of Wang *et al.* (since the liquid fraction is unknown and my simulations are restricted to the quasistatic limit), the dependence of the distributions of the disappearing and created links on liquid fraction and area-disorder presented in this chapter indicate that for the most part the results presented here and the experimental study of Wang et al. are compatible. The only difference that cannot be explained with results in this chapter is the existence of a secondary peak in the distribution of the disappearing link from the experimental study of Wang *et al.*. A secondary peak is observed in the distribution of θ_c in dry foam simulations but not in the distribution of θ_d. However, the statistical information obtained for foams within a range of liquid fraction similar to the experiments of Wang *et al.* may not be adequate to detect a small secondary peak to the distribution of θ_d since these simulations were performed with only 100 bubbles.

5.5.2 Implications of T1 orientation

In this section I consider the implications of the results in this chapter in terms of *T1 localization* and *yielding*. It is the orientation of the disappearing link, θ_d, which is most appropriate in this circumstance since it signifies the onset of a T1 whose occurrence is driven by the applied shear. I summarize the results of this and previous chapters in table 5.1 and include inferences regarding the dependence of the dynamic yield stress,

Results				
Dependent parameter			Control parameter	Figure
Dynamic yield stress, τ_y^d	$\uparrow$ then $\downarrow$	with	area-disorder, μ_2^A	3.9
Dynamic yield stress, τ_y^d	$\downarrow$	with	liquid fraction, ϕ_l	3.15
Localization width, w_{T1}	$\uparrow$	with	area-disorder, μ_2^A	4.10
Localization width, w_{T1}	$\uparrow$	with	liquid fraction, ϕ_l	4.30
Mean orientation, λ_d	$\downarrow$ then $\uparrow$	with	area-disorder, μ_2^A	5.6
Mean orientation, λ_d	$\uparrow$	with	liquid fraction, ϕ_l	5.11
Distribution width, σ_d	$\uparrow$	with	area-disorder, μ_2^A	5.6
Distribution width, σ_d	$\uparrow$	with	liquid fraction, ϕ_l	5.11
Inferences				
Dynamic yield stress, τ_y^d	$\downarrow$	with	Mean orientation, λ_d	
Dynamic yield stress, τ_y^d	$\uparrow$ then $\downarrow$	with	Distribution width, σ_d	
Localization width, w_{T1}	$\downarrow$ then $\uparrow$	with	Mean orientation, λ_d	
Localization width, w_{T1}	$\uparrow$	with	Distribution width, σ_d	

Table 5.1: Summary of results concerning yield stress, localization width and T1 orientation, and resulting inferences. $\uparrow$ and $\downarrow$ stand for "increases" and "decreases" respectively.

τ_y^d, and localization width, w_{T1}, on the mean, λ_d, and width, σ_d, of the distribution of the orientation of the disappearing link.

First I note that the effect of liquid fraction and area-disorder is largely the same, with the exception of the behaviour of the dynamic yield stress and mean orientation of the disappearing link at low area-disorder. From these results I make inferences about the variation of localization width and dynamic yield stress with the mean and width of the distribution of the disappearing link. The relationship of the static yield stress and the orientation of the disappearing link is not considered since the static yield stress is a transient property and θ_d is measured after the transient while the foam is flowing.

The decrease of the dynamic yield stress with liquid fraction and the increase of the mean orientation of the disappearing link with liquid fraction suggests that the dynamic yield stress should decrease with increasing mean orientation. The variation of the dynamic yield stress and mean orientation with area-disorder (above a certain level of

area-disorder) supports this inference.

The width of the distribution of the disappearing link increases with increasing liquid fraction and area-disorder. The dynamic yield stress decreases with increasing liquid fraction and area-disorder, except at low area-disorder, suggesting that the dynamic yield stress should decrease with increasing distribution width, with possible increase at low distribution width (corresponding to low area-disorder).

The localization width increases with increasing liquid fraction and area-disorder. The mean orientation of the disappearing link increases with increasing area-disorder (above a certain level of area-disorder) and increases with increasing liquid fraction. This suggests that the localization width will increase with increasing mean orientation above a certain value of λ_d.

Finally, since the distribution width increases with both liquid fraction and area-disorder, and the localization width increases with both liquid fraction and area-disorder, the localization width should also increase with increasing distribution width.

These inferences can be tested by returning to the data from dry and wet foam simulations. Figure 5.13 shows the relationship between the dynamic yield stress, τ_y^d, and the mean, λ_d, and width, σ_d of the distribution of the orientation of the disappearing link. Data from both the dry and wet methods are in good agreement.

The dynamic yield stress decreases with increasing mean orientation in agreement with the inference in table 5.1. Recall that a low value of the orientation of the disappearing link, θ_d, suggests that a high local strain resulted in a T1, whilst a high value of θ_d suggests that a low local strain resulted in a T1. An accumulation of many T1 events results in a foam flowing and thus as λ_d is the mean of the values of θ_d, it is related to the macroscopic yield strain and therefore the macroscopic yield stress also.

The clear monotonic decreasing relationship between the dynamic yield stress and the mean orientation of the disappearing link, along with the fact that the dynamic yield

stress increases initially and then decreases with area-disorder, supports the weaker evidence in figure 5.6 that λ_d increases with increasing area-disorder following an initial decrease.

The dynamic yield stress increases initially with the width, σ_d, of the distribution of the orientation of the disappearing link, θ_d, and then decreases as σ_d increases further. The origin of the initial increase is unclear since I would expect the yield stress to decrease only as the σ_d increases and a wider range of local bubble configurations can lead to a T1. The result is nevertheless consistent with the prediction from data of σ_d and τ_y^d against liquid fraction and area-disorder.

The experimental study of Wang *et al.* [46] and simulations by Cox [146] show that orientation of the disappearing link decreases with increasing shear-rate. The relationship between the orientation of the disappearing link, θ_d, and the dynamic yield stress now suggests that with increasing shear rate, the dynamic yield stress would also increase and this is consistent with what is observed in the literature [29; 35], once more establishing the link between the orientation of the disappearing link at the microscopic scale and the macroscopic yielding behaviour of the foam.

Figure 5.14 shows the relationship between the localization width and the mean and width of the distribution of the disappearing link. The localization width decreases initially with increasing orientation, corresponding to an increase in area-disorder. The localization width then increases with increasing orientation corresponding to an increase in liquid fraction. The data for dry and wet foams do not match up as for the case of the yield stress. This could be an indication either that there are other factors which determine the localization width and it is not linked solely to the orientation of a T1, or that some finite size effects are present from using a foam with only 100 bubbles. The width of the localized region increases with the distribution width for data obtained for both dry and wet foams but once more the data does not appear to link up. This

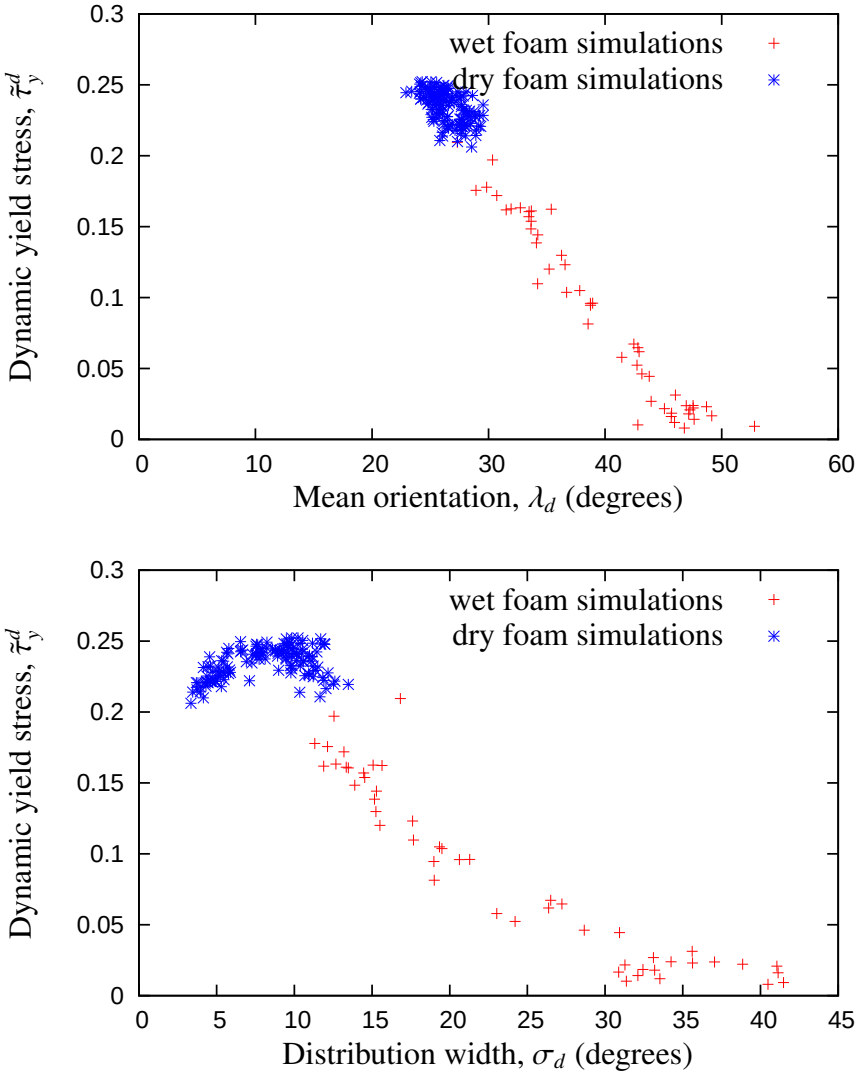

Figure 5.13: The dynamic yield stress, $\tilde{\tau}_y^d$, is related to the mean, λ_d, and width, σ_d, of the distribution of the disappearing link: (a) $\tilde{\tau}_y^d$ decreases with increasing λ_d and (b) $\tilde{\tau}_y^d$ decreases with increasing σ_d after an initial increase.

is an area in which further study would be needed, reducing the liquid fraction further with the wet method and fixing the area-disorder. I do note however that the data for dry foams for the same range of area-disorder in which the wet foam simulations were performed is consistent with the data obtained from wet foam simulations. There is therefore, on balance, a correlation between localization and T1 orientation in that both depend in some way on liquid fraction and area-disorder but the relationship is not as clear as the causal dependence of the dynamic yield stress on T1 orientation.

5.6 Summary

The local bubble configuration of a foam at the instant a T1 is triggered is associated to a particular orientation of the disappearing and created links between bubbles, relative to the direction of shear. The peaks in the distributions of the orientation of the disappearing and created links indicate that there are specific local bubble configurations which are more likely to result in a T1 event than others. The distributions of the T1 orientations depend upon the liquid fraction and area-disorder of the foam as well as the rate at which the foam is sheared. The described dependence of the mean and width of the distributions of the disappearing and created links is compatible with existing experimental results.

For ordered two-dimensional foams, the orientation of the disappearing and created links can be calculated from the strains at which threefold Plateau borders merge and fourfold Plateau borders separate (equations (5.1) and (5.2)). For $\phi_l = 0$, $\theta_d = 30°$ and $\theta_c = 120°$.

For disordered dry two-dimensional foams in the quasistatic limit, the distribution of θ_d is well-fitted by a normal distribution. The mean of the distribution initially decreases with increasing area-disorder, followed by an increase (figure 5.6 (a)). The width of the

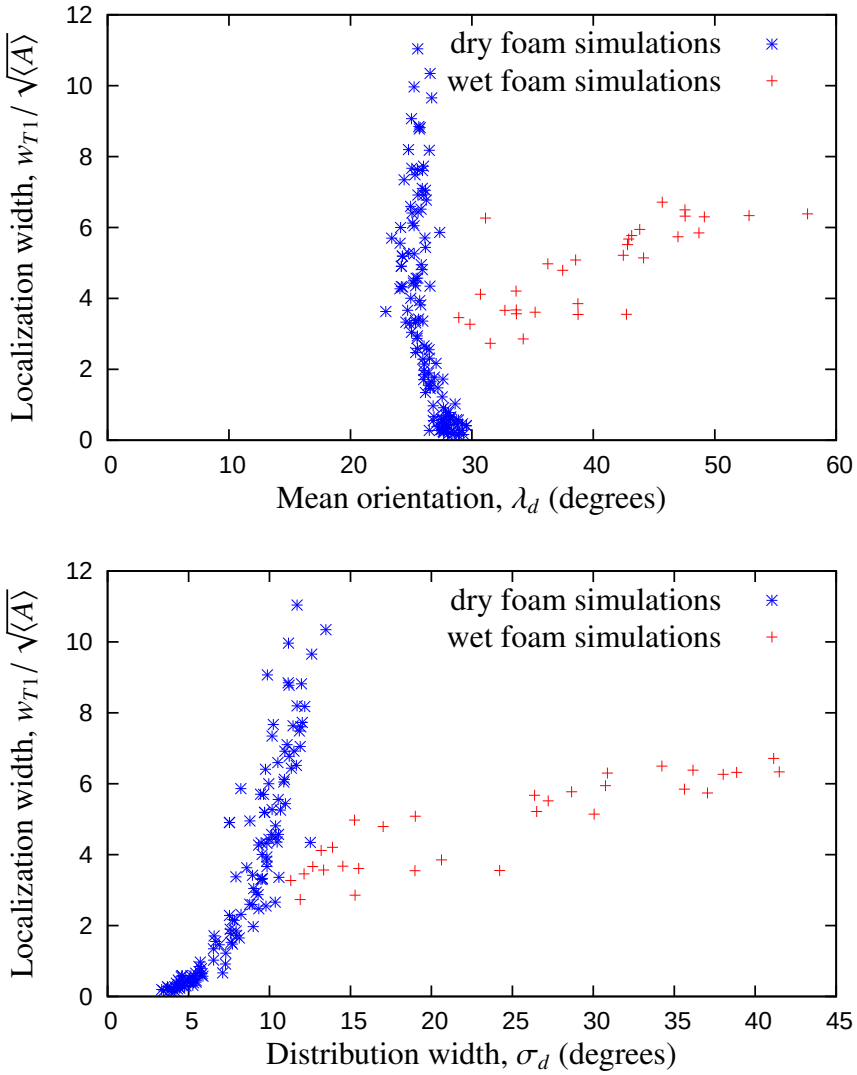

Figure 5.14: The relationship between the localization width, w_{T1}, and the mean, λ_d, and width, σ_d, of the distribution of the disappearing link: (a) w_{T1} decreases with increasing λ_d at low liquid fraction but increases otherwise. (b) w_{T1} increases with increasing σ_d but data from dry and wet foam simulations are not in good agreement.

distribution increases with increasing area-disorder (figure 5.6 (b)). The variation in the mean of the distribution is small relative to the width of the distribution (figure 5.6 (c)).

The distribution of θ_c is a mixture of two normal distributions, suggesting different underlying causes for the T1s. At low area-disorder, the distribution with the largest mean dominates the overall distribution but the distribution with the smallest mean grows in prominence with increasing area-disorder (figure 5.8). The reasons for a bi-modal distribution are not yet known.

The orientation of the disappearing link occurs at the beginning of a T1 when two threefold Plateau borders merge and the mean and width of the distribution of this link correlates with the macroscopic phenomena of yielding regardless of area-disorder and liquid fraction (figure 5.13).

Chapter 6

Conclusions

6.1 Summary

I have probed the response of two-dimensional foams to applied shear in the quasistatic limit through numerical simulation and studied the phenomena of yielding and shear localization in terms of the shear-induced T1 rearrangements. In particular I have focused on the effect of liquid fraction and area-disorder on the flow of the foam and found that in many respects, variation of the two parameters have the same qualitative effect.

I performed oscillatory shear simulations to study the transition from solid-like to liquid-like behaviour in dry two-dimensional foams and found that the complex shear modulus as well as the higher stress harmonics are in good agreement with experimental data for foams and other yield stress materials (figures 3.4 and 3.5).

The yield stress is an important parameter in the solid-liquid transition, and for two-dimensional foams, the static and dynamic yield stress both decrease with increasing area-disorder (figure 3.9) and liquid fraction (figure 3.15). The only exception is for dry foams at low area-disorder, for which the static yield stress is found to be constant with increasing area-disorder whilst the dynamic yield stress increases with increasing area-disorder.

When a two-dimensional foam begins to flow, the T1s can become localized in space. The position and width of the localized region depend on liquid fraction and area-disorder. The position of the localized region is more likely to move and cover larger regions of the foam as the area-disorder is increased, and the width of the localized region increases approximately linearly with increasing liquid fraction (figure 4.30) and as the square root of area-disorder (equation (4.10)). The overall effect is a greater amount of flowing foam with increasing liquid fraction and area-disorder. For sufficiently high values of liquid fraction and area-disorder, the T1s fill the channel and no localization is observed. A combination of liquid fraction, area-disorder and external friction could therefore account for the majority of variation in reported results concerning the shear localization of foams.

For dry two-dimensional foams I presented a one-dimensional measure and a tensorial measure of foam structure which can identify the localized region. Both measures can be calculated from a single still image and are an important first step to a means of predicting the future position and movement of the localized region.

The local bubble configuration at the instant a T1 is triggered gives rise to a particular orientation of the disappearing and created links. The distributions of the disappearing and created links have peaks, indicating that there are certain local bubble configurations which are more likely to result in a T1. The mean and width of the distribution of the disappearing and created links depend on liquid fraction and area-disorder and so therefore does the local bubble configuration leading to a T1.

The mean and width of the distribution of the disappearing link increase with increasing area-disorder (figure 5.6) and liquid fraction (figure 5.11). The distribution of the orientation of the created link for dry two-dimensional foams is a mixture of two normal distributions. At low area-disorder, the overall distribution is dominated by the distribution with the largest mean, but as the area-disorder is increased the distribution

with the smallest mean has an increasing effect on the overall distribution (figure 5.8).

Macroscopic flow behaviour originates at the microscopic scale and I showed that the dynamic yield stress was directly related to the orientation of the T1 events. The localization width is also related to the orientation of T1 events. The relationship is not as clear however, since the data for dry foam simulations in which the area-disorder is a control parameter and data from wet foam simulations in which the liquid fraction is the control parameter do not match up as they did with the dynamic yield stress.

In each chapter I used results from a perfectly ordered two-dimensional foam as a reference. In general, the response of disordered two-dimensional foams differed significantly from that of the ordered foam. The variation of the static and dynamic yield stress of ordered two-dimensional foams with liquid fraction, whilst in qualitative agreement with my results for disordered foams, differs by a significant margin quantitatively. The spatial distribution of T1s and displacement profiles during linear Couette shear change suddenly as area-disorder is introduced and the variation of the orientation of the disappearing and created links of disordered foams differs from the ordered case. When considering the response of real foam systems therefore, it is essential that the role of disorder is considered.

6.2 Future work

The two-dimensional simulations described in this thesis have allowed me to make many deductions concerning foam response to applied shear. The ultimate goal will always be to perform simulations which accurately represent real foam systems. In this respect, there are a number of directions in which my work can be extended.

Perhaps the most obvious extension to the work presented here is to consider three-dimensional foam systems. Three-dimensional simulations are more challenging to

implement as well as more time consuming to run. Nevertheless, with faster processor speeds, three-dimensional simulations are becoming more viable. It would be interesting to consider what effect the volumetric disorder and liquid fraction have on the spatial distribution of topological changes in a three-dimensional foam, and how this in turn effects the flow of the foam.

Wall slip is often eliminated in experimental foam studies, but will undoubtedly be a factor in real world applications. A modification of my numerical method to allow the films in contact with the walls to slip allows the effects of wall slip on foams undergoing linear Couette shear to be studied. Preliminary results with a hundred bubbles suggest that the position of the localized region depends on the boundary conditions at each wall.

There are at least two ways of modelling slip at the walls. One method considers that the motion is governed by static friction. Then a balance of forces where the vertex meets the wall leads to

$$\gamma \cos\alpha_w = \mu_f \gamma \sin\alpha_w \tag{6.1}$$

where γ is the tension of the film, α_w is the contact angle between the film and the wall and μ_f is some coefficient representing the friction between the film and the wall. This effectively defines a critical contact angle, α_w^{crit}, below which the vertices will slip, given by

$$\alpha_w^{\text{crit}} = \tan^{-1}\left(1/\mu_f\right). \tag{6.2}$$

In a simulation, films that meet the wall at an angle less than α_w^{crit} are moved as to increase the angle to the critical one.

Alternatively, one could consider that the motion is governed by dynamic friction and, in the spirit of the Viscous Froth model [42] (see section 2.2.2.2), move the vertices in proportion to their "velocity", v, scaled by a drag coefficient, μ_d, and the contact angle

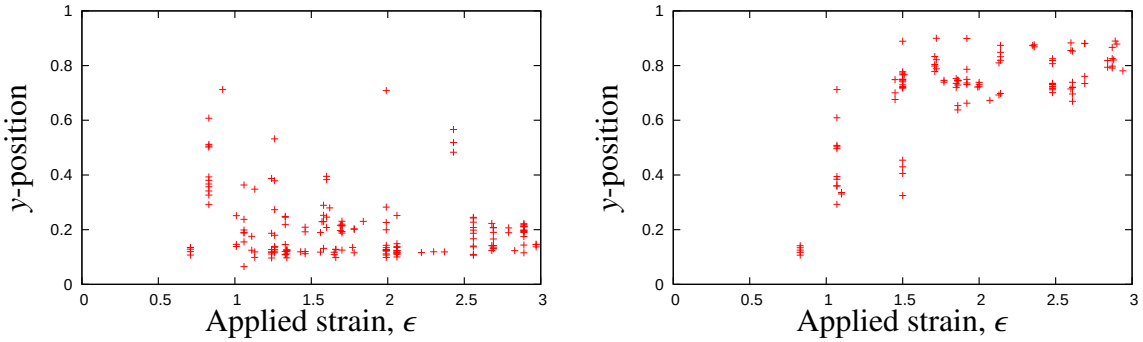

Figure 6.1: (a) T1 y-positions for a foam with no slip boundary conditions at both plates. T1s occur near the bottom plate. (b) T1 y-positions for the same foam as in (a), with a no slip boundary conditions at the top plate, but the films in contact with the bottom plate are allowed to slip. The T1s now occur near the top plate.

between the film and the wall:

$$\mu_f v = \gamma \cos\alpha_w. \tag{6.3}$$

Indeed, a combination of both methods could be used and future work should include investigation of which method is most appropriate and its validity in the quasistatic limit.

Figure 6.1 shows the T1 positions when a 100 bubble foam is sheared between parallel plates, with different boundary conditions. In the first instance (figure 6.1 (a)), a no slip boundary condition is used and the T1s localize in a band near the lower wall. In the second example (figure 6.1 (b)), using the same initial bubble configuration, the films at the lower plate are allowed to move, using the first method described above . This reduces the stress close to the lower wall and, as a result, the T1s move to a location near the upper wall. It may therefore be possible to control the position of the localized region by controlling the degree of slip at the walls, but a more detailed study is required to verify this.

It would also be interesting to extend the comparison between dry foams and glassy systems discussed in section 4.4. One way in which this could be done would be to perform simulations with finite strain rate. Varnik *et al.* [144] observe localized flow

profiles with sheared and non-sheared regions when shearing a Lennard Jones glass at low strain rate, similar to the displacement profiles of dry two-dimensional foams at low area-disorder (figure 4.5 (b)). As the strain rate is increased the position of the interface between the stationary band and the sheared band fluctuates and the flow profiles become linear. My simulations were performed in the quasistatic limit, where the rate of strain is assumed to be very small. The effect of a finite strain rate could be investigated either by implementing existing models, e.g. the Viscous Froth model [42] which includes external dissipation from the bounding plates of a Hele-Shaw cell, or by developing new code to include the internal dissipation of the liquid as it flows in the Plateau borders.

Finally, it may be beneficial to revive the software PLAT and modify it for linear Couette shear. The software is faster than current Surface Evolver methods and would allow simulation of larger foam samples at high liquid fraction. It would be interesting to discover whether the difference in the approach to finding an equilibrium foam configuration would lead to significantly different results.

Bibliography

[1] J. A. F. Plateau. Statique expérimentale et théorique des liquides soumis aux seules forces moléculaires. *Gauthier-Villars, Paris*, 1873.

[2] D. Weaire and S. Hutzler. *The Physics of Foams*. Oxford University Press, 1999.

[3] G. Verbist, D. Weaire, and A. M. Kraynik. The foam drainage equation. *J. Phys. Cond. Matt.*, 8:3751–3731, 1996.

[4] R. D. MacPherson and D. J. Srolovitz. The von Neumann relation generalized to coarsening of three-dimensional microstructures. *Nature*, 446:1053–1055, 2007.

[5] J. von Neumann. *Metal Interfaces*, pages 108–110. American Society for Metals, Cleveland, 1952.

[6] J. J. Chae and M. Tabor. Dynamics of foams with and without wall rupture. *Phys. Rev. E*, 55:598–610, 1997.

[7] A. Bhakta and E. Ruckenstein. Decay of standing foams: drainage, coalescence and collapse. *Adv. Coll. Int. Sci.*, 70:1–124, 1997.

[8] N. D. Denkov. Mechanisms of foam destruction by oil-based antifoams. *Langmuir*, 20:9463–9505, 2004.

[9] A. A. Briggs. Foams for firefighting. In R. K. Prud'homme and S. A. Khan, editors, *Foams: Theory, Measurements and Applications*, volume 57 of *Surfactant Science Series*, pages 465 – 509. Marcel Dekker, New York, 1996.

[10] W. R. Rossen. Foams in enhanced oil recovery. In R. K. Prud'homme and S. A. Khan, editors, *Foams: Theory, Measurements and Applications*, volume 57 of *Surfactant Science Series*, pages 413 – 464. Marcel Dekker, New York, 1996.

[11] R. K. Prud'Homme and G. G. Warr. Foams in mineral floatation and separation processes. In R. K. Prud'homme and S. A. Khan, editors, *Foams: Theory, Measurements and Applications*, volume 57 of *Surfactant Science Series*, pages 511–554. Marcel Dekker, New York, 1996.

[12] M. Rieger. Foams in personal care products. In R. K. Prud'homme and S. A. Khan, editors, *Foams: Theory, Measurements and Applications*, volume 57 of *Surfactant Science Series*, pages 381 – 412. Marcel Dekker, New York, 1996.

[13] T. F. Cooke and D. E. Hirt. Foam wet processing in the textile industry. In R. K. Prud'homme and S. A. Khan, editors, *Foams: Theory, Measurements and Applications*, volume 57 of *Surfactant Science Series*, pages 339 – 380. Marcel Dekker, New York, 1996.

[14] J. E. Taylor. The structure of singularities in soap-bubble-like and soap-film-like minimal surfaces. *Ann. Math.*, 103:489–539, 1976.

[15] D. Weaire and R. Phelan. Vertex instabilities in foams and emulsions. *J. Phys. Cond, Matt.*, 8:37–43, 1996.

[16] D. J. Durian. Bubble-scale model of foam mechanics: Melting, nonlinear behaviour, and avalanches. *Phys. Rev. E*, 55:1739 – 1751, 1997.

[17] A. Saint-Jalmes and D. Durian. Vanishing elasticity for wet foams: Equivalence with emulsions and role of polydispersity. *J. Rheol*, 43:6, 1999.

[18] T. G. Mason, J. Bibette, and D. A. Weitz. Elasticity of compressed emulsions. *Phys. Rev. Lett.*, 75:2051–4, 1995.

[19] F. Bolton and D. Weaire. The effects of Plateau borders in the two-dimensional soap froth. I. Decoration lemma and diffusion theorem. *Phil. Mag. B*, 63:795–809, 1991.

[20] F. Bolton and D. Weaire. The effects of Plateau borders in the two-dimensional soap froth. II. General simulation and analysis of rigidity loss transition. *Phil. Mag. B*, 65:473–487, 1992.

[21] S. Hutzler, D. Weaire, and F. Bolton. The effects of Plateau borders in the two-dimensional soap froth. III. Further results. *Phil. Mag. B*, 71:277–289, 1995.

[22] D. J. Durian. Foam mechanics at the bubble scale. *Phys. Rev. Lett*, 75:4780 – 4783, 1995.

[23] S. Tewari, D. Schiemann, D. J. Durian, C. M. Knobler, S. A. Langer, and A. J. Liu. Statistics of shear-induced rearrangements int two-dimensional model foam. *Phys. Rev. E*, 60:4385–4396, 1999.

[24] V. J. Langlois, S. Hutzler, and D. Weaire. Rheological properties of the soft-disk model of two-dimensional foams. *Phys. Rev. E*, 78:021401, 2008.

[25] E. B. Matzke. The 3-dimensional shape of bubbles in foam - an analysis of the role of surface forces in 3-dimensional cell shape determination. *Am. J. Bot.*, 33:58–80, 1946.

[26] A. M. Kraynik, D. A. Reinelt, and F. van Swol. Structure of random monodisperse foam. *Phys. Rev. E*, 67:031403, 2003.

[27] A. M. Kraynik, D. A. Reinelt, and F. van Swol. Structure of random foam. *Phys. Rev. Lett.*, 93:208301, 2004.

[28] B. S. Gardiner, B. Z. Dlugogorski, and G. J. Jameson. The steady shear of three-dimensional wet polydisperse foams. *J. Non-Newt. Fl. Mech.*, 92:151–166, 2000.

[29] F. Rouyer, S. Cohen-Addad, M. Vignes-Adler, and R. Höhler. Dynamics of yielding observed in a three-dimensional aqueous dry foam. *Phys. Rev. E*, 67:021405, 2003.

[30] H. M. Princen. Rheology of foams and highly concentrated emulsions 1. Elastic properties and yield stress of a cylindrical model system. *J. Coll. Int. Sci.*, 91:160–175, 1983.

[31] D. Weaire and J. P. Kermode. Computer simulation of a two-dimensional soap froth I. Method and motivation. *Phil. Mag. B*, 48:245–249, 1983.

[32] S. A. Khan and R. C. Armstrong. Rheology of Foams I. Theory for dry foams. *J. Non-Newt. Fl. Mech.*, 22:1–22, 1986.

[33] S. A. Khan and R. C. Armstrong. Rheology of foams II. Effects of polydispersity and liquid viscosity for foams having gas fraction approaching unity. *J. Non-Newt. Fl. Mech.*, 25:61–92, 1987.

[34] A. M. Kraynik and M. G. Hansen. Foam and emaulsion rheology: A quasistatic model for large deformations of spatially-periodic cells. *J. Rheol.*, 30:409–439, 1986.

[35] A. M. Kraynik and M.G. Hansen. Foam rheology: A model for viscous phenomena. *J. Rheol.*, 31:175–205, 1987.

[36] F. Bolton and D. Weaire. Rigidity loss transition in a disordered 2D froth. *Phys. Rev. Lett.*, 65:3449, 1990.

[37] T. Okuzono, K. Kawasaki, and T. Nagai. Rheology of random foams. *J. Rheol*, 37:571–587, 1993.

[38] T. Okuzono and K. Kawasaki. Intermittent flow behaviour of random foams: A computer experiment on foam rheology. *Phys. Rev. E*, 51:1246 – 1253, 1995.

[39] Y. Jiang, P. J. Swart, A. Saxena, M. Asipauskas, and J. A. Glazier. Hysteresis and avalanches in two-dimensional foam rheology simulations. *Phys. Rev. E*, 59:5819 – 5832, 1999.

[40] A. Kabla and G. Debregeas. Local stress relaxation and shear-banding in a dry foam under shear. *Phys. Rev. Lett.*, 90:258303, 2003.

[41] S. J. Cox, D. Weaire, and J. A. Glazier. The rheology of two-dimensional foams. *Rheol Acta*, 43:442–448, 2004.

[42] N. Kern, D. Weaire, A. Martin, S. Hutzler, and S. J. Cox. Two-dimensional viscous froth model for foam dynamics. *Phys. Rev. E*, 70:041411, 2004.

[43] S. J. Cox. A viscous froth model for dry foams in the Surface Evolver. *Coll. Surf. A*, 263:81–89, 2005.

[44] L. Bragg and J. F. Nye. A dynamical model of a crystal structure. *Proc. R. Soc. Lond.*, A190:474–481, 1947.

[45] K. Krishan and M. Dennin. Viscous shear banding in foam. *Phys. Rev. E*, 78:051504, 2008.

[46] Y. Wang, K. Krishan, and M. Dennin. Statistics of microscopic yielding in sheared aqueous foams. *Phil. Mag. Lett.*, 87:125–133, 2007.

[47] Y. Wang, K. Krishan, and M. Dennin. Limits of the equivalence of time and ensemble averages in shear flows. *Phys. Rev. Lett.*, 98:220602, 2007.

[48] Y. Wang, K. Krishan, and M. Dennin. Bubble kinematics in a sheared foam. *Phys. Rev. E*, 74:041405, 2006.

[49] Y. Wang, K. Krishan, and M. Dennin. Impact of boundaries on velocity profiles in bubble rafts. *Phys. Rev. E*, 73:031401, 2006.

[50] C. Gilbreth, S. Sullivan, and M. Dennin. Flow transitions in two-dimensional foams. *Phys. Rev. E*, 74:051406, 2006.

[51] M. Dennin. Velocity fluctuations in a slowly sheared bubble raft. *Coll. Surf. A*, 263:78–80, 2005.

[52] M. Twardos and M. Dennin. Comparison between step strains and slow steady shear in a bubble raft. *Phys. Rev. E*, 71:061401, 2005.

[53] M. Dennin. Statistics of bubble rearrangements in a slowly sheared two-dimensional foam. *Phys. Rev. E*, 70:041406, 2004.

[54] J. Lauridsen, G. Chanan, and M. Dennin. Velocity profiles in slowly sheared bubble rafts. *Phys. Rev. Lett*, 93:018303, 2004.

[55] E. Pratt and M. Dennin. Nonlinear stress and fluctuation dynamics of sheared disordered wet foam. *Phys. Rev. E*, 67:051402, 2003.

[56] J. Lauridsen, M. Twardos, and M. Dennin. Shear-induced stress relaxation in a two-dimensional wet foam. *Phys. Rev. Lett.*, 89:098303, 2002.

[57] C. S. Smith. The Shape of Things. *Scientific American*, 190:58–64, 1954.

[58] A. Kabla, J. Scheibert, and G. Debregeas. Quasistatic rheology of foams. Part 2. Continuous shear flow. *J. Fluid Mech.*, 587:47–72, 2007.

[59] G. Debrégeas, H. Tabuteau, and J.M di Meglio. Deformation and flow of a two-dimensional foam under continuous shear. *Phys. Rev. Lett.*, 87:178305, 2001.

[60] C. Raufaste, A. Foulon, and B. Dollet. Dissipation in quasi-two-dimensional flowing foams. *Phys. Fl.*, 21:053102, 2009.

[61] M. E. Rosa and M. A. Fortes. Development of bamboo structure in 2D liquid foam. *Europhys. Lett.*, 41:577–582, 1998.

[62] M. F. Vaz and M. A. Fortes. Experiments on defect spreading in hexagonal foams. *J. Phys. Cond. Matt.*, 9:8921–8935, 1997.

[63] A. Abd. el Kader and J. C. Earnshaw. Stability of two-dimensional foam. *Phil. Mag. A*, 76:1251–1260, 1997.

[64] G. Katgert, M. E. Möbius, and M. van Hecke. Rate dependence and role of disorder in linearly sheared two-dimensional foams. *Phys. Rev. Lett.*, 101:058301, 2008.

[65] G. Katgert, A. Latka, M. E. Möbius, and M. van Hecke. Flow in linearly sheared two-dimensional foams: From bubble to bulk scale. *Phys. Rev. E*, 79:066318, 2009.

[66] C. Quilliet, M. A. P. Idiart, B. Dollet, L. Berthier, and A. Yenki. Bubbles in sheared two-dimensional foams. *Coll. Surf. A*, 263:95–100, 2005.

[67] C. Raufaste, B. Dollet, S. Cox, Y. Jiang, and F. Graner. Yield drag in a two-dimensional flow of foam around a circular obstacle: Effect of fluid fraction. *Eur. Phys. J. E.*, 23:217–228, 2007.

[68] B. Dollet and F. Graner. Two-dimensional foam flow around an obstacle: local measurements of elasticity, plasticity and flow. *J. Fluid Mech.*, 585:181–211, 2007.

[69] C. Quilliet, S. A. Talebi, D. Rabaud, J. Käfer, S. J. Cox, and F. Graner. Topological and geometrical disorders correlate robustly in two-dimensional foams. *Phil. Mag. Lett.*, 88:651–660, 2008.

[70] R. J. Clancy, E. Janiaud, D. Weaire, and S. Hutzler. The response of 2D foams to continuous applied shear in a Couette rheometer. *Eur. Phys. J. E*, 21:123–132, 2006.

[71] E. Janiaud, D. Weaire, and S. Hutzler. Two-dimensional foam rheology with viscous drag. *Phys. Rev. Lett.*, 97:038302, 2006.

[72] N. D. Denkov, S. Tcholakova, K. Golemanov, K. P. Ananthpadmanabhan, and A. Lips. The role of surfactant type and bubble surface mobility in foam rheology. *Soft Matt.*, 5:3389–3408, 2009.

[73] M. F. Vaz and S. J. Cox. Two-bubble instabilities in quasi-two-dimensional foams. *Phil. Mag. Lett.*, 85:415–425, 2005.

[74] S. J. Cox and E. Janiaud. On the structure of quasi-two-dimensional foams. *Phil. Mag. Lett.*, 88:693–701, 2008.

[75] D. Weaire and N. Rivier. Soap, cells and statistics-random patterns in two dimensions. *Contemp. Phys.*, 25:59–99, 1984.

[76] T. C. Hales. The honeycomb conjecture. *Discrete Comput. Geom.*, 25:1–22, 2001.

[77] S.J. Cox and E.L. Whittick. Shear modulus of two-dimensional foams: The effect of area dispersity and disorder. *Euro. Phys. J. E*, 21:49–56, 2006.

[78] S. Vincent-Bonnieu, R. H. Höhler, and S. Cohen-Addad. Slow viscoelastic relaxation and aging in aqueous foam. *Europhys Lett.*, 74:533–539, 2006.

[79] A. Abd. el Kader and J. C. Earnshaw. Shear-induced changes in two-dimensional foam. *Phys. Rev. Lett.*, 82:2610–2613, 1999.

[80] G. L. Thomas, J. C. M. Mombach, M. A. P. Idiart, C. Quilliet, and F. Graner. Simulations of viscous shape relaxation in shuffled foam clusters. *Coll. Surf. A*, 263:90–94, 2005.

[81] R. Höhler and S. Cohen-Addad. Rheology of liquid foam. *J. Phys. Condens. Matter*, 17:R1041–R1069, 2005.

[82] H. M. Princen and A. D. Kiss. Rheology of foams and highly concentrated emulsions 3. Static shear modulus. *J. Coll. Int. Sci.*, 112:427–437, 1986.

[83] A. M. Kraynik and D. A. Reinelt. Linear elastic behaviour of dry soap foams. *J. Coll. Int. Sci.*, 181:511–520, 1996.

[84] D. A. Reinelt and A. M. Kraynik. Simple shearing flow of dry soap foams with tetrahedrally close-packed structure. *J. Rheol*, 44:453–471, 2000.

[85] D. Weaire and M. A. Fortes. Stress and strain in liquid and solid foams. *Advances in Physics.*, 43:685–738, 1994.

[86] J. C. Earnshaw and M. Wilson. Strain-induced dynamics of flowing foam: an experimental study. *J. Phys. Cond. Matt.*, 7:49–53, 1995.

[87] D. A. Edwards, H. Brenner, and D. T. Wasan. *Interfacial Transport Processes and Rheology.* Boston, MA: Butterworth-Heinemann, 1991.

[88] M. Durand and H. A. Stone. Relaxation time of the topological T1 process in a two-dimensional foam. *Phys. Rev. Lett.*, 97:226101, 2006.

[89] S. Tcholakova, N. D. Denkov, K. Golemanov, K. P. Ananthapadmanabhan, and A. Lips. Theoretical model of viscous friction inside steadily sheared foams and concentrated emulsions. *Phys. Rev. E*, 78:011405, 2008.

[90] A. D. Gopal and D. J. Durian. Shear-induced "melting" of an aqueous foam. *J. Coll. Int. Sci.*, 213:169–178, 1999.

[91] S. A. Khan, C. A. Schnepper, and R. C. Armstrong. Foam rheology: III. Measurement of shear flow properties. *J. Rheol*, 32:69–92, 1988.

[92] R. G. Larson. *The Structure and Rheology of Complex Fluids*. Oxford University Press, 1999.

[93] P. Coussot, J. S. Raynaud, F. Bertrand, P. Moucheront, J. P. Guilbaud, H. T. Huynh, S. Jarny, and D. Lesueur. Coexistence of liquid and solid phases in flowing soft-glassy materials. *Phys. Rev. Lett.*, 88:218301, 2002.

[94] S. Rodts, J. C. Baudez, and P. Coussot. From "discrete" to "continuum" flow in foams. *Europhys. Lett.*, 69:636–642, 2005.

[95] P. Marmottant and F. Graner. An elastic, plastic and viscous model for slow shear of a liquid foam. *Eur. Phys. J. E*, 23:337–347, 2007.

[96] I. Cheddadi, P. Saramito, C. Raufaste, and P. Marmottant. Numerical modelling of foam Couette flows. *Eur. Phys. J. E*, 27:123–133, 2008.

[97] D. Weaire, R. J. Clancy, and S. Hutzler. A simple analytical theory of localization in 2D foam rheology. *Phil. Mag. Lett.*, 89:294–299, 2009.

[98] J. Goyon, A Colin, G. Ovarlez, A. Ajdari, and L. Bocquet. Spatial cooperativity in soft glassy flows. *Nature*, 454:84–87, 2008.

[99] A. Wyn, I. T. Davies, and S. J. Cox. Simulations of two-dimensional foam rheology: localization in linear couette flow and the interaction of settling discs. *Eur. Phys. J. E.*, 26:81–89, 2008.

[100] S.J. Cox and A. Wyn. Localization of topological changes in Couette and Poiseuille flows of two-dimensional foams. *AIP Conf. Proc.*, 1027:836–838, 2008.

[101] A. Wyn and S. J. Cox. Orientation and yielding in sheared two-dimensional foams. (in preparation).

[102] P. Marmottant, A. Wyn, F. Rouyer, and S. Cox. Harmonics in oscillatory shear of foams. (in preparation).

[103] K. Brakke. The Surface Evolver. *Exp. Math.*, 1:141 – 165, 1992.

[104] J. L. Higdon. *http://chbe.illinois.edu/Faculty/higdon.php*, [Accessed 4 November 2009].

[105] X. F. Li, H. Zhou, and C. Pozrikidis. A numerical study of the shearing motion of emulsions and foams. *J. Fl. Mech.*, 286:379–404, 1995.

[106] J. P. Kermode and D. Weaire. 2D-FROTH: a program for the investigation of 2-dimensional froths. *Comp. Phys. Comm.*, 60:75–109, 1990.

[107] D. Weaire and J. P. Kermode. Computer simulation of a two-dimensional soap froth II. Analysis of results. *Phil. Mag. B*, 50:379–395, 1984.

[108] D. Weaire, F. Bolton, T. Herdtle, and H. Aref. The effect of strain upon the topology of a soap froth. *Phil. Mag. Lett.*, 66:293–299, 1992.

[109] T. Herdtle and H. Aref. Numerical experiments on two-dimensional foam. *J. Fluid Mech.*, 241:233–260, 1992.

[110] N. Metropolis and S. Ulam. The Monte Carlo Method. *J. Am. Stat. Assoc.*, 44:335–341, 1949.

[111] J. A. Glazier, M. P. Anderson, and G. S. Grest. Coarsening in the 2-dimensional soap froth and the large Q-Potts model - a detailed comparision. *Phil. Mag. B*, 62:615–645, 1990.

[112] Y. Jiang and J. A. Glazier. Extended large-Q Potts model simulation of foam drainage. *Phil. Mag. Lett.*, 74:119–128, 1996.

[113] D. A. Reinelt and A. M. Kraynik. Simple shearing flow of a dry kelvin soap foam. *J. Fl. Mech.*, 311:327–342, 1996.

[114] I. T. Davies and S. J. Cox. Sedimenting discs in a two-dimensional foam. *Coll. Surf. A*, 344:8–14, 2009.

[115] C. Monnereau, M. Vignes-Adles, and N. Pittet. Coarsening of a three-dimensional reconstructed foam under Surface Evolver. *Phil. Mag. B*, 79:1213–1222, 1999.

[116] R. L. Fullman. *Boundary Migration During Grain Growth*, pages pp. 179–207. American Society for Metals, 1952.

[117] I. Cantat and R. Delannay. Dynamical transition induced by large bubbles in two-dimensional foam flows. *Phys. Rev. E*, 67:031501, 2003.

[118] T. E. Green, P. Grassia, L. Lue, and B. Embley. Viscous froth model for a bubble staircase structure under rapid applied shear: An analysis of fast flowing foam. *Coll. Surf. A*, 348:49–58, 2009.

[119] B. S. Gardiner, B. Z. Dugogorski, and G. J. Jameson. Coarsening of two- and three-dimensional wet polydisperse foams. *Phil. Mag. B*, 80:981–1000, 2000.

[120] Q. Sun and S. Hutzler. Lattice gas simulations of two-dimensional liquid foams. *Rheol Acta*, 43:567–574, 2004.

[121] Q. Sun and S. Hutzler. Studying localized bubble rearrangements in 2D liquid foams using a hybrid lattice gas model. *Coll. Surf. A*, 263:27–32, 2004.

[122] H. Sagan. *Introduction to the calculus of variations*. McGraw-Hill, New York, 1969.

[123] K. A. Brakke. 200,000,000 Random Voronoi Polygons. *unpublished, http://www.susqu.edu/brakke/aux/downloads/papers/200.pdf*, 1986.

[124] S. J. Cox, B. Dollet, and F. Graner. Foam flow around an obstacle: simulations of obstacle-wall interaction. *Rheol. Acta.*, 45:403 – 410, 2006.

[125] M. P. Aronson and H M. Princen. Contact angles associated with thin liquid-films in emulsions. *Nature*, 286:370–372, 1980.

[126] M. P. Aronson and H. M. Princen. Contact angles in oil-in-water emulsions stabilized by ionic surfactants. *Coll. Surf.*, 4:173–184, 1982.

[127] T. G. Mason, J. Bibette, and D. A. Weitz. Yielding and flow of monodisperse emulsions. *J. Coll. Int. Sci.*, 179:439–448, 1996.

[128] F. Rouyer, S. Cohen-Addad, R. Höhler, P. Sollich, and S. M. Fielding. The large amplitude oscillatory strain response of aqueous foam: Strain localization and full stress Fourier spectrum. *Eur. Phys. J. E*, 27:309–321, 2008.

[129] S. Marze, R. M. Guillermic, and A. Saint-Jalmes. Oscillatory rheology of aqueous foams: surfactant, liquid fraction, experimental protocol and aging effects. *Soft Matter*, 5:1937–1946, 2009.

[130] P. Saramito. A new constitutive equation for elastoviscoplastic fluid flows. *J. Non-Newtonian Fl. Mech.*, 145:1–14, 2007.

[131] S. Bénito, C. Bruneau, T. Colin, C. Gay, and F. Molino. An elasto-visco-plastic model for immortal foams or emulsions. *Eur. Phys. J. E*, 25:225–251, 2008.

[132] B. S. Gardiner, B. Z. Dlugogorski, and G. J. Jameson. Yield stress measurements of aqueous foams in the dry limit. *J. Rheol.*, 42:1437–1450, 1998.

[133] A. S. Yoshimura, R. K. Prud'Homme, H. M. Princen, and A. D. Kiss. A comparison of techiniques for measuring yield stresses. *J. Rheol.*, 31:669–710, 1987.

[134] H. M. Princen. Rheology of foams and highly concentrated emulsions. II. Experimental study of yield stress and wall effects for concentrated oil-in-water emulsions. *J. Coll. Int. Sci.*, 105:150–171, 1985.

[135] J. C. Baudez and P. Coussot. Abrupt Transition from Viscoelastic Solidlike to Liquidlike Behaviour in Jammed Materials. *Phys. Rev. Lett.*, 93:128301, 2004.

[136] D. Weaire, S. Hutzler, V. J. Langlois, and R. J. Clancy. Velocity dependence of shear localisation in a 2D foam. *Phil. Mag. Lett.*, 88:387–396, 2008.

[137] S. J. Cox. Simulations of Two-Dimensional Foam under Couette Shear. *http://hdl.handle.net/2160/323*, 2007.

[138] L. Arnaud, J. Weiss, M. Gay, and P. Duval. Shallow-ice microstructure at Dome Concordia, Antarctica. *Ann. Glaciol.*, 30:8–12, 2000.

[139] M. Asipauskas, M. Aubouy, J. A. Glazier, F. Graner, and Y. Jiang. A texture tensor to quantify deformations: the example of two-dimensional flowing foams. *Gran. Mat.*, 5:71–74, 2003.

[140] M. Aubouy, Y. Jiang, J. A. Glazier, and F. Graner. A texture tensor to quantify deformations. *Gran. Mat.*, 5:67–70, 2003.

[141] F. Graner, B. Dollet, C. Raufaste, and P. Marmottant. Discrete rearranging disordered patterns, I: Robust statistical tools in two or three dimensions. *Eur. Phys. J. E.*, 25:349–369, 2008.

[142] S. J. Cox, F. Graner, and M. F. Vaz. Screening in two-dimensional foams. *Soft Matt.*, 4:1871–1878, 2008.

[143] A. Tanguy, F. Leonforte, and J.L. Barrat. Plastic response of a 2d Lennard-Jones amorphous solid: Detailed analysis of the local rearrangements at very slow strain rate. *Eur. Phys. J. E*, 20:355–364, 2006.

[144] F. Varnik, L. Bocquet, J. L. Barrat, and L. Berthier. Shear localization in a model glass. *Phys. Rev. Lett.*, 90:095702, 2003.

[145] M. D. Lacasse, G. S. Grest, D. Levine, T. G. Mason, and D. A. Weitz. Model for the elasticity of compressed emulsions. *Phys. Rev. Lett.*, 76:3448–3451, 1996.

[146] S. J. Cox. *private communication*.

[147] S. Vincent-Bonnieu, R. Höhler, and S. Cohen-Addad. A multiscale model for the slow viscoelastic response of liquid foams. *http://arxiv.org/abs/cond-mat/0609363*, 2006.

[148] K. V. Mardia. *Statistics of directional data*. Academic Press, London, 1972.

Appendix A

Publications